THE SYNAPTIC CIRCUITS UNDERLYING OLFACTORY PROCESSING AND
REPRESENTATIONS IN THE INSECT BRAIN: CHARACTERIZATION AND
PLASTICITY OF THE MUSHROOM BODY CALYX

by

Nancy J. Butcher

Submitted in partial fulfillment of the requirements
for the degree of Master of Science

at

Dalhousie University
Halifax, Nova Scotia
August 2010

DALHOUSIE UNIVERSITY

DEPARTMENT OF PSYCHOLOGY/NEUROSCIENCE

The undersigned hereby certify that they have read and recommend to the Faculty of Graduate Studies for acceptance a thesis entitled "THE SYNAPTIC CIRCUITS UNDERLYING OLFACTORY PROCESSING AND REPRESENTATIONS IN THE INSECT BRAIN: CHARACTERIZATION AND PLASTICITY OF THE MUSHROOM BODY CALYX" by Nancy J. Butcher in partial fulfillment of the requirements for the degree of Master of Science.

Dated: August 16th, 2010

Supervisor: _____

Readers: _____

_____

_____

Departmental Representative: _____

DALHOUSIE UNIVERSLTY

DATE: August 16th, 2010

AUTHOR: Nancy J. Butcher

TITLE: THE SYNAPTIC CIRCUITS UNDERLYING OLFACTORY
PROCESSING AND REPRESENTATIONS IN THE INSECT BRAIN:
CHARACTERIZATION AND PLASTICITY OF THE MUSHROOM
BODY CALYX

DEPARTMENT OR SCHOOL: Department of Psychology/Neuroscience

DEGREE: MSc   CONVOCATION: October   YEAR: 2010

Permission is herewith granted to Dalhousie University to circulate and to have copied for non-commercial purposes, at its discretion, the above title upon the request of individuals or institutions.

_____
Signature of Author

The author reserves other publication rights, and neither the thesis nor extensive extracts from it may be printed or otherwise reproduced without the author's written permission.

The author attests that permission has been obtained for the use of any copyrighted material appearing in the thesis (other than the brief excerpts requiring only proper acknowledgement in scholarly writing), and that all such use is clearly acknowledged.

TABLE OF CONTENTS

LIST OF TABLES

LIST OF FIGURES

ABSTRACT

Sensory information is processed and encoded by neural networks. In order to understand how the nervous system is able to rapidly integrate and store sensory information, knowledge of the connections and properties of the neurons in these circuits is required. The fruit fly *Drosophila melanogaster* provides a particularly powerful species to investigate the neural circuits of the olfactory system because in addition to possessing a simple olfactory system amenable to circuit analysis, a host of genetic reagents are available, including the GAL4-UAS system for targeted gene expression. The mushroom bodies, paired structures historically implicated in olfactory learning and memory, receive olfactory information at the mushroom body calyx from second-order olfactory projection neurons (PNs). Within the calyx, individual PN axonal boutons are surrounded by dendritic arborizations from intrinsic Kenyon cells (KCs) and each tiny cluster constitutes a single microglomerulus. Cells that connect the calyx with other areas of the brain, extrinsic neurons (ENs), also contribute to microglomeruli. Most of these contain the neurotransmitter, GABA, and are presumed to be inhibitory. In this study, the synaptic characteristics, neural circuits, and plasticity of calycal cells have been investigated using a combination of serial section electron and confocal microscopy.

The findings reveal several new features of the circuits in the calyx: 1) The calyx contains three ultrastructurally distinct types of PN boutons that are heterogeneous in shape and exhibit subtle differences in synaptic densities. 2) All PN boutons form both ribbon and non-ribbon synapses, and from their smaller size and fewer postsynaptic partners, non-ribbon synapses may possibly become converted to ribbon synapses after activity; the olfactory signal may then be transmitted more strongly and efficiently at ribbon synapses. 3) PN boutons with an electron-dense cytoplasm have the most ribbon synapses per unit area of membrane as well as the highest ratio of ribbon to non-ribbon synapses, and thus may be more active and efficient than other boutons. 4) KC neurites are not exclusively postsynaptic in the calyx and can form occasional ribbon synapses, the functional interpretation of which awaits identification of their postsynaptic partners and vesicle contents. 5) Each PN bouton may contribute input to a single dendritic KC claw at about three presynaptic sites. For the postsynaptic side, a single claw receives input from individual presynaptic sites that must be highly redundant. 6) There may be important processing of the olfactory signal by local circuits formed by ENs in the calyx; ENs form synaptic connections with PNs, KCs, and other ENs. 7) Extensive serial synapses link EN terminals into a network, presumed to be GABAergic and inhibitory, that extends between microglomeruli and may be autaptic. 8) The structure and synaptic connectivity of microglomeruli may undergo changes after adult emergence. 9) vGAT and GAD1-GAL4 lines drive ectopic expression of marker genes in KCs and are not reliable reporters of GABA-positive cells. 10) Previously identified calycal ENs (MB-C1, MB-C2/C3, MB-CP1) are not immunopositive for GAD1, a marker of GABA-containing cells. 11) A network of ENs expressing a GABA phenotype differently innervates anatomically and functionally discrete areas of the honeybee calyx, and in addition the density of innervation may change with alterations in age and/or experience.

LIST OF ABBREVIATIONS USED

3-D	three-dimensional
AL	antennal lobe
AN	antennal nerve
ANOVA	analysis of variance
APL	anterior paired lateral
BR	basal ring
Ca	calyx
CC	central complex
CCV-PN	clear-core vesicle-projection neuron
CO	collar
DB-PN	dark bouton-projection neuron
DCO	dense collar
DCV-PN	dense-core vesicle-projection neuron
GABA	γ-aminobutyric acid
GABA$_A$R	γ-aminobutyric acid A receptors
GABA$_B$R	γ-aminobutyric acid B receptors
GAD1	glutamic decarboxylase-1
GAD1-ir	GAD1-immunoreactive
GFP	green fluorescent protein
HRP	horseradish peroxidase
iACT	inner antennocerebral tract
imACT	inner middle antennocerebral tract
KC	Kenyon cell
KCB	Kenyon cell bodies
kDa	kilodalton
EM	electron microscope, electron microscopy
EN	extrinsic neuron
LCO	loose collar
LH	lateral horn
LP	lip
LPr	lateral protocerebrum
mACT	middle antennocerebral tract
MB	mushroom body
MB-C1	mushroom body-calyx 1
MB-C2/C3	mushroom body-calyx 2/calyx 3
MB-CP1	mushroom body-calyx, peduncle 1
Mi	mitochondrion
NGS	normal goat serum
oACT	outer antennocerebral tract
OL	optic lobes
OSN	olfactory sensory neuron
PB	phosphate buffer
PBS	phosphate buffered saline
PED	pedunculus

plpr	posterior lateral protocerebrum
PN	projection neuron
psmpr	posterior superior medial protocerebrum
Re	retina
sNPF	short neuropeptide F
ssEM	serial section EM
UAS	upstream activating sequence
vGAT	vesicular GABA transporter
vGluT	vesicular glutamate transporter

ACKNOWLEDGEMENTS

CHAPTER 1   INTRODUCTION

1.1 *DROSOPHILA MELANOGASTER AS A MODEL NEUROBIOLOGICAL SPECIES FOR THE STUDY OF OLFACTORY PROCESSING AND REPRESENTATIONS*

Sensory information is processed, encoded, and represented by synaptic networks of neurons. To gain an understanding of the vast capacity of the nervous system to rapidly integrate and store sensory information from the environment, knowledge of the connections and properties of neurons in these circuits is necessary. The recent realization that synaptic wiring is the essential substrate of behaviour is actually a reawakening of old objectives now enabled by new technologies (Bullock, 1990). Initiatives in various labs promote these as the new field of connectomics (Luo et al., 2008; Lichtman and Sanes, 2009). The olfactory system has relatively shallow and compact networks that can be extensively studied to aid our understanding of the neural basis of sensory processing and representation in the nervous system. In vertebrate brains with large populations of neurons, olfactory sensory neurons (OSNs) are separated from the olfactory cortex only by the olfactory bulb. Similarly, in insect brains only the antennal lobe separates OSNs from the mushroom bodies, a higher-order sensory integrative centre. Insect brains have far fewer neurons, however, less than those in vertebrates by a factor of up to 10^9 (Meinertzhagen, 2010), numerical proportions that provide more tractable alternatives to the analysis of neural circuits.

The insect mushroom bodies, or *corpora pedunculata*, are paired structures that are critical for complex activities such as olfactory discrimination, courtship conditioning, context generalization in visual learning, spatial learning, and control of walking activity (Zars, 2000). The mushroom bodies of the fruit fly, *Drosophila melanogaster* have historically been implicated in olfactory learning and memory (Heisenberg et al., 1985; de Belle and Heisenberg, 1994; Zars et al., 2000). *Drosophila* in particular provides a powerful species for investigating the neural circuits of the olfactory system because in addition to possessing a simple olfactory system amenable to circuit analysis, its genes are readily manipulable and behavioural responses to odours quantifiable. Quantification

1

relies especially on the large numbers of flies that can be tested in a single behavioural paradigm, and the consequent suitability of this species for high-throughput screening. By investigating the *Drosophila* olfactory system, we may gain valuable insight into the representation of odours, from the level of sensory neurons to the higher processing and memory areas of the brain, and in turn, the neural basis of learning and memory (Heisenberg, 2003; Keene and Waddell, 2007).

1.2 THE OLFACTORY PATHWAY OF *DROSOPHILA MELANOGASTER*

Odour processing begins with the binding of odour molecules to olfactory receptors proteins located on olfactory sensory neurons (OSNs). There are about 1200 OSNs in the antenna (Stocker, 1994; Figure 1A), and approximately 120 more in the maxillary pulp (Shanbhag et al., 1999). Each OSN typically expresses one of about 60 olfactory receptor proteins (Hallem et al., 2004), and those expressing the same receptor protein have axons that target the same glomerulus in the antennal lobe (Vosshall et al., 2000), although 13 express more than one receptor protein (Vosshall and Stocker, 2007). A total of 46 olfactory receptors have so far been definitively mapped to glomeruli (Vosshall and Stocker, 2007). Glomeruli, "knots or spherical masses of tighter weave than the surrounding neuropil" (Bullock and Horridge, 1965) are repeating units within the antennal lobe, and there are about 43 glomeruli in total, albeit there are some differences in the nomenclature and number of glomeruli in the literature (Vosshall and Stocker, 2007). Most of these receive targeted input from OSNs that express receptor proteins with seven membrane-spanning domains that have no homology to G protein-coupled receptors (Vosshall and Stocker, 2007), although at least one glomerulus receives input from ionotropic glutamate receptor chemosensory OSNs (Benton et al., 2009). The numbers, sizes and relative locations of the glomeruli are invariant (Laissue et al., 1999; Fishilevich and Vosshall, 2005). The dendrites of approximately 150-200 projection neurons (PNs) form synaptic contacts with the OSNs within the glomeruli, with each PN receiving synaptic input from only one or two specific glomeruli. Odorant specific activity in identified glomeruli has been reported by various means, including optogenetic probes such as cameleon (Fiala et al., 2002). Genetically expressed cameleon in *Drosophila* is used to visualize olfactory information in PNs, aided by the shallow,

frontal location of the glomeruli. These recordings confirm the anatomy of the antennal lobe and permit specific patterns of activation in the glomeruli to be visualized in response to any given olfactory stimulus. PNs project their axons primarily through the inner antennocerebral tract and give rise to axon collaterals that innervate the mushroom body calyx, the main input region of the mushroom bodies, en route to the lateral horn, where they terminate (Figure 1A; Vosshall and Stocker, 2007). The PNs express a cholinergic phenotype (Yasuyama et al., 2002; Leiss et al., 2009) and are excitatory (Turner et al., 2008).

Within the calyx, PN boutons provide synaptic input to the other calycal neurons (Figure 1B), mostly intrinsic neurons of the calyx called Kenyon cells (KCs; Kenyon, 1896) but also occasionally to extrinsic neurons (ENs; Schürmann, 1987; Yasuyama et al., 2002), defined here as neurons that connect the mushroom bodies with other areas of the brain, not including PNs. KC dendrites branch extensively within the calyx (Strausfeld et al., 2003), and their axons, numbering approximately 2000, exit the calyx to converge as the stalk-like pedunculus before forming the MB lobes (Figure 1A; Aso et al., 2009). There are three types of KCs, classified by the MB lobes in which they terminate, and also distinguished by their birth order (Crittenden et al., 1998; Lee et al., 1999). The γ KCs are generated first, followed by the α'/β' neurons, and lastly, the α/β KCs form (Lee et al., 1999). In the adult MB, the axons of α/β and α'/β' KCs bifurcate to form the vertical (α and α') and horizontal (β and β') lobes. The γ KC axons do not bifurcate, and form the horizontal γ lobe (Figure 1A; Crittenden et al., 1998; Ito et al., 1998). The lobes appear to play different roles in short- and long-term memory (Zars, 2000). In contrast to the KCs, the origins and branching patterns of ENs have been little characterized. In the calyx, GABA-immunoreactive ENs form synaptic contacts with KCs and the occasional PN (Figure 1B), although the origin(s) of these fibres has either never been closely addressed or is inconclusive (Yasuyama et al., 2002). Recently, Liu and Davis (2009) identified a neuron that expresses a GABA phenotype and provides a widespread innervation to the mushroom bodies, including the calyx, and both suppresses and is suppressed by olfactory learning. There have also been reports of calycal input from octopaminergic cells (Busch et al., 2009). There are possible contributions from

dopamine- (Nässel and Elekes, 1992; Johard et al., 2008; Tanaka et al., 2008; Mao and Davis, 2009) or serotonin-immunoreactive neurons (Vallés and White, 1988; Sitaraman et al., 2008) or even from neurons belonging to other neurotransmitter systems, but these remain unclear.

1.3 RATIONALE AND OBJECTIVES

1.3.1 Investigating the ultrastructure and synaptic characteristics of neurons in the mushroom body calyx

Although advances have been made in our understanding of the neural basis of odor representations at the level of the primary olfactory centres (Namiki et al., 2009), for example in the olfactory bulb of mammals and the antennal lobe of insects, we still lack detailed information on the neural circuits of higher olfactory brain centres, such as the insect mushroom bodies. In particular, many questions remain unresolved regarding the circuits of the neurons in the calyx, the main input neuropile of the mushroom bodies. It is obvious at the light microscope level that the calyx is organized into an overlapping array of more or less discrete microglomeruli. A PN synaptic bouton lies at the centre of each microglomerulus, and is surrounded by tiny profiles of KC dendrites. GABA-immunoreactive ENs and GABA-immunonegative ENs also contribute to the organization of the microglomeruli (Figure 1B; Yasuyama et al., 2002; Leiss et al., 2009). In a previous report, which still provides the major evidence on this topic in *Drosophila*, Yasuyama et al. (2002) used immuno-electron microscopy in an attempt to resolve these circuits more fully. They found that PNs form frequent synapses on to KC dendrites, but rarely do so onto GABA-immunopositive ENs; ENs were also presynaptic to KCs, and sometimes to PNs (Figure 1B).

The synaptic circuits of the calyx cannot be completely characterized using single section EM, however. The neurons have complex forms, and are not easily recognized from single profiles alone, so that the morphology of the neurons and the complete inventory of their input and output synapses both still remain largely unknown, and require investigation with serial section EM (ssEM). Although because of the technical difficulty associated with cutting serial sections such studies have been few, ssEM has already

provided important insights into the structure and function of a number of nervous systems. These provide a basis for the ones to be presented in this study. The foremost precedent comes from the entire wiring diagram of the nematode *Caenorhabditis elegans* (White et al., 1986) as recently augmented (http://www.wormatlas.org/), but earlier examples come from the input neuropiles of various arthropod visual systems: the crustacean *Daphnia* (Macagno et al., 1973), the horseshoe crab *Limulus* (Fahrenbach, 1985), and *Drosophila* itself (Meinerzhagen and O'Neil, 1991; Meinertzhagen and Sorra, 2001). Other examples less relevant to this thesis are given by Ware and LoPresti (1975). Many examples of such studies have been reported from single neurons. For example, crustacean motor terminals that release neurotransmitter tonically are larger in area and contain more synapses than phasic releasing terminals (Msghina et al., 1998). The numbers and spacing of synaptic sites are also reported for neuromuscular junctions in flies (Meinertzhagen et al., 1998). In addition, ssEM has been used to extensively characterize the surface distribution of synaptic sites in photoreceptor terminals of *Musca* and *Drosophila* (Meinerzhagen and O'Neil, 1991; Meinertzhagen and Sorra, 2001), providing novel evidence that synaptic site selection occurs during synaptogenesis (Meinerzhagen and Hu, 1996).

Studies using ssEM have been particularly revealing for investigating age- and experience-based neural changes that accompany behavioural changes in social insects. For example, the ant *Pheidole dentata* has a complex behavioural repertoire that expands with age. Young worker ants care for the brood within the nest, and older worker ants also perform tasks such as foraging outside the nest (Wilson, 1976). Seid et al. (2005) showed that neural remodeling in the lip of the calyx coincides with this period of behavioural maturation. In Hymenoptera, the calyces are paired cup-like structures often organized into two major regions known as the lip and the collar; the lip is solely innervated by the olfactory system and the collar by the visual system (Gronenberg, 2001). ssEM reconstructions have shown that as ants age and their behavioural repertoire expands, the number of PN boutons decreases, while the number of synapses and size of the PN boutons increases, as does the number of synaptic vesicles and the average size of the postsynaptic partners (Seid et al., 2005). Furthermore, ssEM reconstructions revealed

that in the ant *Cataglyphis albicans* PN boutons that innervate the lip and collar, respectively, differ in both structure and synaptic connectivity. PN boutons in the lip are larger, with larger synapses and more synaptic vesicles, while PN boutons in the collar have more postsynaptic partners per synapse (Seid and Wehner, 2008). The latter feature refers to the usual arrangement of synaptic contacts in insect brains, which is polyadic (Meinertzhagen, 2010), with multiple postsynaptic elements abutting a single release site, so as to constitute multiple-contact synapses, dyads, triads, tetrads and so on, like those of the vertrebrate retina (Dowling and Boycott, 1966). Based on the morphological observations in *Cataglyphis*, it has been suggested that olfactory signals carried by PNs in the lip are stronger and are more likely to propagate in the calyx than the visual signals, which are integrated among more postsynaptic partners, possibly for spatial processing for visual navigation (Seid and Wehner, 2008). Quite how reliably structural evidence can be interpreted in such a functional way remains to be seen, however.

The mushroom body calyx of *Drosophila* is an ideal anatomical region to be characterized using ssEM. Not only does it provide input to a region of the brain important in olfactory learning and memory, there is also some evidence that, as in social insects (Groh et al., 2004; Seid et al., 2005; Stieb et al., 2010), the adult *Drosophila* calyx is a plastic structure, its volume and composition being influenced both by age and environmental conditions (Technau, 1984; Heisenberg et al., 1995). As examples of its plasticity, the number of KC fibres changes as flies age, and flies living together in an "enriched" environment have more KC fibres than those housed alone with minimal sensory experience (Technau, 1984). Similarly, the number of KC fibres appears to be dependent on the density and sex of the co-habitating flies (Heisenberg et al., 1995). The exact behavioural correlate(s) of the change in KC fibres remain(s) unclear, but the changes can be seen both in axon and in neurite volume (Heisenberg et al., 1995). Even greater changes are visible in other insect species, for example in volumetric differences between the solitary and gregarious phases in locusts (Ott and Rogers, 2010) but the *Drosophila* brain has the significant advantage of being genetically manipulable, opening the door to studies investigating plasticity at the level of individual cells and their synapses in the calyx. Here, ssEM will be used to investigate and characterize the

synapses and circuits of the calyx in a wild-type mature fly, providing fundamental, yet important, knowledge of the neural connections underlying olfactory processing in the *Drosophila* calyx. These results will be compared with those from a young fly to determine whether observable differences might occur in microglomerulus structure.

1.3.2 Characterizing the phenotypically GABAergic network of the mushroom body calyx using the GAL4-UAS system

The main relay pathway in the calyx, from PNs to KCs, has been previously identified (Yasuyama et al., 2002), but it is the ENs that relay information from other brain regions and possibly between different microglomeruli, that provide synaptic complexity to this neuropile. ENs probably make important pre- and postsynaptic contributions to the transmission of the olfactory signal from PNs to KCs, but ENs have so far been difficult to characterize thoroughly in the *Drosophila* calyx, chiefly because the cells of origin are not well described. Immunolabeling has shown that at least three octopamine-containing cells sparsely distribute presynaptic varicosities over the entire calyx (Busch et al., 2009), but it is GABA-immunopositive cells that appear to be the largest contributors of ENs to the calyx (Yasuyama et al., 2002; Enell et al., 2007; Liu and Davis, 2009). It would therefore be of enormous value to analyze more completely the structure of these GABA cells and the synaptic microcircuits to which they contribute in the calyx, by means of serial section EM. It is hard, however, to combine ssEM with immunolabeling, which is largely restricted to single section EM, because either the pre- or post-embedding method must be used and neither is easily compatible with ssEM. During pre-embedding, detergents are used to permeabilize the membranes to facilitate antibody penetration into the dense neuropile. These holes in the membranes are visible at the EM level, and clear, intact membranes are essential to align serial sections in the z-dimension and identify individual cells. For post-embedding, it is not technically feasible to stain all sections of a large series separately without incurring risk of loss or damage to some of the sections. As an alternative, however, the *Drosophila* toolbox includes the GAL4-UAS system, which could be an important tool to resolve ENs further by removing the need to use antibodies. This genetic system will now be described.

7

The GAL4-UAS system of yeast transgenes (Brand and Perrimon, 1993) is widely utilized in *Drosophila* to drive expression of target genes in a time and cell or tissue-specific manner (Phelps and Brand, 1998). An endogenous promoter or enhancer (called a driver) controls the pattern of expression of the yeast transcription factor GAL4, which in turn directs the transcription of the UAS target gene. Thus the promoter drives expression of the UAS target gene in a spatiotemporal pattern identical to that of the endogenous gene. The GAL4 gene and the UAS target gene are initially located in two different transgenic lines, and transcription of the UAS target gene is normally absent or minimal, driven only by GAL4. One parental fly line carries the gene that encodes GAL4 under the control of the driver, while the other carries the transcriptionally inactive gene of interest, such as a reporter gene (e.g. the gene for green fluorescent protein, GFP), fused to the upstream activating sequence (UAS), which is the GAL4 binding site. In the progeny of the two transgenic lines, GAL4 binds to UAS and causes transcription of the target gene (e.g. GFP) in the spatial and temporal pattern dictated by the driver. GAL4 can also drive expression of an effector target gene, for example in a mutant form, in a strategy not adopted in this study.

Here, the GAL4-UAS system will be used to identify the number and location of cells providing candidate GABA input into the calyx. GABA is the chief neurotransmitter at inhibitory synapses in invertebrate brains (Gerschenfeld, 1973; Sattelle et al., 1991), acting on ion channel receptors for fast, inhibitory transmission and on G-protein-coupled receptors for a slow or modulatory action (Sattelle et al., 1991; Mezler et al., 2001; Buckingham et al., 2005). Both receptor types have been detected in the calyx (Enell et al., 2007) and *in vitro* electrophysiological recordings from KCs show that their fast inhibitory postsynaptic currents are mediated by picrotoxin-sensitive, chloride-conducting GABA receptors (Su and O'Dowd, 2003). The number and arborization pattern(s) of inhibitory inputs to the calyx may have important functional implications for the processing and transformation of olfactory information in the mushroom bodies. Additionally, the identification of a GAL4 line with a promoter that selectively drives expression of GABA-positive neurons in the calyx could permit detailed circuit analysis by ssEM of candidate GABAergic pathways provided by ENs. Two phenotypic markers

8

for GABA-positive neurons are vGAT (vesicular GABA transporter; Fei et al., 2010) and GAD1 (glutamic acid decarboxylase-1; Featherstone et al., 2000), both of which are available GAL4 lines used in this study, which should drive expression in candidate GABAergic neurons. In addition, three GAL4 lines identified by Tanaka et al. (2008) are reported to drive expression in ENs, and these were also investigated. Given the widespread arborization of GABA-positive neurites in the calyx (Yasuyama et al., 2002; Enell et al., 2007; Liu and Davis, 2009), it was hypothesized here that at least one of the lines isolated by Tanaka et al. (2008) may be a source of GABA-positive projections to the calyx. These lines permit the visualization of specific neurons, the MB-C1 cell, the MB-C2/C3 cells, and the MB-CP1 cells, that project to the calyx. The cells are named according to the areas of the mushroom body in which they arborize (e.g. Mushroom Body-Calyx: MB-C; Mushroom Body-Calyx, Peduncle: MB-CP). MB-C2 and MB-C3 also form large arborizations in various areas of the lateral protocerebrum, and MB-C1 in the lateral horn (Tanaka et al., 2008). MB-C1 was considered an excellent candidate for a GABA-positive EN (Tanaka et al., 2008) because it drives expression in calycal cells in a coarse reticulum, reminiscent of the reticulum previously obtained by directly immunolabeling the calycal neuropile with a GABA antibody (Yasuyama et al., 2002). Furthermore, GABA-positive ENs connect the lateral horn and the calyx in other insect species (Nishino and Mizunami, 1998; Perez-Orive et al., 2002), not yet identified in *Drosophila*.

CHAPTER 2   MATERIALS AND METHODS

2.1 FLY STOCKS AND GENETICS

Flies were raised on standard cornmeal molasses medium at 23°C for all crosses, unless otherwise noted. Adult female offspring between 7 and 14-days old were used for all immunocytochemical experiments. Oregon R wild-type flies, either 1-day old or 5-days old (supplied by G. Boulianne, Hospital for Sick Children, Ontario, Canada) were used to investigate the neural circuitry of the calyx with serial section electron microscopy (ssEM).

GAL4 lines were used to drive expression in all phenotypically GABAergic neurons in the brain, some of which are thought to be mushroom body ENs, with many ENs being GABA-positive (Yasuyama et al., 2002). Two phenotypic drivers for GABA neurons were used: GAD1-GAL4 flies were crossed into a stable line with w*; P{UAS-GFP.S65T}T2 (P. Salvaterra, University of California, Riverside, California, USA); and vGAT-GAL4 flies (J. Simpson, Janelia Farm, Virginia, USA) were crossed with yw; P{w+; UAS-superGFP}T2-1/CyOy+ flies (K. Ito, University of Tokyo, Tokyo, Japan). Six insertions of the vGAT gene (CG8394) into the genome were examined and all were predicted to show the same pattern of gene expression.

To investigate GAL4 lines previously reported by Tanaka et al. (2008) to drive expression of marker genes in ENs, as candidate sources of GABA-positive input to the calyx, female GAL4-NP2331 flies were crossed with male yw; P{w+; UAS-superGFP}T2-1/CyOy+ flies or with y1w*; PinYT/CyO; P{UAS-mCD8::GFP.L}LL4 flies (Bloomington Stock Center, Indiana University, Indiana, USA) to visualize the MB-C1 neuron. Flies were incubated at 29°C for at least 24 hours prior to dissection to increase the level of GFP expression (Duffy, 2002). To visualize the MB-C2/C3 neurons, female GAL4-NP6029 flies were crossed with male UAS-mCD8:GFP flies. To drive expression in MB-CP1, female GAL4-NP2297 flies were crossed with male UAS-GFP

(S65T) T2 flies. All lines were supplied by K. Ito (University of Tokyo, Tokyo, Japan), except where otherwise stated.

2.2 ANTIBODIES

A polyclonal antiserum to full-length gel-purified *Drosophila* glutamic acid decarboxylase-1 (GAD1) protein (kindly provided by F. R. Jackson, Tufts University, Boston, USA) was raised in rabbit and characterized by a complete absence of labeling of tissue in homozygous mutant *Drosophila* embryos lacking the *gad1* gene, and Western blotting, which showed that the antiserum recognizes endogenous GAD protein of the expected size of 57 kDa (Featherstone et al., 2000).

A mouse monoclonal antiserum raised against green fluorescent protein (GFP) isolated from the jellyfish *Aequorea victoria* (Invitrogen Molecular Probes, A11120) was used to enhance the GAL4 driven expression of GFP. Demonstrating its specificity, it did not give signal in tissue that lacked the GFP transgene.

The following secondary antibodies were used: goat anti-rabbit conjugated with Cy3 (Jackson Immunoresearch Laboratories, 111-165-003) and goat anti-mouse Alexa 488 (Invitrogen Molecular Probes, A11001).

2.3 IMMUNOCYTOCHEMISTRY AND CONFOCAL MICROSCOPY

After decapitation, fly heads had their probosces removed in 0.1M phosphate buffer (PB), then fixed immediately in 4% formaldehyde in PB for 4 hours or overnight at 4°C. The heads were washed three times for 10 minutes in PB, and at least once in phosphate buffered saline (PBS), before being embedded in 7% agarose in PBS and sectioned at a thickness of 80-100μm on a Vibratome (Leica). The sections were washed once in PBS with 2% Triton-X 100 for 10 minutes and twice in PBS with 0.2% Triton-X 100, then blocked in PBS with 0.2% Triton-X 100 and 10% normal goat serum (NGS) for 1 hour. Tissues were incubated in mouse anti-GFP (1:500) and rabbit anti-GAD1 (1:1000) in PBS with 0.2% Triton-X 100 and 5% NGS at 4°C for 4 days, then washed six times in PBS with 0.2% Triton-X 100 for at least 10 minutes each, and incubated in goat anti-

mouse Alexa 488 (1:250) and goat anti-rabbit Cy3 (1:250) in PBS with 0.2% Triton-X 100 with 2% NGS for 2 days at 4°C or 2 hours at 23°C. The protocol was developed after titrating the GAD1 antibody at dilutions of 1:500, 1:1000 and 1:2000 with incubations times of 2, 3 or 4 days. The sections were then rinsed six times in PBS for at least 10 minutes each, mounted in Vectashield (Vector Laboratories) on glass slides under 00 coverslips, and sealed with clear nail polish. Images were captured using an immersion objective, either 63x/1.4 Plan Apochromat or 40x/1.3 Plan Neofluar, with a LSM 510 confocal microscope with Meta (Zeiss) and edited with Adobe Photoshop CS2.

2.4 TISSUE PREPARATION FOR ELECTRON MICROSCOPY

Female Oregon R flies, either 1-day old or 5-days old were used for serial section EM and subsequent three-dimensional (3-D) reconstructions. The flies were immobilized on ice and decapitated under a drop of modified Karnovsky's fixative (2.5% glutaraldehyde, 2.5% paraformaldehyde in 0.1M cacodylate buffer with a pH of 7.3 and 0.04% calcium chloride). The mouthparts were dissected off to aid with penetration of the fixative into the brain. The heads were fixed for 2 hours on ice, then rinsed for 10 minutes with 0.3M cacodylate buffer in 2% osmium tetroxide, and post-fixed for 1 hour at 4°C in veronal acetate buffer (pH=7.2). The heads were washed three times in 50% ethanol, before further dehydration in a graded ethanol series (10 minutes each in 70%, 80%, 90%, 95% ethanol, and twice for 5 minutes in 100% ethanol) followed by propylene oxide. The tissues were embedded in a 1:1 ratio of propylene oxide and Poly/Bed 812, left overnight in an open container for solvent to evaporate, then transferred from the mixture into fresh resin for 4 hours and placed into a 60°C oven for 48 hours. Semithin 1-2μm sections were cut in a tangential plane from the postero-dorsal surface of the head at a depth until they contained the cortex of Kenyon cell bodies overlying the mushroom body calyx, which was then cautiously sectioned through until the most distal surface of the calyx was encountered. Serial ultrathin sections (Figure 2) were then cut at 50nm, collected on Pioloform-coated 1 x 2 mm slot grids, and stained with saturated aqueous uranyl acetate for 10 minutes and then with lead citrate for 5 minutes. Sections were examined at 80kV in a Philips Tecnai 12 EM, and digital images captured from 117 serial sections for the 1-day old fly and 196 sections for the 5-day old fly. A complete section covered an area of

about 257µm^2 (13.5µm in length x 19µm in width) for the 1-day old fly and 176µm^2 (11µm in length x 16µm in width) for the 5-day old fly, although sections were often rotated on the grid, and counter-rotated for alignment so that the complete area of each section was not always in vertical alignment, and not therefore useable. Tissue preparation, sectioning, and some EM was performed by Zhiyuan Lu. Folds in the tissue were corrected and each section manually aligned in Photoshop CS2. Areas of tissue that were not visible because of a fold in the section were substituted with an insertion of the same area from an adjacent section to permit accurate vertical alignment. Fine alignment was completed in Reconstruct (Fiala, 2005). Cell profiles were traced and 3-D reconstructions then generated in Reconstruct. The tissue was sparsely reconstructed, insofar as only some cells were reconstructed rather than every cell in the entire volume of tissue, a less frequently pursued objective that is both more laborious and time-consuming (Helmstaedter et al., 2008).

2.5 CLASSIFICATION OF CELL PROFILES

Cell types were identified according to a previous report (Yasuyama et al., 2002) that used immuno-EM to characterize projection neurons (PNs), Kenyon cells (KCs), and GABA-immunoreactive extrinsic neurons (ENs) of calycal microglomeruli (Figure 3A,B). PNs form synaptic boutons, the largest elements of the calyx, containing numerous presynaptic sites and a dense population of synaptic vesicles in any given section plane (Yasuyama et al., 2002). The PNs are largely presynaptic to numerous, tiny, vesicle-free profiles of KC dendrites (Yasuyama et al., 2002). ENs profiles are identifiable by their sparsely filled cytoplasm, marked by an occasional presynaptic site accompanied by a halo of small clear-core vesicles and a few dense-core vesicles (Yasuyama et al., 2002). These profiles are smaller than those of the PNs, and typically larger than those of KCs. Their GABA-immunoreactive profiles provide structural inputs, presumed to be inhibitory, to both PNs and KCs (Yasuyama et al., 2002). Neurons classified here as ENs exhibit these synaptic contacts in addition to the morphological characteristics described. Reconstructed ENs could still include both GABA-positive and GABA-negative profiles in the unlabeled EM series examined.

13

2.6 IDENTIFICATION OF SYNAPSES AND POSTSYNAPTIC PARTNERS

Synapses and postsynaptic partners were identified as in previous studies of the calyx using both single (Yasuyama et al., 2002) and serial section EM (Seid et al., 2005; Seid and Wehner, 2008). Synapses were identified by locating presynaptic dense bodies, visible by electron-dense staining of the presynaptic site at the plasmalemma, known as the active zone, with a population of small, clear-core vesicles in close proximity. Synapses were classified as ribbon (Figure 3C) or non-ribbon synapses (Figure 3D). Ribbon synapses contain a characteristic presynaptic density T-shaped in cross section, and non-ribbon synapses do not. A few synapses could not be categorized, for instance if a fold in the tissue obscured part of the synapse. No membrane specializations at the postsynaptic site were obvious. Each active zone was characterized as a single synapse, although more than one postsynaptic partner was almost always present. The number of postsynaptic partners counted for each synapse included all that fell in direct contact with the large, dense active zone (Figure 3C,D). The active zone was most often coextensive with the full width of each postsynaptic element. Occasionally a postsynaptic element made only partial contact at the periphery of the active zone and such sites were still counted as a postsynaptic site. Each postsynaptic profile in contact with the active zone in consecutive sections was counted as a single contact to provide a measure of the total number of postsynaptic partners at the entire active zone. To measure the area of the presynaptic plasmalemma covered by each active zone, the length of the active zone in every section was multiplied by the section thickness and summed per synapse. Every synapse was characterized and its postsynaptic partners counted for the entire reconstructed region of the cell.

2.7 MEASUREMENT OF SYNAPTIC VESICLE DIAMETERS

The electron density of their intravesicular contents distinguished clear-core from dense-core vesicles. The diameters of vesicle profiles were measured in Reconstruct from one outer edge of the membrane profile to the other. Clear-core vesicles were measured in three non-adjacent sections of PN boutons but every section of the ENs, where they were less numerous. The diameters of all dense-core vesicles were measured in the entire reconstructed region of both the PN boutons and ENs. In a novel bouton that was

unidentifiable as either a PN or EN, all dense-core vesicles in five non-adjacent sections were measured, and in a small cell containing large dense granules, the granules were measured in each section plane they were visible.

The EM series used here provides an uncommon advantage for measuring vesicles and granules, because profiles that are split during sectioning are measured only once, reducing the need for correction factors (Abercrombie, 1946) that can introduce biases into the data (Williams and Rakic, 1988). Thus, if a vesicle or granule straddled two adjacent sections, it was measured only in the section plane containing the actual diameter; this method guarantees measurement of the true diameter, and thus helps to reduce the measurement of vesicle or granule caps. When vesicles were not measured in every section, as in the case of the clear-core vesicles in the PNs, vesicle profiles were chosen for measurement in which the membrane outline was sharply defined, compatible with that vesicle being captured at its true diameter. I cannot exclude, however, that some vesicle caps were still measured.

CHAPTER 3   RESULTS

3.1 ELECTRON MICROSCOPIC ANALYSIS OF THE CALYX

The main EM features of calycal microglomeruli are illustrated in Figure 3. The
neuropile field comprises an array of microglomeruli, but these lack clear boundaries, or
obvious glial partitions, and are obvious mainly from the repeated profiles of large,
vesicle-laden PNs. One of these is enclosed in a box (Figure 3A) and reconstructed in
3-D in Figure 3B, to reveal a surrounding halo of KC neurites and several associated EN
terminals. Synapses either had presynaptic T-bar ribbons (Figure 3C) or, in non-ribbon
synapses (Figure 3D), lacked these. The number of postsynaptic partners for each
synapse were those that came into contact with the active zone (Figure 3C,D).

3.2 PROJECTION NEURONS (PNs)

3.2.1   Identification of three subpopulations of PNs

The synaptic boutons formed by PNs were the most prominent ultrastructural feature of
the calycal region, as reported previously in *Drosophila* (Yasuyama et al., 2002) and
other insect species (Ganeshina and Menzel, 2001; Seid et al., 2005). Profiles of the PN
boutons were irregular in shape, usually contained at least one mitochondrial profile, and
ranged from approximately 1 to 4µm in diameter (Figure 4A-D). PN boutons differed in
terms of vesicle phenotype and cytoplasmic electron density, and were sub-divided here
for the first time as PN boutons containing: 1) exclusively clear-core synaptic vesicles
(clear-core vesicle-projection neurons, CCV-PNs; Figure 4A); 2) clear-core vesicles as
well as dense-core vesicles (dense-core vesicle-projection neurons, DCV-PNs; Figure
4B,D); and 3) a dark cytoplasm, containing clear-core vesicles as well as dense-core
vesicles (dark bouton-projection neurons, DB-PNs; Figure 4C). PN boutons containing
dense-core vesicles have not previously been explicitly reported in *Drosophila*, although
they have been reported in the honeybee *Apis mellifera* (Ganeshina and Menzel, 2001)
and two species of ants (Seid et al., 2005; Seid and Wehner, 2008). DB-PNs have also
not been previously reported in *Drosophila*. Ganeshina and Menzel (2001) describe a
population of PN boutons darker than others in the honeybee calyx, although these are

lighter than those found here. Dark PN boutons are also visible in published photomicrographs of the ant, *Cataglyphis albicans* (Seid and Wehner, 2008), and have been purported to reflect a functional state (Steiger, 1967). The different types of PN boutons in the honeybee differ in their synaptic connections (Ganeshina and Menzel, 2001), for which reason the synaptic characteristics and circuits of all three PN subtypes have been extensively investigated here.

3.2.2 Quantification of synaptic vesicles

Diameters of the dense-core (Figure 5A,B) and clear-core (Figure 5D) vesicles of the DCV-PNs and the CCV-PNs were measured, but the electron-dense cytoplasm of the DB-PNs often obscured the membranes of individual vesicles so these could not be measured. Although the mean vesicle diameter measured from EM photomicrographs is typically reported for vesicle populations in the literature (e.g. Ganeshina and Menzel, 2001; Yasuyama et al., 2002), here the distributions of these diameters will be presented for individual vesicle profiles. The mean value is not actually the mean diameter of the vesicles present in the cell, but rather a mean of the distribution of sectioned vesicles projected from a three-dimensional to a two-dimensional plane (Kim et al., 2000). The mean of a measured distribution of vesicle diameters thus does not necessarily indicate the true vesicle diameter, and does not inform us if several populations of different vesicle sizes coexist within the same cell. By presenting histograms of the measured vesicle diameters one can better estimate if more than a single population of vesicles is present (Kim et al., 2000).

All dense-core vesicle profiles with well-defined, and membranes that were therefore presumed to be orthogonal to the section plane containing a true diameter were measured from outer-membrane to outer-membrane in 7 DCV-PNs (n=565 vesicles total). Two DCV-PNs had a population of dense-core vesicles that often appeared denser than the others (compare Figure 4B with 4D), and had distributions shifted towards larger diameters (Figure 5B), and thus possibly have different contents. These observations were supported by a 1-way ANOVA, which revealed significant differences between the vesicle diameters of the individual DCV-PNs ($F_{(6, 558)}=17.56$, $p<0.001$). Post-hoc

analyses (Tukey HSD) showed that DCV1 was significantly different from all other DCV-PNs (p<0.001), and DCV5 was significantly different from all other DCV-PNs (DCV1, p<0.001; DCV3, p=0.023; DCV4, p=0.001; DCV6, p=0.016) except DCV-2 (p=0.996) and DCV7 (p=0.056). No other significant differences were observed. The number of dense-core vesicles in each bouton ranged from 37 to 139, but the number of vesicles per bouton correlated positively with bouton volume (Figure 5C, r=0.84). This correlation indicates that the internal trafficking of dense-core vesicles, the contents of which are presumed to modulate synaptic transmission in surrounding neurons, is the same for boutons of different sizes. The dense-core vesicles ranged from about 40-100nm (Figure 5A,B), a range larger than the 40-65nm reported in the ant (Seid et al., 2005), but narrower than the 60-120nm reported for the honeybee, which were also of varying electron densities (Ganeshina and Menzel, 2001).

All clear-core vesicles with well-defined membranes were measured from outer-membrane to outer-membrane in three non-adjacent sections from three CCV-PNs and three DCV-PNs. The average vesicle size was about 34nm for both CCV-PNs (n=257) and DCV-PNs (n=335), similar to the mean vesicle diameter reported by Yasuyama et al. (2002) of 32nm±4 for ChAT-immunoreactive PNs. A two-tailed t-test showed there was no significant difference in vesicle diameters between the two types of PNs (p=0.70). Additionally, no significant differences were observed within the three PNs measured for the two groups (F(2,254)=0.401, p=0.67 for CCV-PNs and F(2,332)=0.632, p=0.53 for DCV-PNs).

The DCV-PNs appear to have slightly fewer clear-core vesicles within the diameter range of 26-30nm and slightly more in the range of 36-40nm, when compared with the CCV-PNs. The overall distributions, however, were very similar (Fig. 5D), correlating well with the suggestion that all PN boutons contain the classical fast neurotransmitter acetylcholine (Yasuyama et al., 2002; Leiss et al., 2009). Vesicle diameters ranged from about 20-75nm, compared with 30-60nm found in the honeybee (Ganeshina and Menzel, 2001) and 10-60nm in the ant (Seid et al., 2005). Collectively, these measurements indicate that there is a large range in size of clear-core vesicles that are presumed to

contain acetylcholine, or that there could even be a "large" and "small" population of vesicles within the same terminal. If the latter were true, multiple Gaussian distributions fitted to each peak of the data should provide a higher correlation between the theoretical and observed distribution of vesicle diameters, than a single Gaussian distribution fitted to the single highest peak. Fitting more than one Gaussian curve to counts of clear-core vesicle diameters, however, did not substantially improve this correlation (not shown). For example, for the CCV-PNs, a Gaussian curve fitted to the distribution at its highest peak (31nm) yielded a strong correlation (r=0.97) between the observed and theoretical distribution. The addition of curves that were fitted to the much lower peaks at larger vesicle diameters (e.g. 36 and 59nm) failed to improve the correlation beyond a value of 0.98. The reason for the large range of vesicle diameters is unclear, but could be due to transient states in the vesicle recycling pathway or possibly caused by a disequilibrium introduced during the process of chemical fixation. A large range of vesicle diameters has also been reported in cholinergic antennal olfactory sensory neurons of the moth, *Manduca sexta* (Tolbert and Hildebrand, 1981).

3.2.3 Morphology

Three PN terminals of each group that could be reconstructed in their entireties were traced and rendered using Reconstruct (Figure 6). PNs were packed closely together (Figure 3A, Figure 6J,K), and the three types intermingled in no apparent pattern. There were no obvious differences in morphology between the three subtypes of PNs based on the three-dimensional reconstructions, although considerable heterogeneity of shape existed within each group that would have made differences in shape hard to discern. It is now clear as a result that the terminal boutons of PNs are of varying size and shape. The polymorphic bouton shapes were classified as elongated (Figure 6A,E,F), uni-lobed (B,D,H,I), or bi-lobed (C,G). Long, slender axons were visible in some reconstructions (Figure 6A,E,F,G,H), but for technical reasons only short segments of axon could be reconstructed in others (Figure 6B,C,D,I). The axons did not contain presynaptic sites, although they occasionally received input from other cells, presumed to be ENs, at ribbon synapses.

3.2.4 Quantitative morphometric comparision of PNs

Despite differences in their shape, the three groups of PNs were similar in size, their types of synapses, and the density of their presynaptic sites, although some differences were also noted (Table 1). Each of the boutons of the three DCV-PNs measured had a consistent surface area of approximately $14\mu m^2$, and while some CCV-PNs and DB-PNs also had boutons of a similar size, they also had terminals twice or more this size. The smaller PN boutons typically each contained 30 to 35 synapses, while the larger boutons contained a commensurately larger number of synapses. The number of synapses was comparable to those reported in PN boutons in the lip of the ant calyx, although the volume of the PN boutons here was up to three times as large (Seid et al., 2005; Seid and Wehner, 2008).

When the effect of membrane surface area was controlled for by calculating the number of synapses per μm^2 of plasma membrane, DCV-PN and DB-PN boutons, which both contain DCVs, had identical mean areal synaptic densities (2.33±0.15; 2.33±0.26 respectively), greater than that of the CCV-PNs (1.84±0.27). Despite this lower value, no significant effect of PN bouton subtype on synaptic density was found (F=2.552, p=0.119, df=2). Synapses in all three groups of PN boutons were classified as ribbon or non-ribbon synapses depending on the presence or absence of a T-bar ribbon, and this partition of synapse type did affect synaptic density (F=106.397, p<0.001, df=1), as ribbon synapses were more prevalent than non-ribbon ones in every bouton (Table 1). There was no interaction between PN subtype and synapse type (F=1.884, p=0.2, df=2), however, showing that these two independent variables affect the dependent variable, synaptic density, in an independent fashion. On average, DB-PNs had approximately 3.5 times more ribbon than non-ribbon synapses per μm^2 of plasma membrane, CCV-PNs had three times more, and DCV-PNs twice as many. DB-PNs also had the highest density of ribbon synapses per μm^2 of plasma membrane, and DCV-PNs had more in turn than CCV-PNs. DCV-PNs had the highest density of non-ribbon synapses, followed by DB-PNs and CCV-PNs.

3.2.5   Synaptic arrangements of PN synapses

In all three groups of PNs, the numbers of postsynaptic partners at non-ribbon synapses tended to be fewer than at ribbon synapses (Figure 7). The postsynaptic profiles were primarily KC dendrites, but infrequently also included ENs (Yasuyama et al., 2002), identified here by their morphology and synaptic characteristics. The number of profiles postsynaptic to ribbon synapses, identified by contacts with the dense, presynaptic active zone, was most often six for all three groups of PNs, but ranged from two to fourteen. Non-ribbon synapses were most often arranged as dyads or triads, with a range of one to ten postsynaptic partners. These distributions differed dramatically from the results obtained when the number of postsynaptic partners was counted in a single section, as has been done previously (e.g. Ganeshina and Menzel, 2001; Seid et al., 2005). From single sections, both ribbon and non-ribbon synapses most often form triads, with a maximum of six postsynaptic partners. A similar finding has been reported by Tolbert and Hildebrand (1981) for synaptic connections in the antennal lobe of the moth: when the number of postsynaptic partners was counted on individual sections, synapses typically appeared as dyads, but when counts were made using serial sections the number of postsynaptic partners ranged from two to seven. These results collectively indicate that counts of postsynaptic partners from single EM sections should always be interpreted with caution, as they are likely to be only lower-limit estimates.

3.2.6   Relationship between synapse size and number of postsynaptic partners

Since the number of postsynaptic partners at ribbon and non-ribbon synapses ranged so widely, it was suspected that as the number of postsynaptic partners increased, so did the area of the presynaptic site. For one DCV-PN, the most frequently observed type of PN bouton, the surface area of each ribbon and non-ribbon synapse was therefore reconstructed and measured (Figure 8). The surface area of the electron-dense presynaptic membrane positively correlated with the number of its postsynaptic partners (r=0.83 for all synapses, Figure 8F; r=0.94 for non-ribbon synapses; r=0.70 for ribbon synapses). Non-ribbon synapses were significantly smaller ($57,500\pm46,100nm^2$, range $13,400$-$157,100nm^2$, p=0.004) than ribbon synapses ($108,300\pm43,100nm^2$, range $37,500$-

214,100nm^2). Ribbon and non-ribbon synapses were interspersed (Figure 8A-E), and synapses were often very close to each another, although one side of the bouton was almost bare of presynaptic sites (Figure 8A). These results are compatible with PN synapses being at various stages of development, with the larger ribbon synapses and their larger number of postsynaptic partners being in a more mature state than the smaller non-ribbon synapses. Alternatively, the latter may represent regressive stages of ribbon synapses that are in the process of being eliminated.

3.3 KENYON CELLS (KCS)

KCs were presumed to contribute the tiny profiles postsynaptic to the large PN boutons (Figure 3A,B). This has been assumed in previous studies (e.g. Ganeshina and Menzel, 2001; Yasuyama et al., 2002) based on the small size and large number of these, now confirmed below by the reconstructions identified in this study. The KC dendrites were extremely fine and branched extensively in the calyx, making them very difficult to trace even in EM series. Nevertheless, the sparse and mostly partial reconstructions obtained showed that the KCs encircle PN terminals, forming microglomeruli (Figure 9A,B), and that some exhibited characteristic claw-like processes (Figure 9C,D), conforming very well with those previously demonstrated using confocal microscopy (Leiss et al., 2009). Multiple claws embracing a single PN bouton were reconstructed (Figure 9C), in a configuration also observed at the light microscope level (Leiss et al., 2009). One KC was postsynaptic to the CCV-PN that it abutted with its claw, and extended a long, narrow branch that ran around a DCV-PN (non-synaptic contact), before forming two separate sites away from the PN boutons that were both presynaptic (Figure 9D). This is the first report of KC presynaptic sites in the calyx. Both were ribbon synapses surrounded by a small halo of vesicles (e.g. Figure 9E). These ribbon synapses lacked large active zones of the sort found at PN synapses (Figure 4), but were nevertheless unambiguous and extended through one or three consecutive sections. One synapse formed a small triad (Figure 9E) with postsynaptic partners that could not be identified because they could only be traced for a short distance within the series. Two of the postsynaptic elements appeared to be long axons, and the third formed a terminal with a ribbon synapse that was similar in appearance to the presynaptic KC profile (Figure 9E),

although it had a denser active zone. The other KC presynaptic site formed a monad, which was cautiously identified as an EN because of its ultrastructural appearance. A handful of dense-core vesicles were dispersed within the KC. These were about 60nm in diameter and possibly contained a neuropeptide, consistent with reports of weak, punctate labeling of short neuropeptide F (sNPF), the orthologue of mammalian neuropeptide Y, in the intrinsic neurons of the calyx (Johard et al., 2008). sNPF was recently identified (Johard et al., 2008) in an effort to determine what peptide gives rise to FMRFamide immunolabeling in the fly mushroom bodies (Nässel, 1993). No other neuropeptides so far have been identified in the mushroom bodies, even some that localize to KCs in other insect species (e.g. tachykinin, Winther et al., 2003; orkokinin, Hofer et al., 2005; longNPF, corazonin, insulin-like peptide 7, Nässel et al., 2008). It is thus not clear what other neuropeptides (if any) might also express in KCs, nor whether different classes of KCs might express different neuropeptides.

3.4 ESTIMATING PN-KC CONVERGENCE

From the nine reconstructions of PNs, it appears that PN boutons form 17-22 active zones per KC, based on the following arithmetical reasoning. The average total number of presynaptic sites constituting the synaptic regions of nine PN boutons (three of each subtype) was about 40. So for the estimated 1,115 PN boutons in the calyx (Turner et al., 2008), there would be a total of roughly 44,600 synapses. Distributing these equally among the 2,500 KCs that arborize in the calyx yields an average of 17 presynaptic sites for each, or for a more recent estimate of 2,000 genetically identifiable KCs (Aso et al., 2009), a total of 22 presynaptic sites per KC. These estimates may be slightly inflated because some PN presynaptic sites are in contact with EN synapses, but these are very rare compared with PN input to the KCs. Each KC probably receives its synaptic inputs from five or so PN boutons, because a KC typically has between five and seven claw-like branches in the calyx (Lee et al., 1999; Zhu et al., 2003), and each of these branches contacts a single PN bouton (Leiss et al., 2009). Therefore, distributing the 17-22 presynaptic sites evenly among the 5-7 claw-shaped branches would imply that each PN bouton may contribute input to a single KC claw at roughly only three presynaptic sites. This estimate corresponds to the number of synaptic inputs observed here from a PN

bouton to a claw-shaped KC. These inputs derive from any combination of ribbon and/or non-ribbon synapses.

The average number of synapses counted in nine boutons, three of each subtype, was used for the above calculations because each fell within a reasonably similar range of number of synapses per bouton (Table 1). More precise estimates will require an estimate of the relative frequencies and distributions of CCV-PNs, DCV-PNs, and DB-PNs in the calyx, which would require the reconstruction of a much larger area of the calyx, as may eventually become possible with automated methods for computer-aided 3-D reconstruction. Despite the limited sample presented here, the methods used to obtain these estimates are still much more precise than the rough estimates previously derived from the total number of synapses in the calyx based on the number of synapses in a single profile of a single PN bouton and the approximation that PN boutons are perfectly spherical (Turner et al., 2008).

The numbers above refer only to the number of PN presynaptic sites that contact a single KC, however, and ignore the complex arrangement of postsynaptic dendrites also now reported in this study. Given that there are 2000-2500 KC axons that extend dendritic arborizations into the calyx (Aso et al., 2009), and that each KC forms an average of six claw-like branches in the calyx (Lee et al., 1999; Zhu et al., 2003) that each contact a different PN bouton (Leiss et al., 2009), then the calyx must contain a total of approximately 12,000-15,000 KC claws. Distributing these evenly among the estimated 1,115 boutons in the calyx (Turner et al., 2008), there would be about 11-13 claw-like branches per bouton. From the counts made here, each of these boutons contains approximately 40 presynaptic sites, about 30 with presynaptic ribbons, which typically each have six postsynaptic partners, and 10 non-ribbon synapses, which each have about two to three postsynaptic partners. By these counts, a single PN bouton in this series has about 200-210 postsynaptic elements, all of which must originate from the 11-13 claw-like branches. Each claw must thus contribute roughly 17 postsynaptic profiles to a PN bouton. From the presynaptic calculations given above, each claw corresponds on average to about 3 presynaptic sites per bouton. It therefore follows that a single claw

24

receives multiple input from individual presynaptic sites that must be highly redundant, indeed confirming this conclusion, even within the limited samples reconstructed in this study branched KC dendrites were sometimes found to be postsynaptic at two sites at the same synapse.

3.5 EXTRINSIC NEURONS (ENs)

Profiles of ENs were identifiable by their sparsely filled, pale cytoplasm and synaptic contacts, as previously reported (Yasuyama et al., 2002) and illustrated in Figure 10. The previous report (Yasuyama et al., 2002) only categorized GABA-immunopositive EN profiles but the unlabelled ENs here could include elements other than those that express a marker for GABA. Unlike PNs, ENs rarely formed synapses; each reconstructed EN made only one to three synapses (Table 2). Furthermore, ENs formed exclusively ribbon synapses, and these were found for every 0.13 to 0.32 μm^2 of plasmalemma surface, with the exception of an EN terminal (EN3) with a synaptic density of approximately 1 synapse/μm^2 (Table 2). Small populations of clear-core vesicles clustered around the ribbon synapses (Figure 10A,C,E) and, not surprisingly, the EN with the highest density of synapses also had the greatest concentration of vesicles (Table 2). The most common diameter of vesicles in this EN was 26-30nm, unlike the other three ENs, which all had profiles that mostly ranged between 31 and 40nm (Figure 10B). The latter group is more consistent with previous observations that clear-core vesicles in GABA-immunopositive ENs are 43±11nm in diameter (Yasuyama et al., 2002) and range from 30-60nm (Ganeshina and Menzel, 2001), suggesting that EN3 was not GABA-positive, or at least belonged to a different group of EN type. Three of the four ENs also contained dense-core vesicles (Table 2), and the profiles of these vesicles ranged from 50-60nm. These were smaller than those measured in the honeybee (80-120nm), perhaps suggesting that dense-core vesicles in ENs in the two species may contain different amines or peptides. Dense-core vesicles were much more prevalent in EN2 (Table 2) than the others, perhaps offering a further indication that the observed population of ENs here was heterogeneous.

The ENs provided synaptic input to all elements of the microglomerular microcircuits, the KCs (Figure 10A), the PNs (Figure 10A,C), and to other ENs (Figure 10C,E).

Connections between ENs have not clearly been reported previously, neither in *Drosophila* (Yasuyama et al., 2002) nor *Apis* (Ganeshina and Menzel, 2001). The ENs are long, narrow and branched, and occasionally show small swellings (Figure 11). Some seem to encircle PN boutons (e.g. Figure 11B), while others run in parallel with each other (Figure 11D). At sites of contact with the PN boutons, the ENs can be postsynaptic (Figures 10D,11A), but are more often presynaptic (Figure 10A,C; 11A-C),in a ratio of about 1:4 between these two types of elements (Figure 12). ENs formed synaptic arrangements of various compositions, and the number and identity of postsynaptic partners varied greatly (Figure 12). As previously identified (Yasuyama et al., 2002), ENs provided input to KC dendrites. This was sparse compared with input from PN boutons to KCs however. In one microglomerulus (Figure 12), the PN bouton was presynaptic to 206 profiles of putative KC dendrites (not shown). Of these KCs, only three also received input from an EN.

ENs also appeared to form a local network, for example, EN4 contacted a PN bouton (reconstructed in Figure 6G) directly through a synapse, and indirectly through synaptic inputs via EN3, which was presynaptic both to the bouton as well as other ENs, which in the case of EN1 also provided synaptic input to the PN (Figure 12). Thus EN4 provided monosynaptic, disynaptic and trisynaptic input to the PN bouton. If these ENs all provided tonic or simultaneous phasic GABAergic transmission, and if this were in all cases inhibitory, then together the ENs would provide input to the PN bouton that was not only inhibitory but also disinhibitory. Similarly, EN3 provided a direct synaptic input to a KC profile, as well as indirectly by EN1, again providing potentially both inhibitory and disinhibitory inputs. These results indicate anatomical substrates for extensive shaping of the PN olfactory signal within the calyx.

3.6 CHARACTERIZING THE PHENOTYPICALLY GABAERGIC NETWORK OF THE MUSHROOM BODY CALYX USING THE GAL4-UAS SYSTEM

To resolve the number and circuits of cells that contribute GABA-containing neurons to the calyx it would be extremely valuable to identify such cells by means of GAL4 lines that reliably drive expression of a marker gene (e.g. GFP) in GABA-positive cells. To

correlate the EM observations from this study with identified ENs, because the former derived from labour-intensive methods that could not be extended to larger regions of the cell(s), GAL4 lines were sought that would drive expression of GFP visible by confocal microscopy. Not all lines drove expression of GFP as previously reported, however. In particular, to evaluate the contributions of the MB-C1 neuron to EN profiles in the calyx, female GAL4-NP2331 flies were crossed to two different UAS lines. When crossed with y1w[*]; PinYT/CyO; P{UAS-mCD8::GFP.L}LL4 flies as previously reported (Tanaka et al., 2008), the MB-C1 neuron was not visible and there was only faint GFP expression in other cell bodies and neurites. When crossed with yw; P{w+; UAS-superGFP}T2-1/CyOy+, the MB-C1 neuron was visible in a small number of progeny, although other cells were visible in all preparations. There is no clear reason why the two UAS-GFP lines yielded different levels of expression. Although different UAS reporters usually label the same set of GAL4-expressing neurons, sometimes neurons that cannot be readily visualized with one UAS-reporter are apparent with a different reporter line (Ito et al., 2003; Tanaka et al., 2008).

Problems also existed with the specificity of the GAL4 lines used. The two lines generated so far to target candidate GABAergic neurons, vGAT-GAL4 and GAD1-GAL4, were both found to promote ectopic expression of GFP in the KCs of the mushroom bodies (Figure 13). All lines carrying insertions of the vGAT gene (CG8394) into the genome showed the same pattern of gene expression except one that lacked expression entirely. As well as possibly labeling ENs, the KC dendrites were obvious in the calyx as the outer ring of individual microglomeruli (Figure 13B,D). The KC axons were clearly visible as four bundles exiting the calyx (Figure 13C), and the lobes of the MBs, which largely comprise KC axons and terminations, are also well-labeled (Figure 13A). Furthermore, the cell bodies of the KCs were labeled, and the pattern of GAD1-driven GFP expression did not correspond with GAD1-immunolabeling (Figure 13B).

Since neither the vGAT nor the GAD1-GAL4 lines were useful for identifying GABA-positive cells that project to the calyx, three GAL4 lines that drive expression in calycal ENs (Tanaka et al., 2008) were next tested for GAD1-immunoreactivity. Neurons were

identified by the location of their cell bodies (Figure 14), MB-C1 in the lateral cell body region in the posterior lateral protocerebrum (plpr), MB-C2/C3 in the posterior superior medial protocerebrum (psmpr), and MB-CP1, ventrolateral to calyx, in the plpr. None was GAD1-immunoreactive (Figures 15-17). The MB-C1 driver was found here to promote expression of GFP (Figure 15) in cells in addition to MB-C1, including PNs of the outer antennocerebral tract, which terminate in the lateral horn (not shown), as well as visual projection neurons (Otsuna and Ito, 2006), and other cell bodies throughout the brain (not shown). The driver for the MB-C2/C3 neurons was specific to those cells only, and these branched extensively in the lateral protocerebrum (Figure 16). No arborizations were clearly visible in the calyx, as previously reported (Tanaka et al., 2008). The MB-CP1 driver (Figure 17) promotes expression of GFP in many cell bodies, with pronounced labeling of the fan-shaped body and noduli (not shown), as well as in a small population of PNs originating from the inner antennocerebral tract (Figure 17C,F). Long, slender neurites extended from the MB-CP1 cell body into the calyx (Figure 17C,F).

Thus, none of these drivers drove expression in the mushroom body calyx compatible with ENs that have previously been shown to contain GABA (Yasuyama et al., 2002), frustrating our further characterization of EN input to the calyx.

3.7 OTHER CELL TYPES

Two cells were identified in the EM series that did not meet the criteria for PNs, KCs, or ENs (Figure 18). One cell had a cytoplasm filled with dense-core vesicle profiles up to 70nm in diameter (Figure 18B,C), as well as some clear-core vesicles and synapses (Figure 18B). Although closest in appearance to a PN, its membrane surface area ($10.47\mu m^2$), volume ($2.34\mu m^3$), and density of (exclusively ribbon) synapses (1.53 synapses per μm^2) were all lower than the values observed for PNs (Table 1), indicating that this cell may instead be a terminal from an EN that has not been previously identified, at least at the EM level. Reconstruction of the cell revealed a bulbous structure that appeared bi-lobed (Figure 18A). The second cell was much smaller, with a membrane surface area of $5.00\mu m^2$ and a volume of $0.47\mu m^3$. Profiles ranged in length

from 0.3 to 1.3μm, and most were filled with large, dense granules up to 160nm in diameter (Figure 18E,F). Similar profiles containing large, dense granules have been previously reported in *Drosophila* (Yasuyama et al., 2002) and *Apis* (Ganeshina and Menzel, 2001). The cell contained one putative ribbon synapse (not shown) and mitochondrion, and its three-dimensional structure was elongated and bi-lobed (Figure 18D). It appeared to be presynaptic to a PN bouton, as well other small profiles unidentifiable because of the short distance over which they were captured in the series (not shown). A clearly identifiable ribbon synapse was reported by Yasuyama et al. (2002) in this type of cell, and interestingly, Ganeshina et al. (2001) reported that dense granule-containing cells were occasionally postsynaptic to PN boutons. Collectively, these results indicate that there may be rare reciprocal contacts between PN boutons and these dense granule-containing cells.

3.8 COMPARISON WITH MICROGLOMERULI FROM A 1-DAY OLD FLY

As in the older fly, the calyx of the 1-day old fly contained microglomerular units with indistinct boundaries, with a single PN bouton at their centres surrounded by tiny profiles of KC dendrites. There were however several notable differences. The PN boutons seen in the 1-day old fly were all DCV-PNs; CCV-PNs or DB-PNs were not observed. DB-PNs were also absent in single sections from a second 1-day old fly. These sections were not used to identify CCV-PNs and DCV-PNs because these can only be distinguished from one another in section series. A single microglomerulus was encircled by thin glial processes, and two others were partially ensheathed. The three PN boutons reconstructed were inhomogeneous in shape and had a less regular, more swollen morphology than those of the 5-day old fly (Figure 19A, compare with Figure 6B,E,H). They also appeared larger in size, although this difference was not significant (p=0.16 for membrane surface area, p=0.06 for volume; Figure 19C,D).

The synapses and pre- and postsynaptic partners of one PN bouton (leftmost in Figure 19A) were compared with those from three DCV-PNs of the older fly (Figure 6B,E,H). The bouton had a total of 57 synapses, for a synaptic density of 2.22 synapses per μm^2 of membrane. Of these 57, 38 were ribbon synapses (1.48 synapses per μm^2) and 11 non-

ribbon synapses ($0.43\mu m^2$). Eight synapses could not be clearly identified as ribbon or non-ribbon. These synaptic densities were similar to those in the boutons from the 5-day fly (Table 1), as was the finding that ribbon synapses had more postsynaptic partners than non-ribbon synapses. The ribbon synapses in the 1-day fly most commonly had 7 or 10 postsynaptic partners (Figure 19B), however, more than in the 5-day old fly (Figure 7B,E,H). Non-ribbon synapses most often had five postsynaptic partners (Figure 19B) compared with two or three in the older fly (Figure 7B,E,H). These results should of course be interpreted with caution, because only a single DCV-PN bouton was characterized for the 1-day old fly, compared with three in the 5-day old fly, and the eight unclassified synapses must make unidentified contributions to the distribution of postsynaptic partners (Figure 19B). The total number of postsynaptic partners could also not be counted for two large ribbon synapses because of poor membrane preservation in some of the sections they spanned, but these had at least 11 and 17 postsynaptic partners each.

Ribbon and non-ribbon synapses were interspersed over the presynaptic membrane (Figure 20A-E), as in the 5-day old fly (Figure 8A-E), and the surface area of the electron-dense presynaptic membrane again correlated positively with the number of its postsynaptic partners (r=0.82 for all synapses, Figure 20F; r=0.86 for non-ribbon synapses; r=0.75 for ribbon synapses; r=0.82 for unclassified synapses). The contact areas of non-ribbon synapses in the 1-day old fly were significantly smaller ($54,900\pm29,800nm^2$, range $21,350-124,850nm^2$, p<0.001) than ribbon synapses ($155,840\pm67,610nm^2$, range $33,000-322,400nm^2$), as also reported in the older fly. Interestingly, the ribbon synapses of the 1-day old fly were significantly larger than those of the 5-day old fly (p=0.001). There was no difference in the size of non-ribbon synapses between the two ages (p=0.88), however. Provided direct comparisons are possible, the decreased size of ribbon synapses and the number of postsynaptic partners in the 5-day old fly together indicate that ribbon synapses become smaller and have fewer postsynaptic partners as the fly ages from day 1 to day 5. It is unclear why the number of postsynaptic partners is larger for non-ribbon synapses if the synapses are not

significantly larger, but the significance of these findings may be limited by the small number of non-ribbon synapses counted (n=11).

Other preliminary findings include the fact that by the first day post-emergence, the calyx is innervated by the small cells containing large dense granules, and rare PN bouton-bouton synapses exist, although the numbers of these remain to be determined.

3.9 TABLES AND FIGURES

Table 1   Quantitative morphometric and synaptic comparison of terminals of three clear-core vesicle-projection neurons (CCV-PNs), three dense-core vesicle-projections neurons (DCV-PNs) and three dark bouton-projection neurons (DB-PNs). Mean±standard deviation, where shown.

	CCV-PNs			DCV-PNs			DB-PNs		
Surface area of bouton (μm^2)	32.21	19.58	13.69	13.96	14.43	13.53	12.94	24.21	25.31
Mean surface area of bouton (μm^2)	21.82±9.46			13.97±0.45			20.82±5.59		
Volume of bouton (μm^3)	6.95	4.86	4.26	3.46	4.87	2.43	2.78	6.13	6.74
Mean volume of bouton (μm^3)	5.35±1.41			3.59±1.23			5.21±2.13		
Number of ribbon synapses	53	24	18	24	24	19	28	42	39
Ribbon synapses per μm^2	1.65	1.23	1.31	1.72	1.66	1.40	2.16	1.73	1.54
Mean ribbon synapses per μm^2	1.40±0.22			1.59±0.17			1.81±0.32		
Number of non-ribbon synapses	16	8	6	11	9	11	3	19	13
Non-ribbon synapses per μm^2	0.50	0.41	0.44	0.79	0.62	0.81	0.23	0.79	0.51
Mean non-ribbon synapses per μm^2	0.45±0.05			0.74±0.10			0.51±0.28		
Number of unknown synapses	0	0	0	0	0	0	0	1	1

	CCV-PNs			DCV-PNs			DB-PNs		
Total number of synapses	69	32	24	35	33	30	31	62	52
Mean of all synapses	42			33			48		
All synapses per μm^2	2.14	1.63	1.75	2.50	2.29	2.22	2.39	2.56	2.05
Mean synapses per μm^2	1.84±0.27			2.33±0.15			2.33±0.26		

Table 2   Quantitative morphometric and synaptic comparison of four extrinsic neurons (ENs).

	EN1	EN2	EN3	EN4
Total surface area (μm^2)	4.40	3.08	2.82	15.86
Number of ribbon synapses	1	1	3	2
Ribbon synapses per μm^2	0.23	0.32	1.06	0.13
Total volume (μm^3)	0.25	0.28	0.24	1.58
Number of clear-core vesicles	10	21	56	8
Clear-core vesicles per μm^3	40	75	233	5
Number of dense-core vesicles	0	6	1	1
Dense-core vesicles per μm^3	0	21.43	4.17	0.64
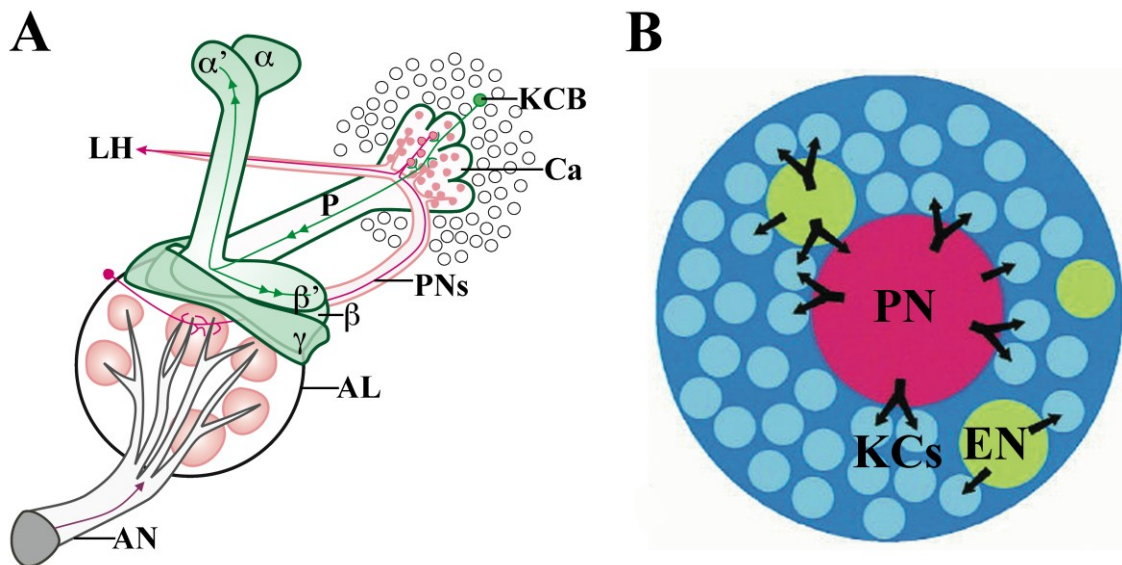
Figure 1   A) Schematic diagram of the olfactory pathway in *Drosophila melanogaster*, represented in the right brain hemisphere as seen in a frontal plane from the anterior aspect (adapted from Kasuya et al., 2009). Olfactory information (purple arrow) is first received by olfactory sensory neurons and transmitted to the antennal lobe (AL), primarily through the antennal nerve (AN). In the antennal lobe, the olfactory sensory neurons synapse upon the dendrites of projection neurons (PNs), which in turn project in tracts to the mushroom body calyx (Ca). The path of a single PN is shown (pink cell). The PNs innervate the calyx with axon collaterals before terminating in the lateral horn (LH). These collaterals contact the dendrites of the intrinsic neurons of the calyx called Kenyon cells, whose cell bodies (KCB) surround the calyx as a cortex. The Kenyon cell axons converge in the pedunculus (P) and arborize to form the MB lobes. The axons of α/β and α'/β' Kenyon cells bifurcate to form the vertical (α and α') lobes and the horizontal (β and β' lobes). An example of a bifurcating α'/β' KC is shown; arrows indicate direction of projection. The γ Kenyon cell axons form the γ lobe. B) Diagram of the synaptic connections in one microglomerulus in the calyx (adapted from Yasuyama et al., 2002). In the calyx, PN boutons provide synaptic input onto other calycal neurons, both Kenyon cells (KCs) and extrinsic neurons (ENs).
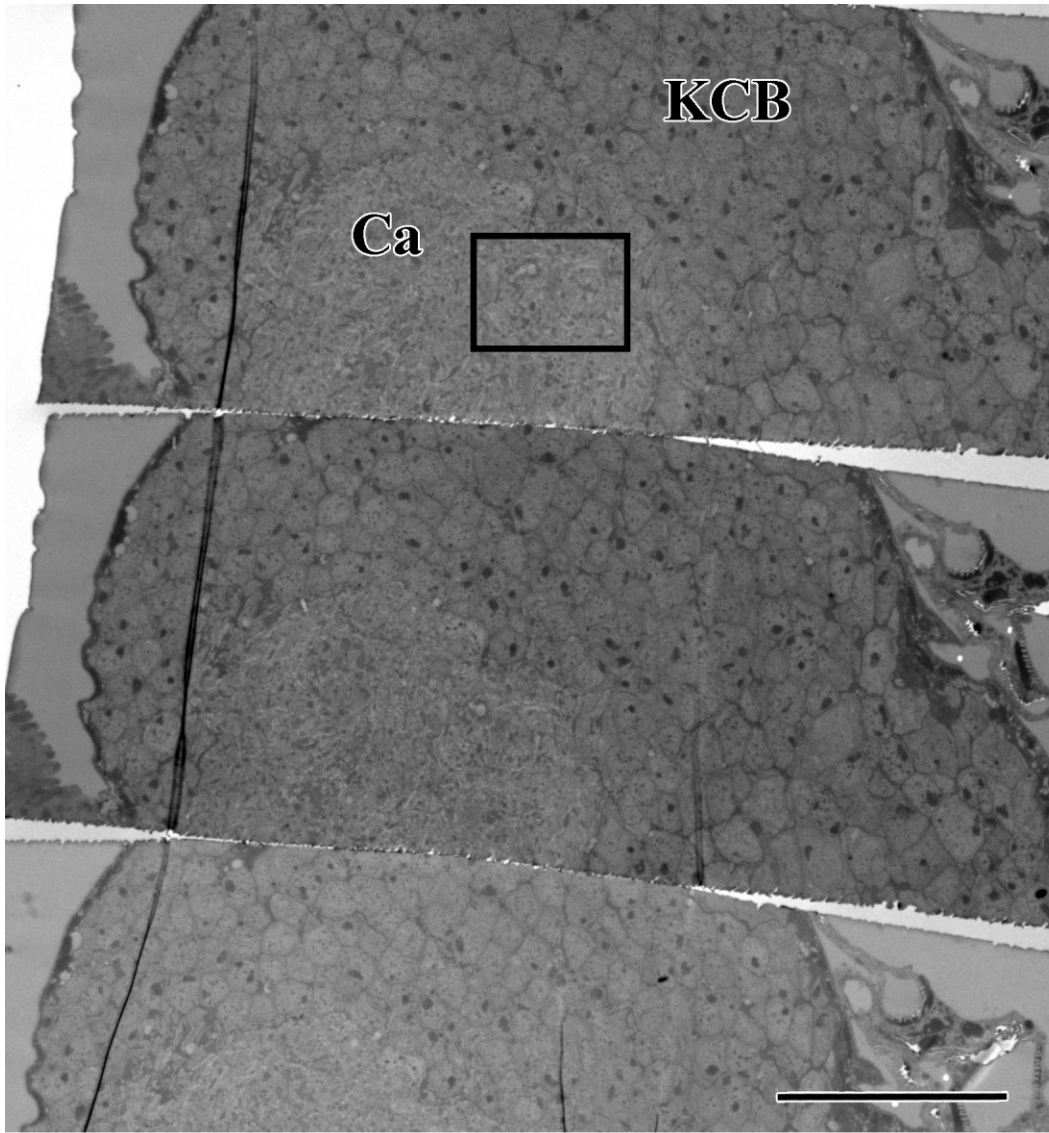
Figure 2   Sparse three-dimensional reconstructions were generated from a dorso-medial region (square) of the calyx (Ca) in the right hemisphere. Three consecutive sections from the series reveal the general characteristics of the cortex of Kenyon cell bodies (KCB), surrounding a central neuropile region. A fold runs down the length of the ribbon of sections on the right-hand side; scale bar, 20µm.
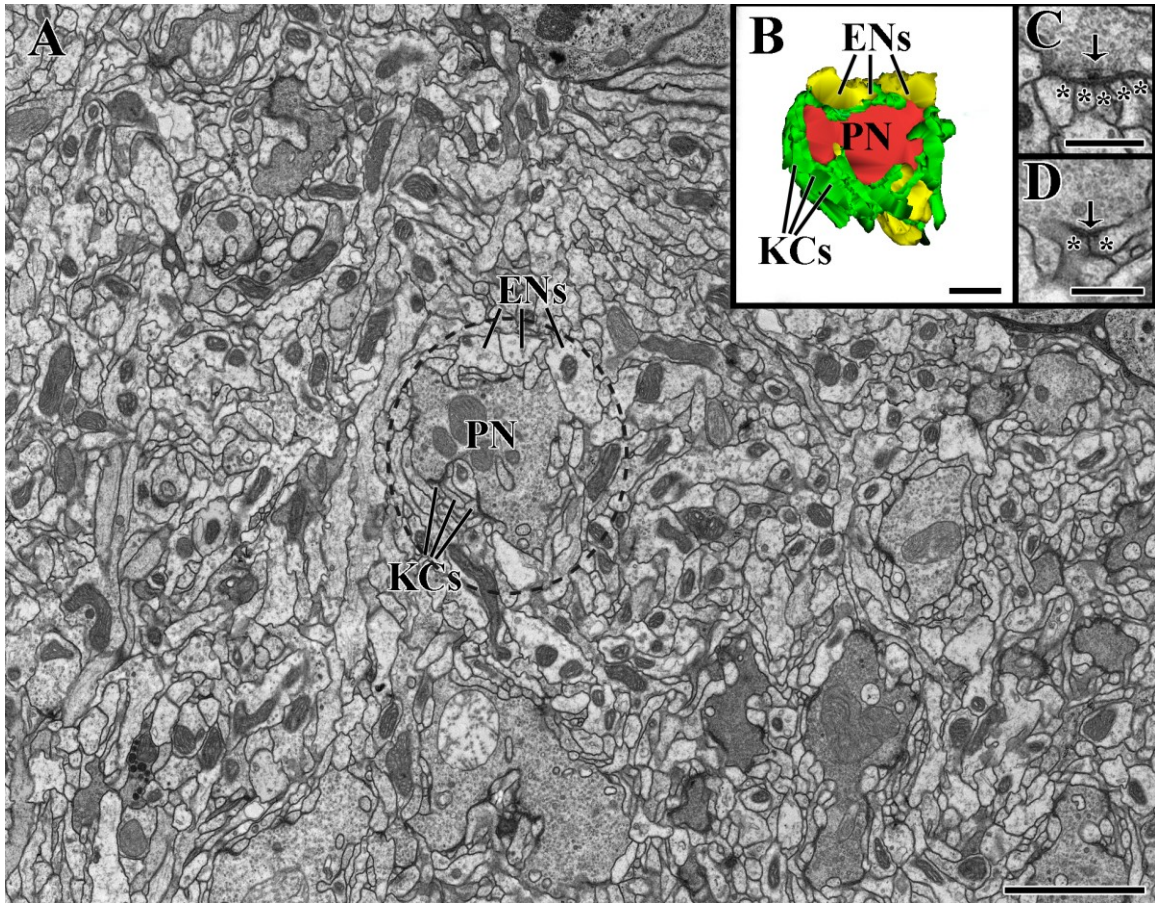
Figure 3   A) Microglomeruli that comprise a large vesicle-laden projection neuron (PN) bouton surrounded by tiny Kenyon cell dendrites (KCs) are densely packed in the region of the calyx photographed for three-dimensional reconstruction. Extrinsic neuron profiles (ENs) also contribute to microglomeruli. B) Plan view of a three-dimensional rendering of a single microglomerulus (dashed outline in A shows the approximate area of reconstruction on one section). Note the microglomerular boundaries are indistinct at the EM level and are only approximated here. Cells are colour-coded and do not appear individually in the reconstruction. C,D) Presynaptic sites in PNs are either ribbon (C) or non-ribbon (D) synapses. Non-ribbon synapses lack the T-bar presynaptic density characteristic of ribbon synapses. Asterisks, postsynaptic partners; arrows, presynaptic sites showing the presumed direction of transmission; scale bar in A, 2µm; B, 1µm; C,D, 0.5µm.
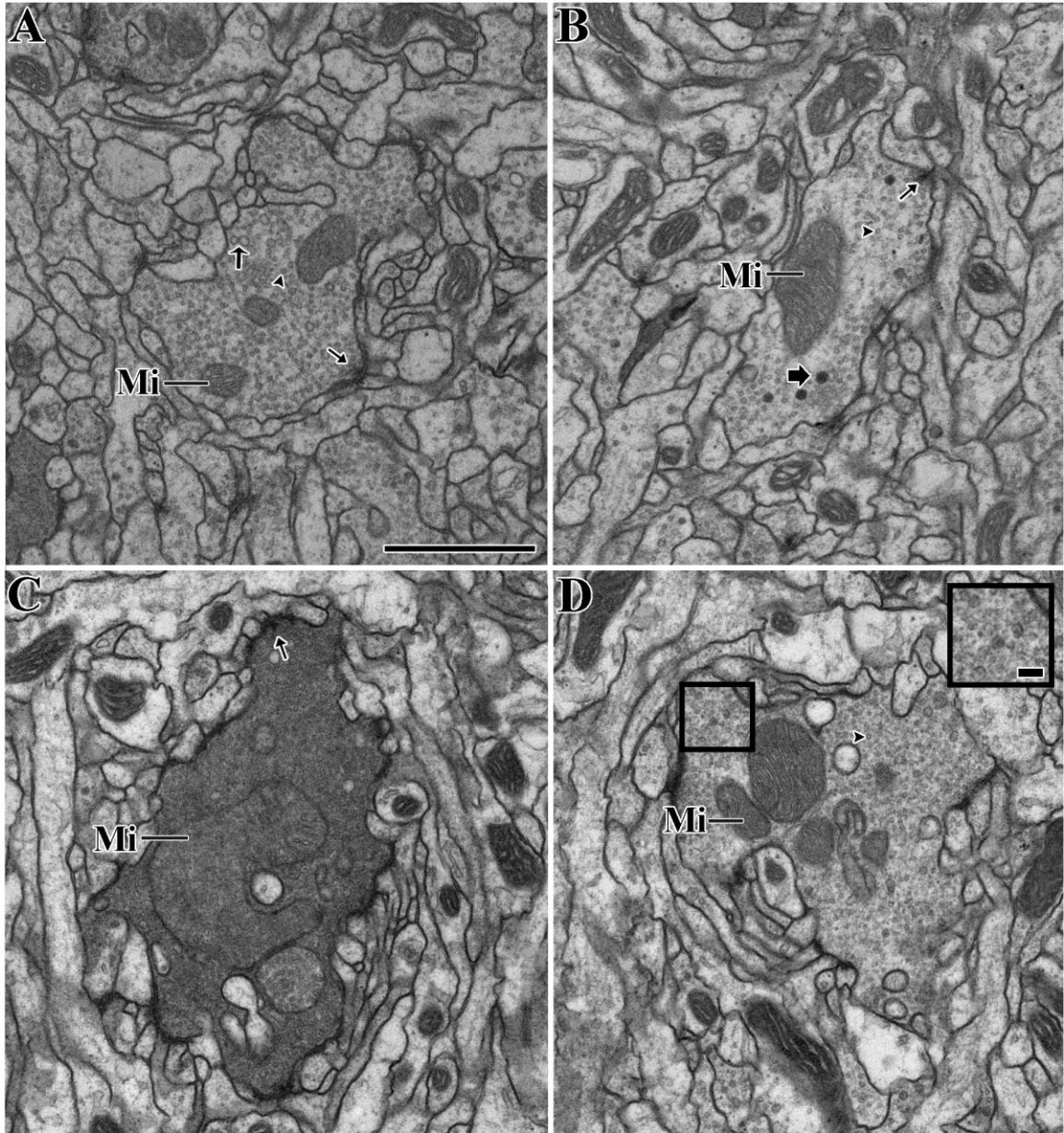
Figure 4   The calyx contains three subtypes of projection neuron boutons (PNs). A)
Clear-core vesicle-projection neuron boutons (CCV-PNs) contain vesicles that
are exclusively clear-core. B) Dense-core vesicle-projection neuron boutons
(DCV-PNs) also contain dense-core vesicles (B,D) that are larger than the
clear-core vesicles and filled with electron dense material. C) Dark bouton-
projection neurons (DB-PNs) also have both types of vesicle profiles and are
further characterized by their dark cytoplasm. Arrowheads, small clear-core
vesicles; slender arrows, synapses with a presynaptic ribbon visible in the
section plane; Mi, mitochondria; bold arrow in A, large clear-core vesicles;
bold arrow in B, dense-core vesicles; square inset in D, dense-core vesicles;
scale bar in A, 1µm; scale bar of square in D, 100nm. Scale in A applies to B-
D.
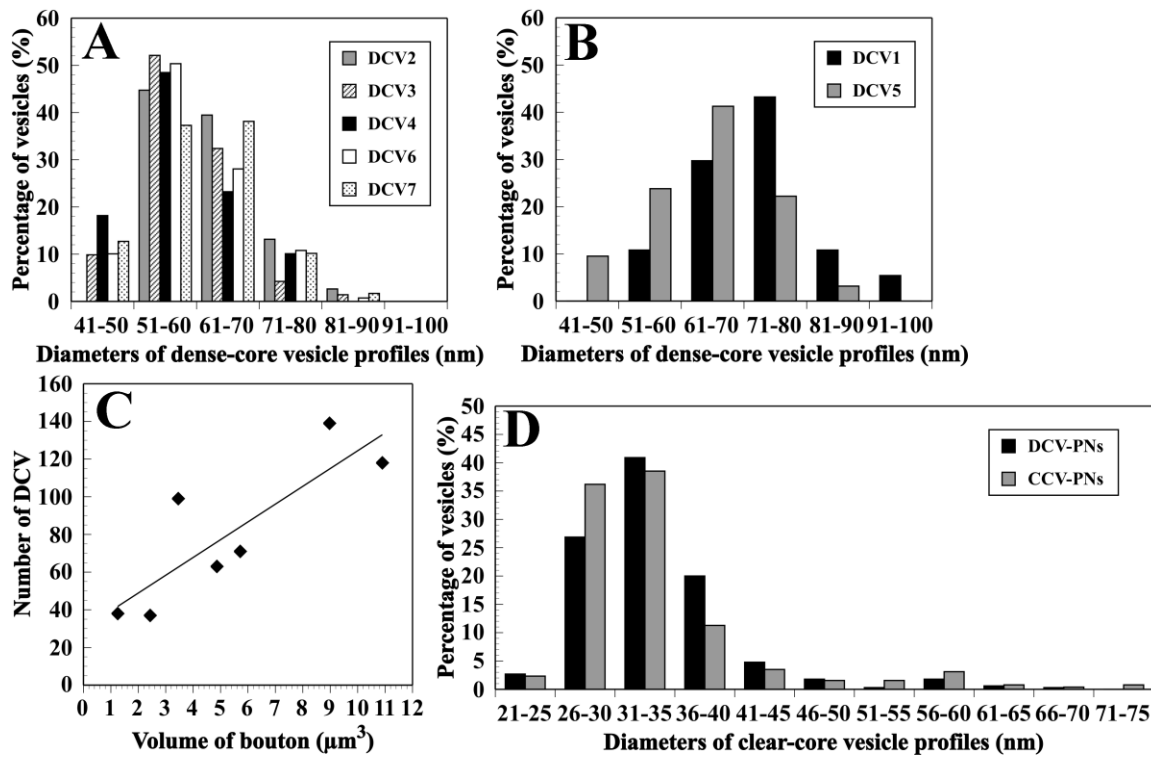
Figure 5   Distribution of sizes of clear-core and dense-core vesicles in projection neuron
             boutons. A) The distribution of dense-core vesicle diameters is similar for
             five DCV-PNs (DCV2, n=38; DCV3=71; DCV4, n=99; DCV6, n=139;
             DCV7, n=118) although two DCV-PNs (DCV1=37; DCV5=63) show
             distributions shifted towards larger diameters (B). C) The number of dense-
             core vesicles (DCV) in PN boutons positively correlates with bouton volume
             (r=0.84). D) The diameters of clear-core vesicles in both DCV-PNs (n=257)
             and CCV-PNs (n=335) vary in size.

CCV-PNs　　DCV-PNs　　DB-PNs

A　　B　　C

D　　E　　F

G　　H　　I

J　　K
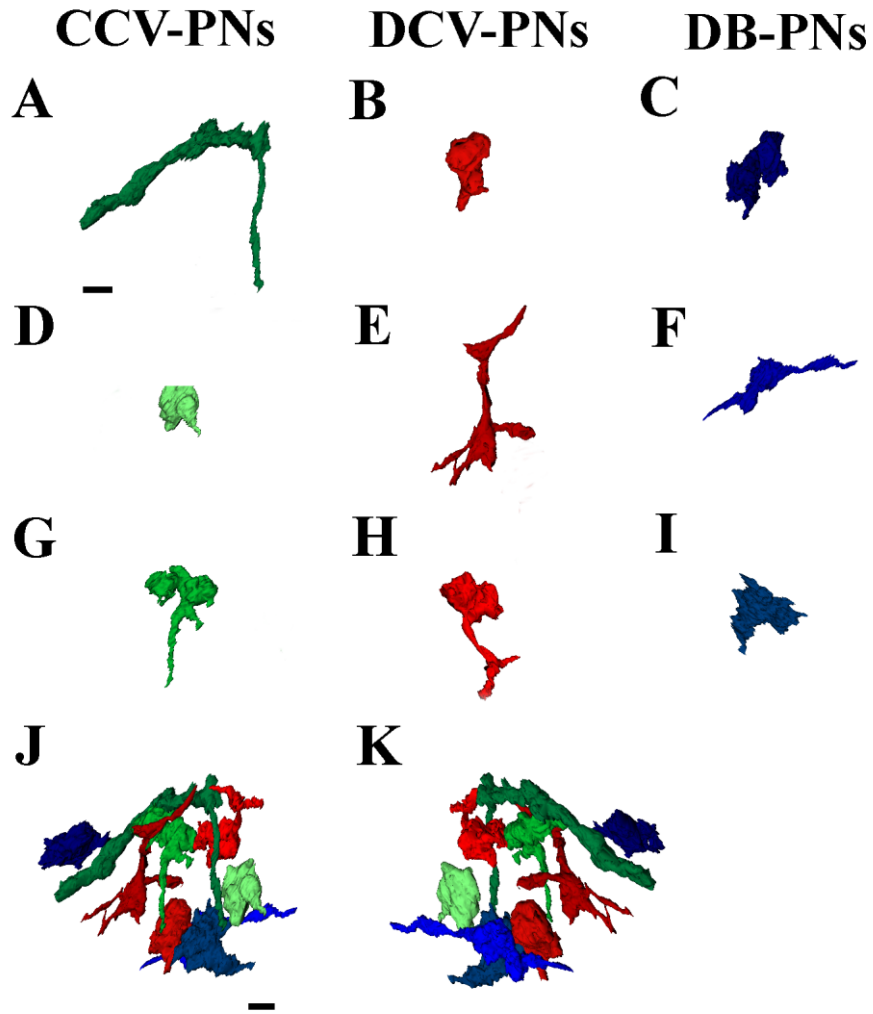
Figure 6　Projection neurons (PNs) are polymorphic. PNs of all three groups (CCV-PNs, clear-core vesicle-projection neurons; DCV-PNs, dense-core vesicle-projection neurons; DB-PNs, dark bouton-projection neurons) can be elongated (A,E,F), uni-lobed (B,D,H,I), or bi-lobed (C,G). J,K) Compilation of all reconstructed PN boutons, colour coded as in A-I, to show their relative positions. PNs are densely packed and subtypes intermingle within the calyx (J, rotated 180 degrees in K). All scale bars, 2μm; scale in A applies to B-I; scale in J applies to K.
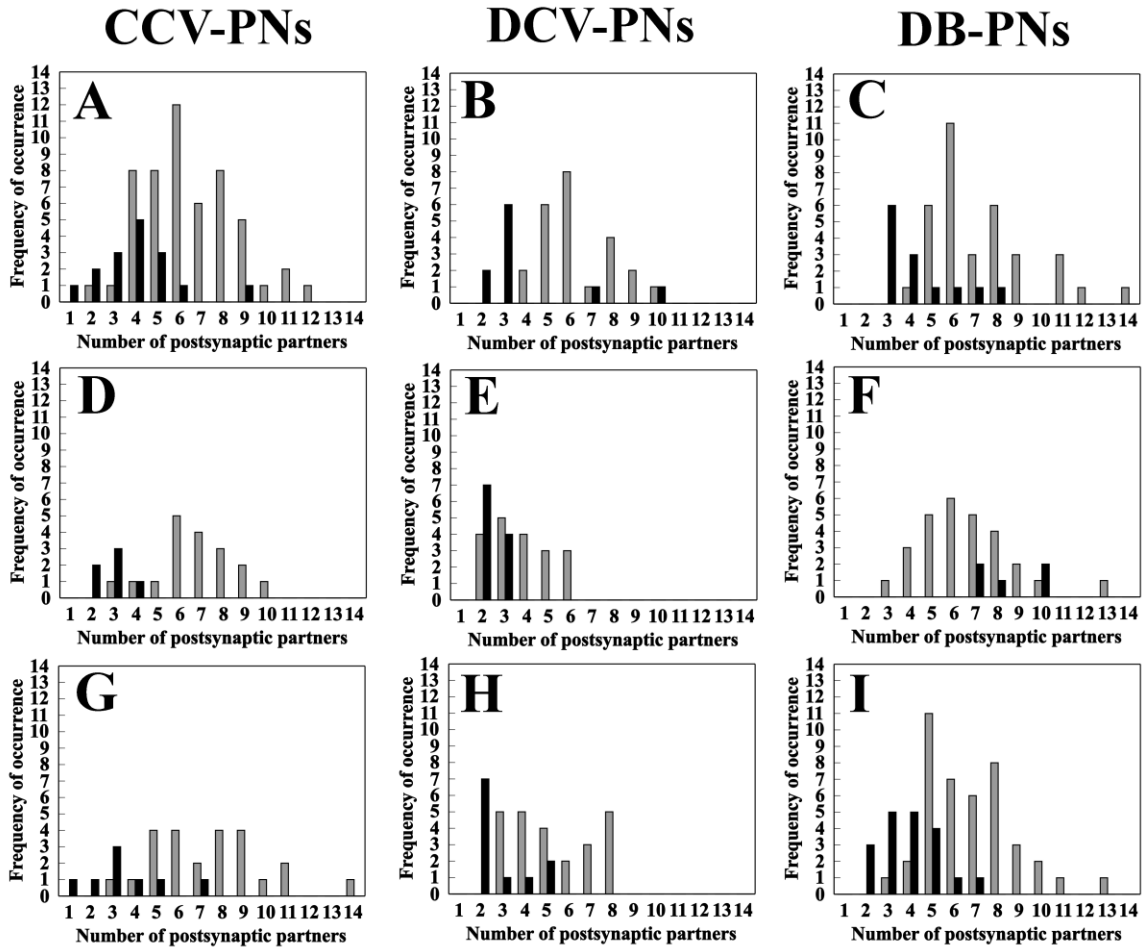
Figure 7   Distribution of postsynaptic partners for ribbon (grey) and non-ribbon (black) synapses in three clear-core vesicle-projection neurons (CCV-PNs; A,D,G), three dense-core vesicle-projections neurons (DCV-PNs; B,E,H) and three dark bouton-projection neurons (DB-PNs; C,F,I). Graphs correspond to the images reconstructed in Figure 6A-I. Non-ribbon synapses tend to have fewer postsynaptic partners at each synapse than ribbon synapses, except in F.
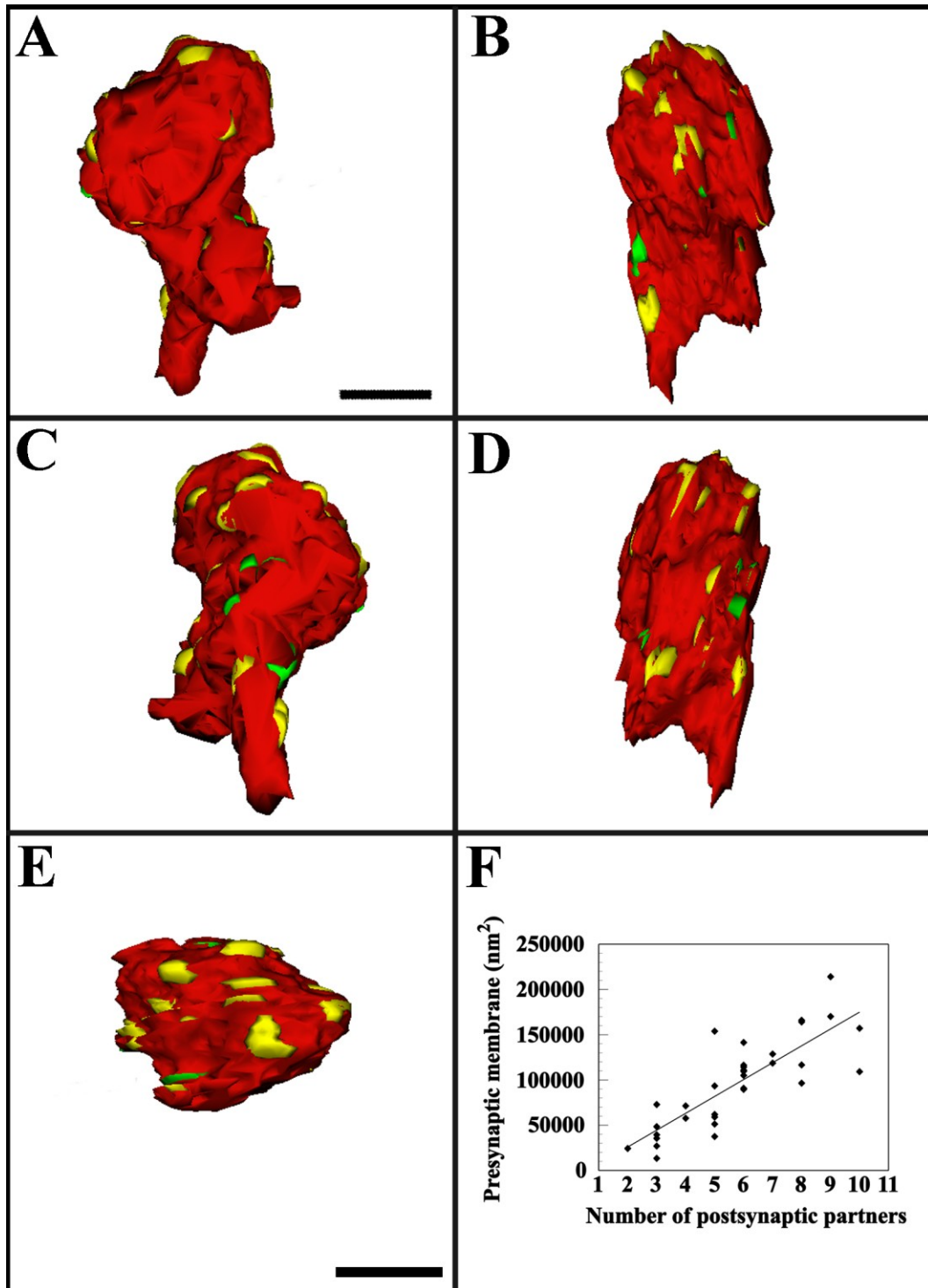
Figure 8   Three-dimensional reconstruction of a dense-core vesicle-projection neuron (DCV-PN, Figure 6B) and its individual synapses (ribbon, yellow; non-ribbon, green) shown in four views in successive 90° rotations (A-D) as well as an overhead view (E). F. The number of postsynaptic partners correlates positively with the surface area of presynaptic membrane (r=0.83). Scale bars, 1μm; scale in A applies to B-D.
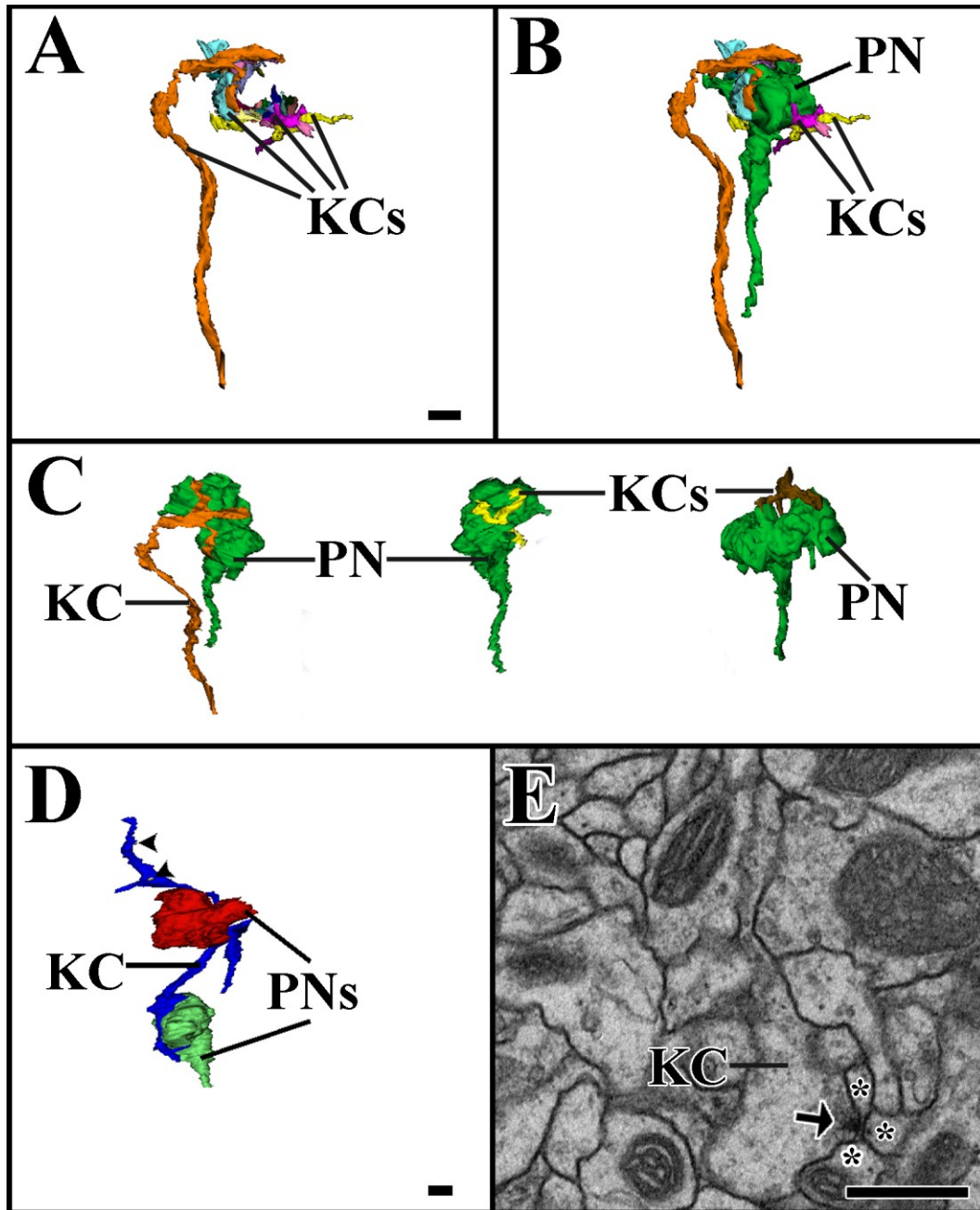
Figure 9   Kenyon cells (KCs) make both pre- and postsynaptic contributions to neural circuits of the calyx. A,B) A conglomeration of sparsely reconstructed KCs envelops a bouton of a projection neuron (PN). Each colour represents an individual KC body, some of which may originate from the same KC, beyond the possible extent of the reconstruction. C) Multiple claw-shaped KC dendrites are postsynaptic to a single PN. D) A single KC (blue) that is postsynaptic to a CCV-PN (green) and encircles a DCV-PN (red), is also presynaptic (arrowheads) at two ribbon synapses; one of these is shown in E. Asterisks, postsynaptic partners (E); arrow, presynaptic site (E); all scale bars, 1μm; scale in A applies to B and C.
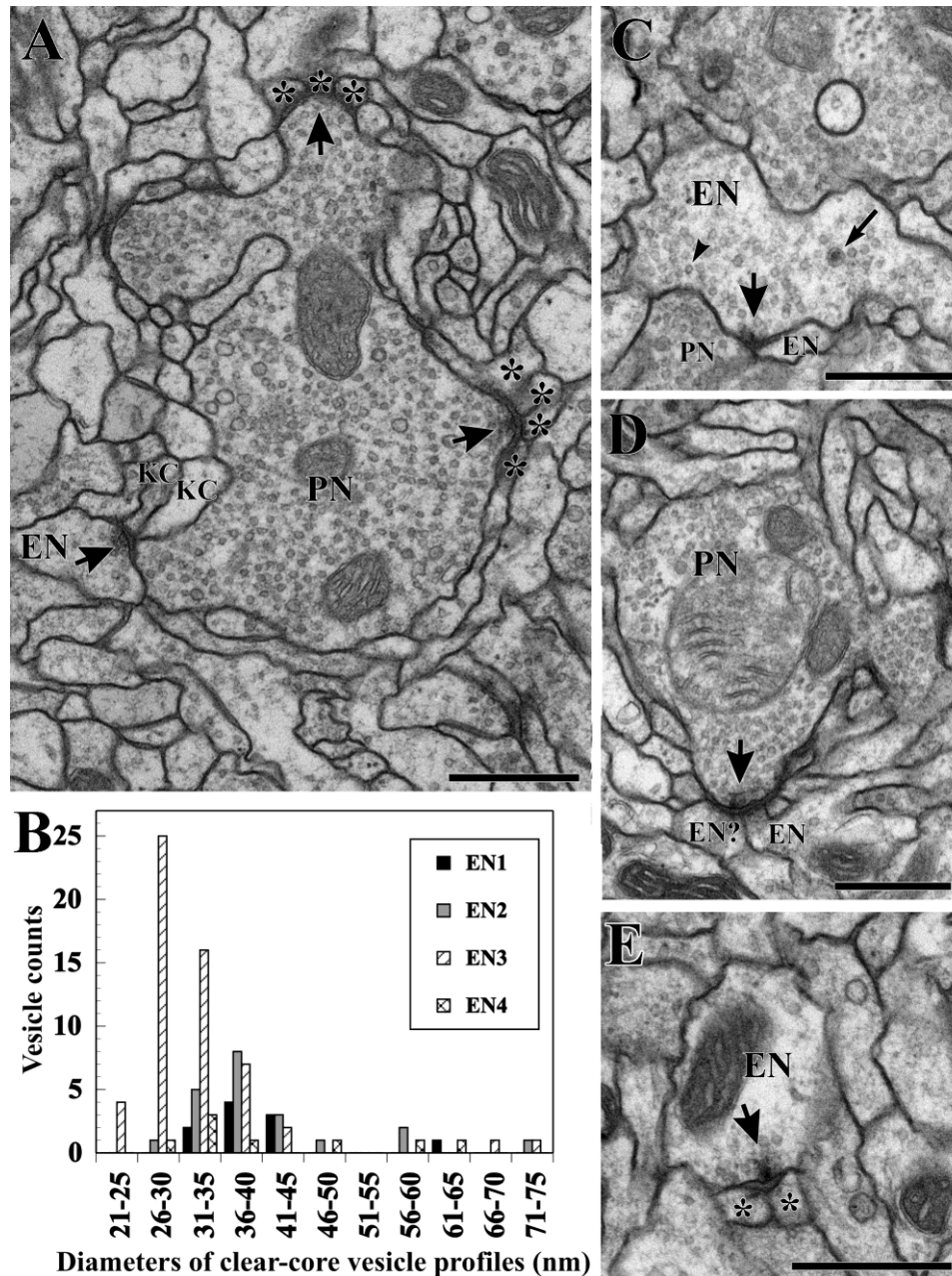
Figure 10 Calycal circuits of extrinsic neurons (ENs). A) An EN profile forms a ribbon synapse (arrow) upon Kenyon cell (KC) dendrites, together with a projection neuron bouton (PN). The PN is in turn presynaptic (arrows) to small KC profiles (asterisks). B) Distribution of all clear-core vesicle diameters in four ENs (EN1-EN4). C) An EN profile is presynaptic to a PN as well as another EN at a ribbon synapse (arrow), constituting a serial synapse between the two ENs. The presynaptic EN profile contains clear-core vesicles (arrowhead) and a dense-core vesicle (small arrow). D) The profile of a PN contacts an EN and a putative EN at a ribbon synapse (arrow). E) An EN profile forms a ribbon synapse (arrow) upon two other ENs (asterisks), creating a divergent serial arrangement between ENs. All scale bars, 0.5µm.

44
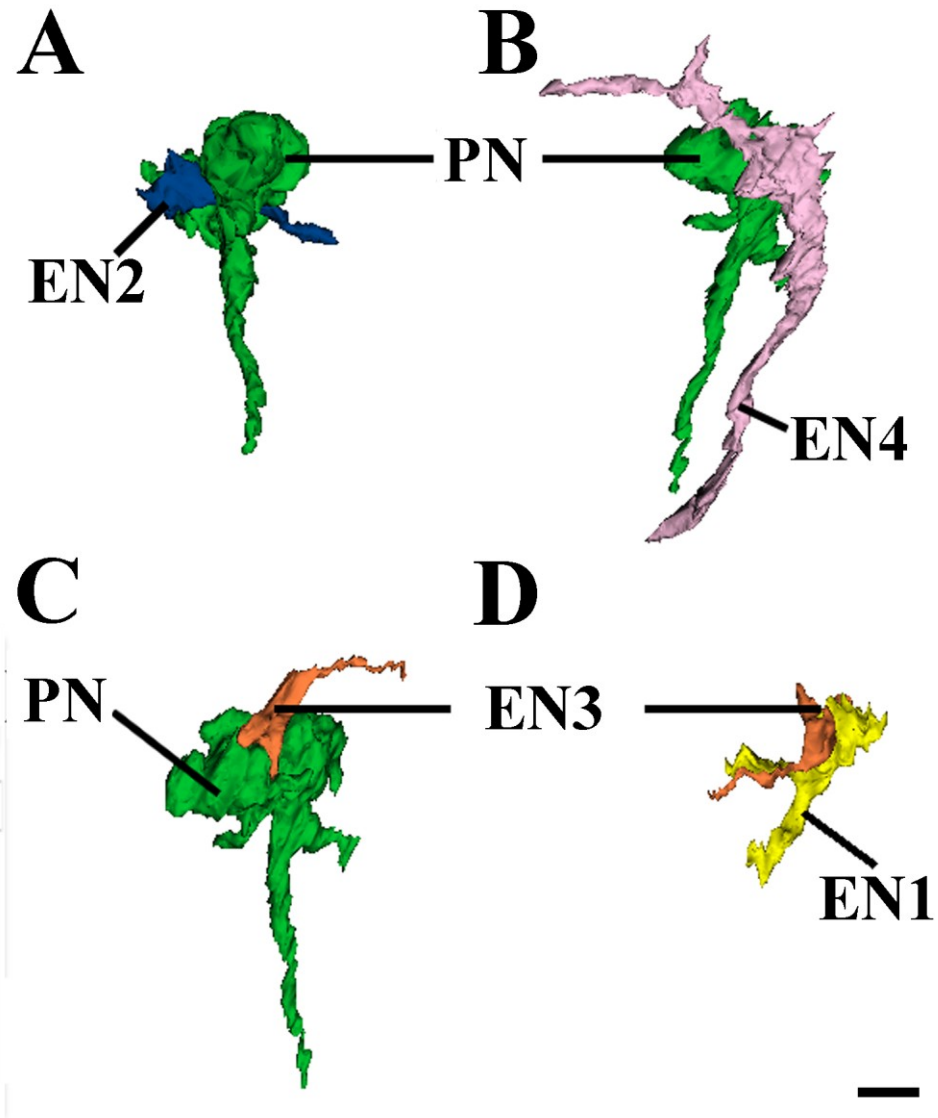
Figure 11   Three-dimensional reconstructions of extrinsic neurons (EN1,2,3 and 4).
Multiple ENs are presynaptic to a single projection neuron (A-C). D) EN3 is
in turn presynaptic to EN1. Scale bar, 1μm.
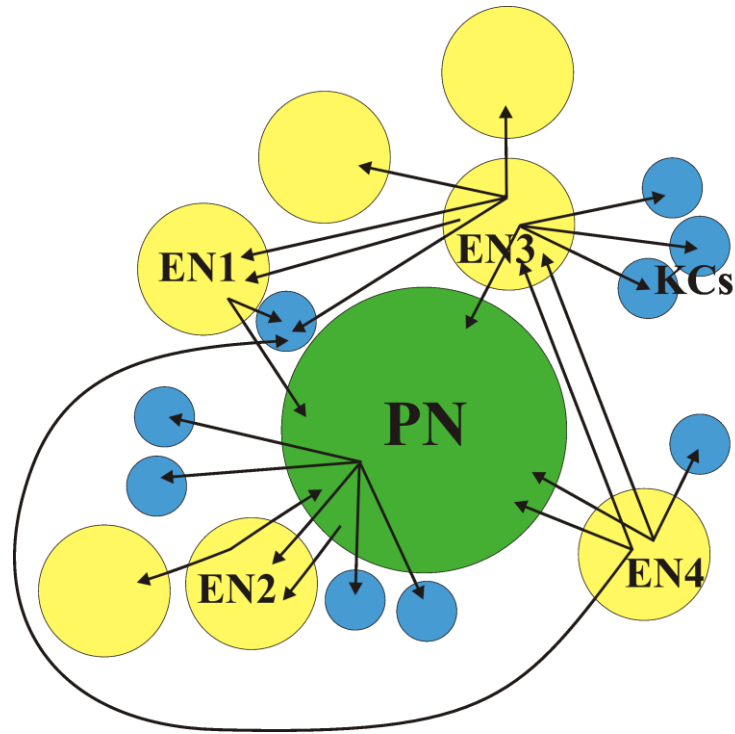
Figure 12 Schematic diagram of the pre- and postsynaptic partnerships of the four extrinsic neuron (EN) terminals (yellow) presynaptic to a single (green) projection neuron bouton (PN bouton reconstructed in Figure 6G) and corresponding clusters of Kenyon cell (KC) dendrites (blue). Only KCs that are postsynaptic to these four ENs, or share a site of presynaptic input with an EN are included, although many other KC dendrites exist locally that receive PN input alone. Note KCs and possibly ENs may belong to the same cell that branches beyond the reconstructed volume for which the connections are shown here. Unlabeled ENs are only tentatively identified. Arrows having a common origin represent divergence at a single presynaptic site.
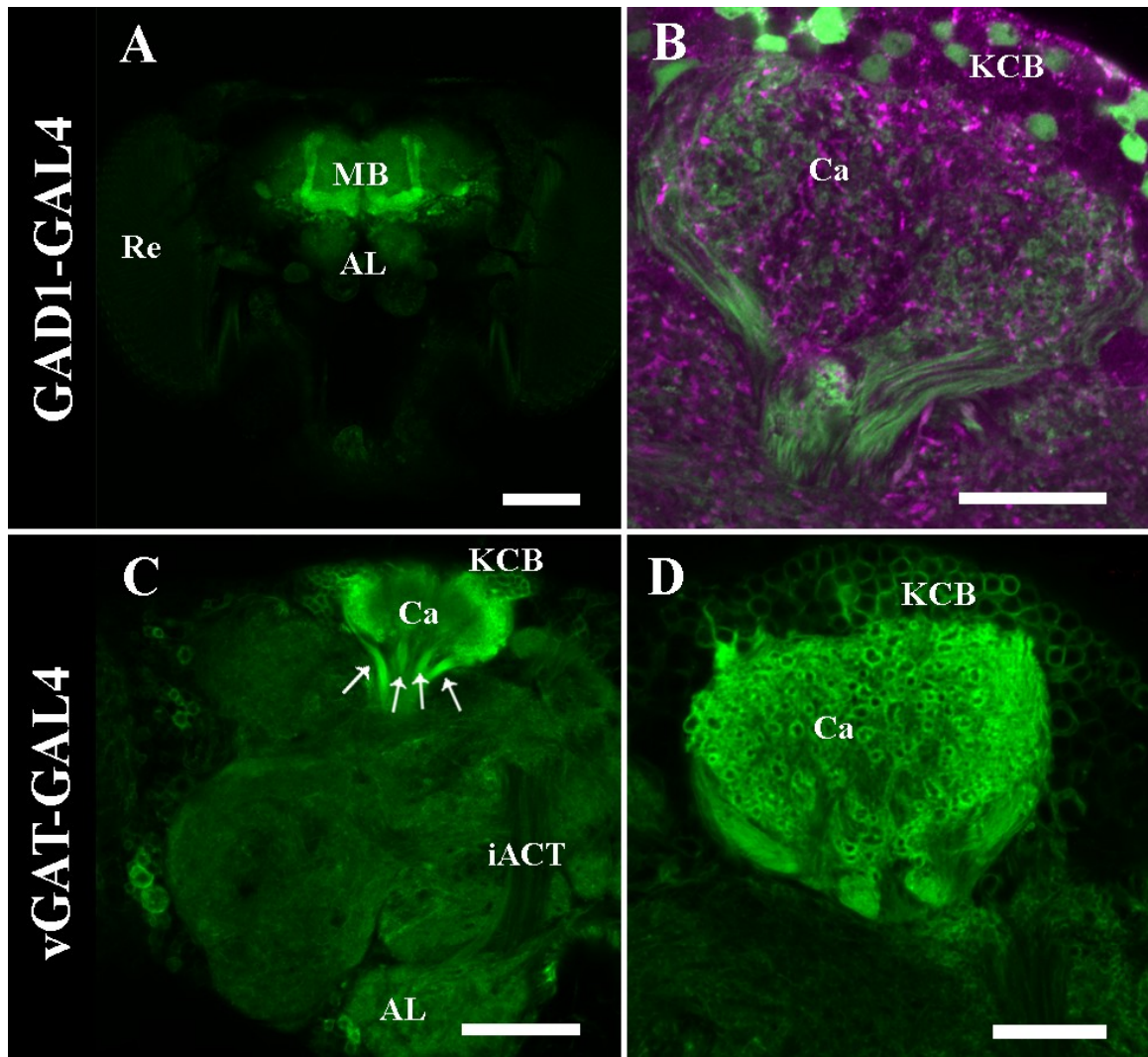
Figure 13 The GAD1-GAL4 and vGAT-GAL4 drivers promote ectopic expression of GFP (green) in the Kenyon cells of the mushroom bodies (MB). A) The lobes of the MBs are well-labeled, as are the Kenyon cell bodies (KCBs; B-D). The halo-like organization of KC dendrites characteristic of microglomeruli (B,D) was visible and did not colocalize to antibody labeling of GAD1 (magenta in B). The four tracts of KC axons exiting the calyx (Ca) are also clearly identifiable (C, arrows). Re, retina; AL, antennal lobes; iACT, inner antennocerebral tract; scale bar in A, 100µm; B,D, 20µm; C, 50µm.
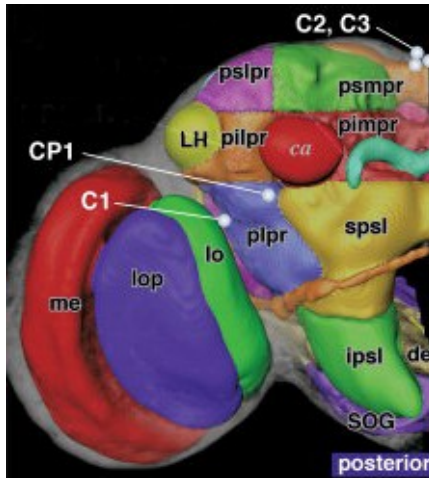
Figure 14 Schematic representation of the posterior view of a brain showing the positions of the cell bodies of MB-C1, MB-C2/C3, MB-CP1 (adapted from Tanaka et al., 2008). ca, calyx; de, deutocerebrum other than the AL; LH, lateral horn; lo, lobula; lop, lobula plate; me, medulla; SOG, suboesophageal ganglion; m-, middle; p-, posterior; -s-, superior; -i-, inferior; -lpr, lateral protocerebrum; -mpr, medial protocerebrum.
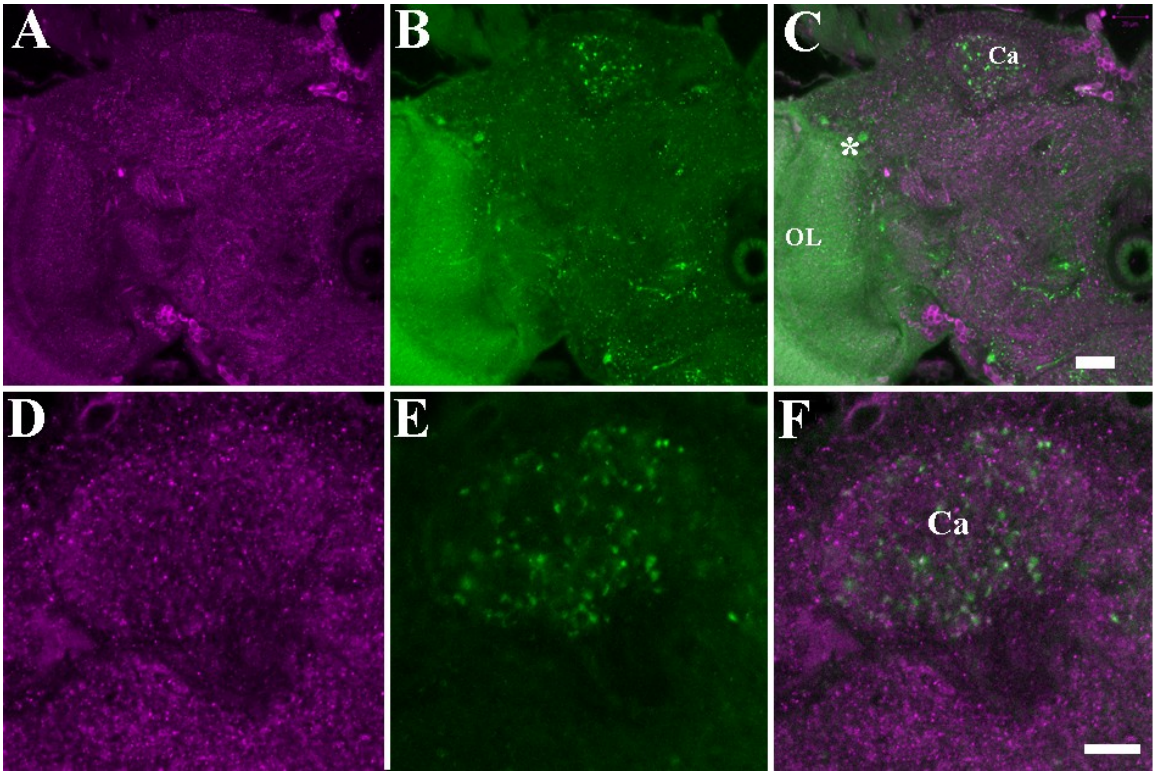
Figure 15 The MB-C1 neuron innervating the mushroom body calyx (Ca) is not GAD1-immunopositive. A) GAD1 antibody (magenta) immunolabels cell bodies and neurites in the brain. B) The NP2331-GAL4 driver promotes expression of cytosolic GFP (green) in visual projection neurons of the optic lobes (OL; Otsuna and Ito, 2006) as well as MB-C1, which arborizes in the calyx (Tanaka et al. 2008). C) A merged image of A and B fails to show overlap. D-F) Higher magnification images of the calyx shown in A-C. Asterisk in C, MB-C1 cell body; scale bar for A-C, 20µm; D-F, 10µm.
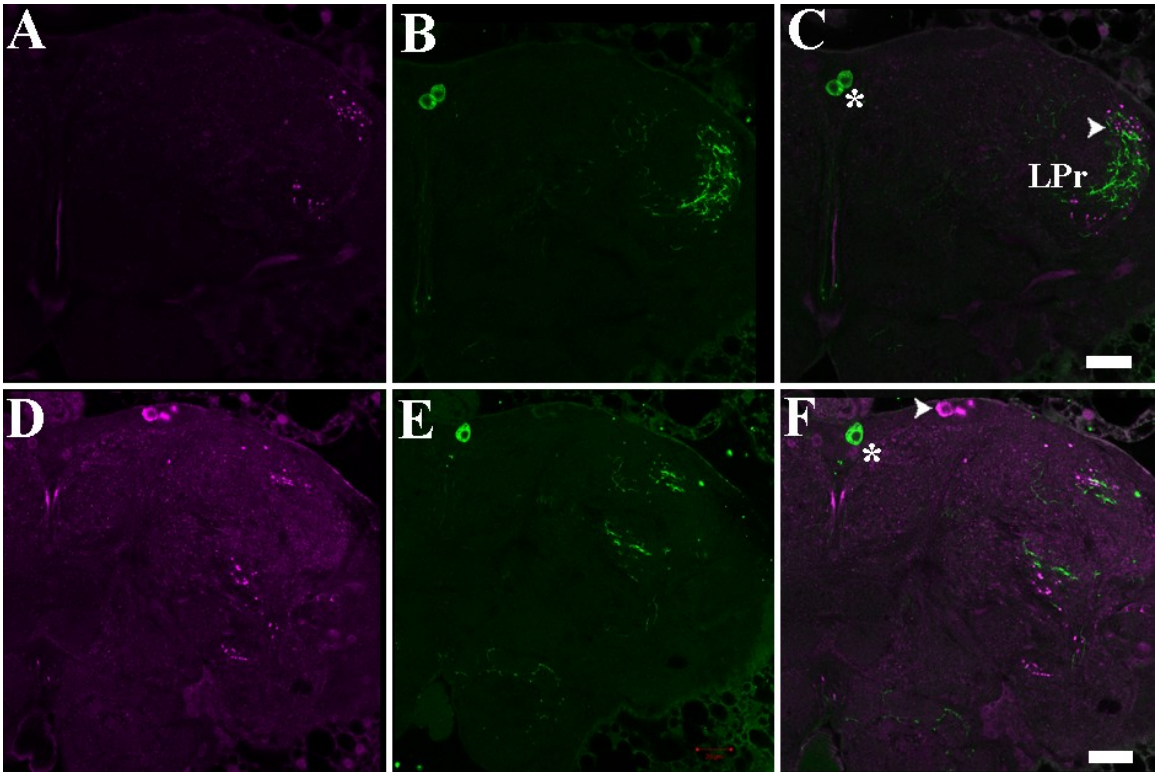
Figure 16 The cell bodies of the MB-C2/C3 neurons innervating the mushroom body calyx (calyx not shown) are not GAD1-immunopositive. GAD1 antibody (magenta) immunolabels neurites (A) and cell bodies (D). The NP6029-GAL4 driver promotes expression of membrane bound GFP exclusively in the MB-C2/C3 neurons (B,E). A merged image of A and B shows in C that punctate GAD1 profiles are interspersed with MB-C2/C3 neurons in the lateral protocerebrum (arrowhead; LPr). A merged image of D and E is shown in F. Asterisks, MB-C2/C3 cell bodies; arrowhead in F, GAD1-immunopositive cell body; scale bars, 20μm.
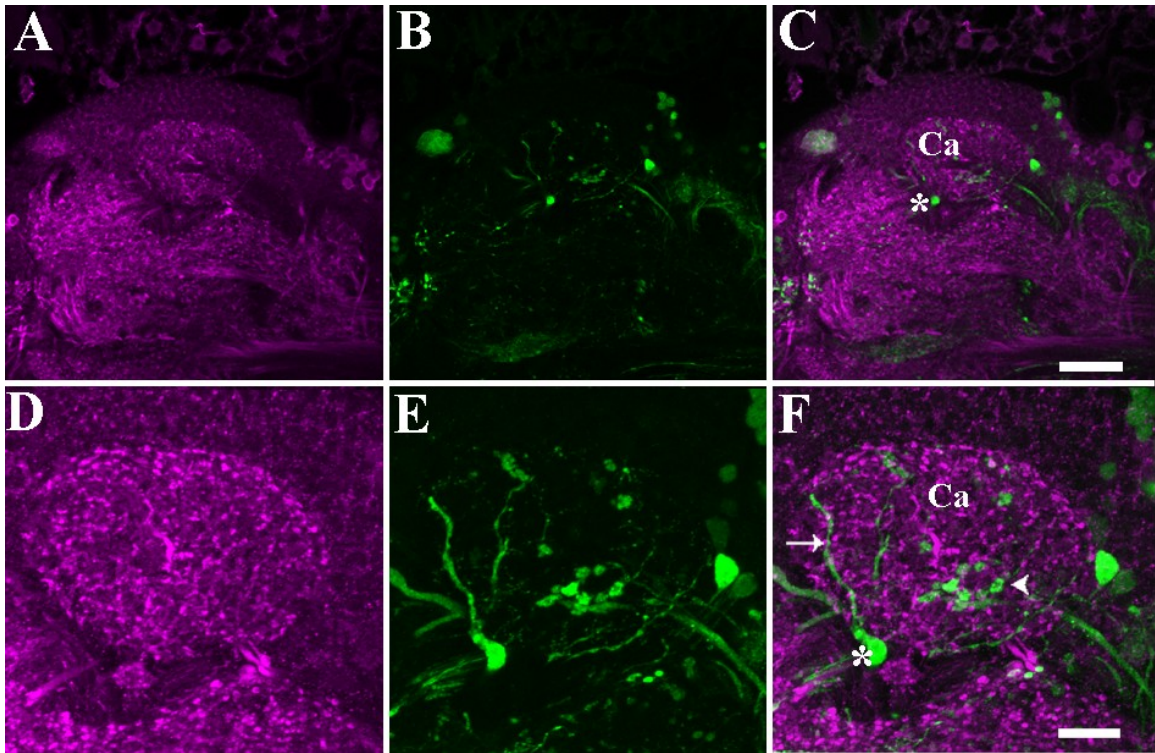
Figure 17 The MB-CP1 neuron innervating the mushroom body calyx (Ca) is not
GAD1-immunopositive. GAD1 antibody (magenta) immunolabels neurites
and cell bodies (A,D). The NP2297-GAL4 driver promotes expression of
cytosolic GFP (green) in the cell body and neurites of the MB-CP1 neuron
(identified by cell body position), as well as other cell bodies and neurites
(B,E), including a putative population of projection neurons (arrowhead, F).
A merged image of A and B is presented in C. Higher magnification images
of the calyx are shown in D-F (7 sections, 1µm intervals). Long, slender
neurites project from the MB-CP1 cell body into the calyx (arrow, F).
Asterisk, MB-CP1 cell body; scale bar for A-C, 25µm; D-F, 10µm.
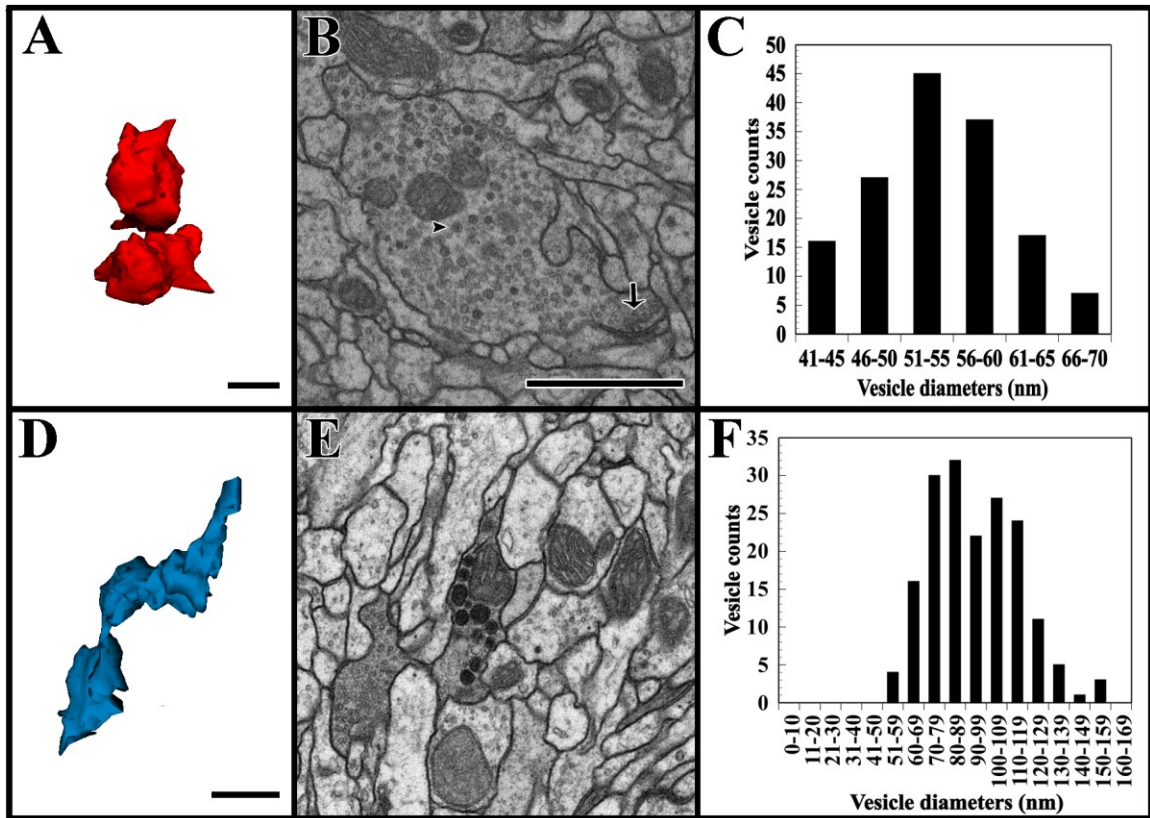
Figure 18 Neurons of unidentified origin in the calyx. A) A cell that is at least bi-lobed predominately contains small dense-core vesicles (B, arrowhead), up to 70nm in diameter (C). D) A cell with an elongated, lobed morphology is filled with dense granules (E) up to 160nm in diameter (F). Arrow, presynaptic site; all scale bars, 1µm; scale in B applies to E.
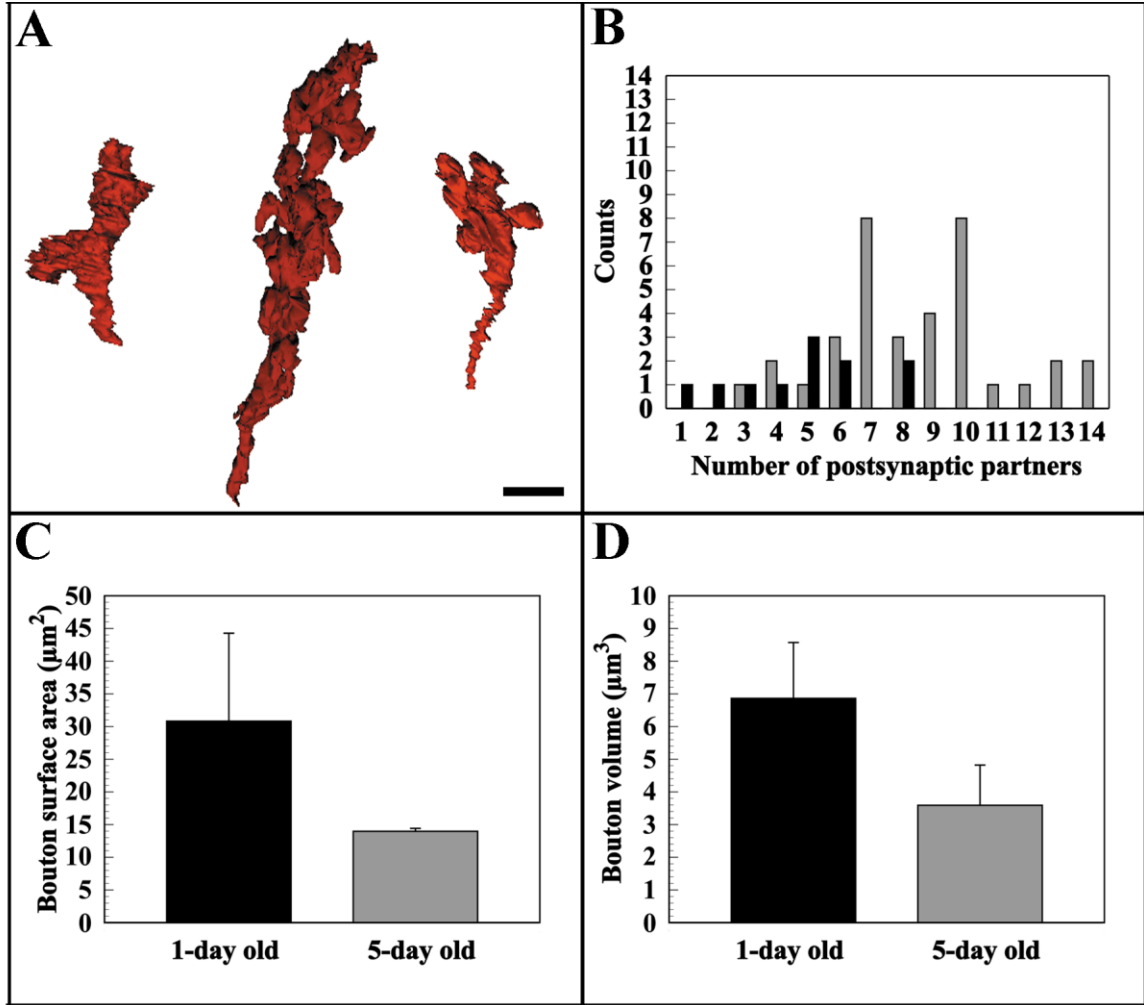
Figure 19 Characteristics of sampled PN boutons in the calyx of a 1-day old fly. A) All PN boutons sampled are DCV-PNs and these are polymorphic. B) Distribution of postsynaptic partners for ribbon (grey) and non-ribbon (black) synapses in one DCV-PN (leftmost in A). The surface area (C) and volume (D) of three DCV-PNs in a 1-day old and a 5-day old fly are compared. Scale bar, 2µm.
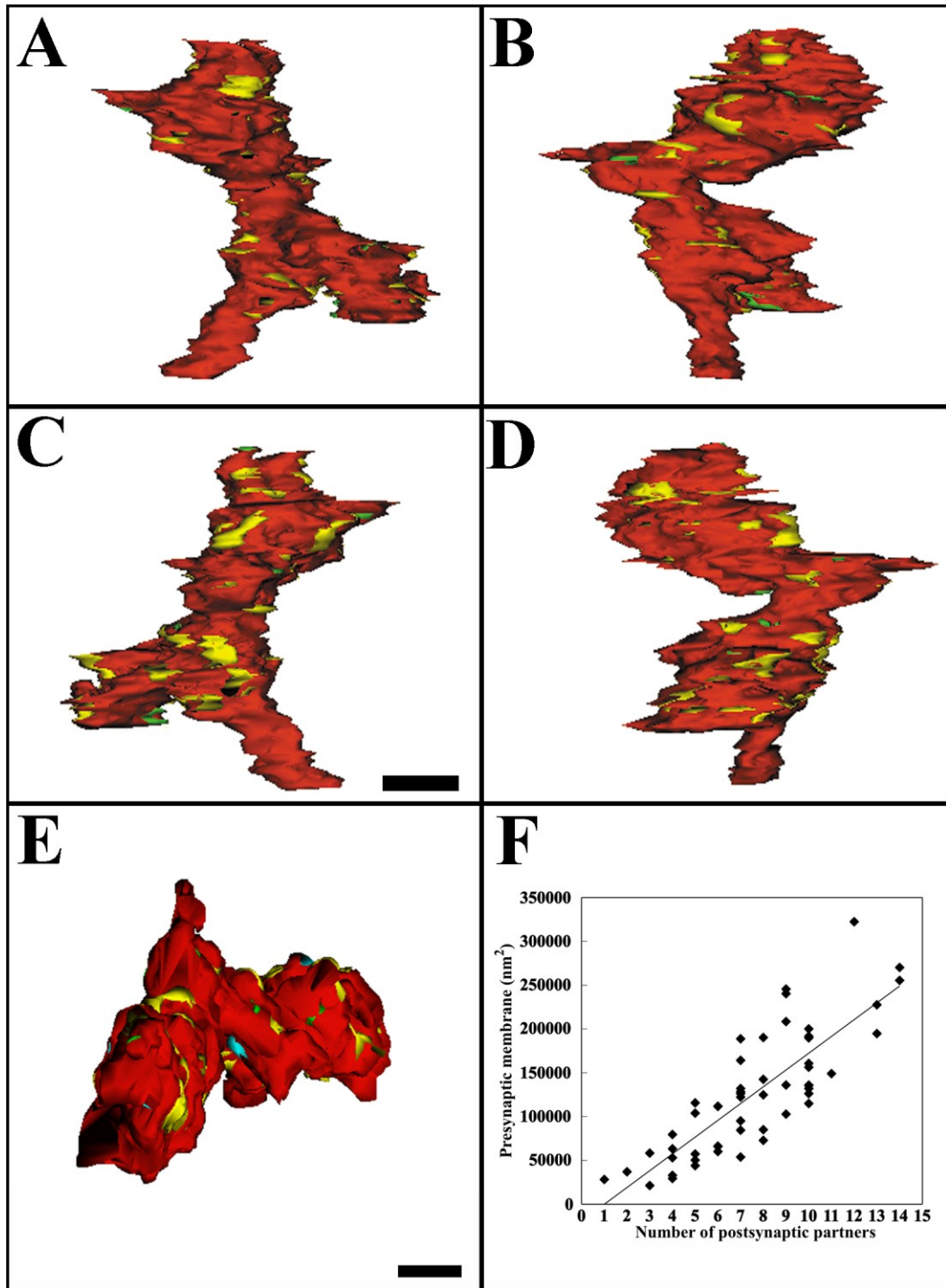
Figure 20 Three-dimensional reconstruction of a dense-core vesicle-projection neuron in the calyx of a 1-day old fly (DCV-PN, Figure 19A) and its individual synapses (ribbon, yellow; non-ribbon, green; unclassifiable, blue) shown in four views through successive 90° rotations (A-D) as well as an overhead view (E). F) The number of postsynaptic partners correlates positively with the surface area per presynaptic site (r=0.82). Scale bars, 1μm; scale in A applies to B-D.

CHAPTER 4   DISCUSSION

4.1   SYNAPTIC CHARACTERISTICS AND FUNCTIONAL IMPLICATIONS OF THREE PN SUBTYPES

Three ultrastructurally distinct populations of PN boutons were identified based on vesicle type and cytoplasm electron density. The first point on which assurance should be sought is whether the three types of PN boutons identified here from ultrastructural criteria truly differ from each other functionally. Thus, CCV-PNs might have been those in which dense-core vesicles were missed, and DB-PNs might have been those in which the PN was electron-dense because it was undergoing degenerative changes resulting from damage during dissection. Such changes, for example in photoreceptor neurons, are rapid (Brändstatter et al., 1991). Neither of these possibilities is likely, however. CCV-PN boutons were reconstructed in their entirety, permitting identification of every vesicle in the bouton as clear-core or dense-core, and DB-PNs did not exhibit any other morphological or ultrastructural features associated with degenerating cells (Brändstatter et al., 1991).

The shape of the PN boutons provides no clear basis to distinguish between the three types. The three-dimensional reconstructions revealed that the PN boutons of each group are polymorphic, classifiable as elongated, uni-lobed, or bi-lobed bodies. Each PN bouton is at the centre of a single microglomerulus, confirming that each microglomerulus contains only a single PN (Leiss et al., 2009). Although PN boutons are tightly packed, they never form synapses with each other, although bouton-bouton synapses exist in the ant (Seid et al., 2005), one of several differences between species revealed by this study. Characteristics such as synapse type, density, and number of postsynaptic partners were also investigated extensively, to help determine whether there are functional differences between the PNs that are revealed from their respective connectivities. For example, synapse number has been implicated in enhanced olfactory perception (Acebes and Ferrús, 2001) and synapse size has been related to synaptic efficacy (Tanaka et al., 2005). Furthermore, at least at lobster neuromuscular synapses the active zone density appears to correspond to the rate of neurotransmitter release,

being three times higher at high-output neuromuscular varicosities than at low-output terminals of the same excitatory axon (Govind and Chiang, 1979).

All subtypes of PN boutons contained two types of presynaptic specializations, either an electron-dense region of the presynaptic plasma membrane (non-ribbon synapse), or the same density at the presynaptic membrane but accompanied by a T-bar ribbon (ribbon synapse). These ribbons, which are identified sites of vesicle release in photoreceptor terminals of the housefly (Saint Marie and Carlson, 1982), feature a distinct protein architecture comprising a pedestal surmounted by a thin platform. Presynaptic ribbons in *Drosophila* photoreceptor synaptic terminals have been compared to the synaptic ribbons of vertebrate photoreceptors, with which they share many structural features (Meinertzhagen, 1993; Zhai and Bellen, 2004; Sanes and Zipursky, 2010). In vertebrate photoreceptors the ribbon is thought to act as a conveyor belt to funnel vesicles towards the presynaptic membrane (Parsons and Sterling, 2003). Ribbons support the high rates of tonic neurotransmitter release typical of photoreceptor synapses and identified in *Drosophila* (Stuart et al., 2007).

As in the PN boutons of the *Drosophila* calyx, non-ribbon and ribbon synapses are found together in salamander (Yang et al., 2003) and goldfish (Midorikawa et al., 2007) bipolar cells. The two types of synapses are also interspersed and located close together in these cells (Midorikawa et al., 2007). Interestingly, ribbon synapses are associated with clusters of calcium channels and presynaptic calcium entry at the ribbon sites can diffuse to the non-ribbon sites. Induction of presynaptic calcium current accordingly causes a transient rate of high-frequency vesicle fusion, followed by a delayed, sustained fusion outside the ribbon region (Midorikawa et al., 2007). It is possible that ribbon and non-ribbon synapses have a similar function in the *Drosophila* PN boutons. Ribbon synapses could be readily activated in response to an olfactory stimulus to provide strong, rapid transmission to KCs, and the non-ribbon synapses activated, when necessary, to provide a more sustained input.

As an alternative explanation, ribbon and non-ribbon synapses in PN terminals may be different stages of single synaptic sites, and thus non-ribbon synapses may simply be ribbon synapses that have either lost their ribbon or that have yet to assemble one. Such a proposition raises the intriguing possibility that non-ribbon synapses may be in a non-functional state until they develop into ribbon synapses, or they may simply play a different functional role in synaptic transmission, as in goldfish bipolar cells (Midorikawa et al., 2007). Ribbon synapses, it is known, can both assemble and disassemble rapidly (Rybak and Meinertzhagen, 1997) and exhibit ultrastructural plasticity in response to circadian or other environmental signals (Schmitz, 2009). Furthermore, non-ribbon synapses in the PN boutons are typically smaller than ribbon synapses, with fewer postsynaptic partners. Their difference in size suggests they may be ribbon synapses in the process of expanding but before assembling a ribbon. Some large non-ribbon synapses were also observed, and these may be undergoing disassembly. Since it was found that the size of the presynaptic PN site relates to the number of postsynaptic partners, if ribbon synapses are in a constant flux of assembly and disassembly, the number of postsynaptic partners must also vary. Indeed, PN boutons are presynaptic to KC dendrites, which are highly enriched in filamentous actin and thus may be a site of synaptic plasticity (Leiss et al., 2009), but although anatomy may suggest such propositions, it offers no proof for them.

The finding that there are multiple postsynaptic partners at individual presynaptic sites is not unique to the calyx. It is the most common arrangement of synapses in the insect brain (Meinertzhagen, 2010), and contrasts with the vertebrate nervous system, in which most synapses are monadic except in specialized sites such as the retina (Dowling, 1987). The reason for the prevalence of this type of multiple-contact synapse in the insect brain is uncertain, but several explanations have been advanced, based largely on findings from the fly's visual system (Meinertzhagen and Sorra, 2001). It could be that circuit complexity and synaptic divergence are achieved in flies by increasing the number of postsynaptic elements, rather than by increasing the number of neurons, an alternative strategy possible in vertebrates with large numbers of neurons in their nervous systems. Alternatively, having numerous elements postsynaptic to a single presynaptic site may be

energy efficient, providing a means to reduce the metabolic cost of presynaptic transmitter release (Laughlin et al., 1998). In yet a third alternative, the presence of multiple elements postsynaptic to a single source of input could allow several target neurons to receive evenly-balanced synaptic inputs. Since a single PN contacts multiple classes of KCs (Tanaka et al., 2004), this synaptic arrangement could permit each lobe to receive equally balanced input from a presynaptic PN carrying a component of the odour signal.

The ratio of ribbon to non-ribbon synapses was not the same for each ultrastructural type of PN bouton. The DB-PNs had the most ribbons relative to non-ribbon synapses, followed by the CCV-PNs and then the DCV-PNs. DB-PNs also had the most ribbon synapses per μm^2 of plasmalemma, and sometimes had two presynaptic ribbons at a single active zone. Since ribbon synapses are generally larger and contact more postsynaptic partners than non-ribbon synapses, they may represent sites of higher transmitter output and greater divergence of transmission of the olfactory signal among the KCs. Together these results suggest that DB-PNs may have special requirements for transmission at their terminals, or have had a different functional history by which they accumulated more numerous ribbon synapses. Certainly the recruitment of presynaptic dense bodies to existing synapses has been reported after long-term facilitation at the neuromuscular junctions of decapod crustaceans, without the formation of new presynaptic sites for release (Chiang and Govind, 1986; Wojtowicz et al., 1994). DCV-PN activation may cause the gradual enlargement of existing non-ribbon presynaptic sites and the assembly of T-bar ribbons, as well as recruitment of additional KC dendrites. If these changes were marked by an increase in cytoplasmic electron density, at least in part from the dense packing of vesicles and the numerous filaments that tether these to each other (Butcher, 2008), a means would then exist for olfactory activity to convert DCV-PNs to DB-PNs. Confirmation of such a chain of events would require experimental activation of DCV-PNs followed by counts of DB-PNs. Such a confirmation would support the early suggestion that DB-PNs represent activated DCV-PN boutons. This would then support only a single distinction between PN boutons, between those with dense-core vesicles (DCV-PNs, DB-PNs) and those without (CCV-PNs). Preliminary

evidence obtained here supports this hypothesis, insofar as DB-PN were not observed in the calyx of a 1-day old fly, which presumably experienced less olfactory stimulation than an older fly. The functional implications of increased neurotransmitter output are unclear, as is the influence of the contents of the dense-core vesicles as a possible modulator of transmission of the olfactory signal. Finally, it is not clear why PN boutons require their synapses to be so densely packed, at approximately 2 synapses per μm^2 of the PN bouton's plasma membrane. This value is more dense than those at some other known synaptic terminals. In the tonically active photoreceptor terminals of the housefly compound eye, for example, each T-bar ribbon occupies a patch of membrane about $1.6\mu m^2$ in area, only about 0.6 synapses per μm^2 of plasma membrane (Nicol and Meinertzhagen, 1982). At neuromuscular varicosities on the other hand there are more than 3 synapses per μm of plasma membrane (Feeney et al., 1998).

If the three groups of PN boutons observed here are indeed separate subtypes, it is possible that they relate to the different tracts in which PN axons project from the antennal lobe to the calyx. Most PNs project through the inner antennocerebral tract (iACT; Stocker et al., 1990) before forming axon collaterals in the calyx, but some project instead through the outer antennocerebral tract (oACT), the inner middle antennocerebral tract (imACT, Tanaka et al., 2008) or the middle antennocerebral tract (mACT, Stocker et al., 1990). It seems unlikely, however, that the small area of the calyx sampled here would contain numerous examples of each subtype given that the oACT, imACT and mACT appear to contribute few boutons to the calyx (Stocker et al., 1990; Tanaka et al., 2008). In theory this possibility could be investigated using available GAL4 lines for each PN tract (Tanaka et al. 2008) using serial EM of horseradish peroxidase (HRP) labeled tissue, but these drivers have so far been proved too weak to effectively drive expression of a marker protein such as HRP at the EM level (C. Groh, personal communication).

The three ultrastructural subtypes of PNs also appear not to correspond in any way to the three classes of KCs. The KC dendrites of all three classes appear to arborize broadly in the calyx (Tanaka et al., 2004) and individual PN boutons contact multiple classes of KC

dendrites (Leiss et al., 2009). This arrangement allows the possibility that each lobe of the mushroom bodies receives olfactory input from each activated PN. More interesting is the possibility that ribbon and non-ribbon synapses preferentially associate with the different KC classes. Ribbon synapses have a larger area, and synapse size has been related to synaptic efficacy (Tanaka et al., 2005). Similarly, the different types of KCs exhibit different levels of responsivity to PN input; α'/β' KCs are more responsive than α/β KCs, which are more responsive in turn than the γ KCs (Turner et al., 2008). However, individual branched KC dendrites were sometimes observed here to receive inputs from both ribbon and non-ribbon synapses, and so a partition of inputs to different KCs is not true in detail and so may in fact not be the general case either.

A final possibility for the origins of the three ultrastructural types of PNs identified here is that DB-PNs are those undergoing degeneration. Cells with dark cytoplasm after being prepared for electron microscopy are often suspected of incipient degeneration, perhaps from being damaged during dissection or as part of normal developmental pruning. It seems unlikely that the DB-PNs are dying however, because other morphological and ultrastructural features associated with degenerating cells were not observed. Neurons that are degenerating might be smaller, have fewer synapses, and/or enlarged mitochondria (Brändstatter et al., 1991), but the DB-PNs observed here have synapses of a similar or larger size and density than those of PNs with lighter cytoplasm. Some mitochondria did appear slightly bloated, but this was not unique to the DB-PNs and was also observed in the DCV-PNs and the CCV-PNs. Furthermore, dark PN boutons have been reported in other insect species (Ganeshina and Menzel, 2001; Seid and Wehner, 2008) and DB-PNs were not a feature of just one 5-day old fly, but were also found in another fly of the same age.

The CCV-PNs and the DCV-PNs or DB-PNs were distinguished from one another because CCV-PNs lack dense-core vesicles. Each PN axon, however, forms multiple axon collaterals in the calyx, and so it is theoretically possible that another bouton originating from the same axon as the CCV-PN bouton, but outside the range of reconstruction, contains dense-core vesicles. Although the targeting of vesicles to

specific axon collaterals seems unlikely, and we would expect all boutons from a single PN either to have or to lack dense-core vesicles, it is nevertheless important to emphasize that these terminologies refer only to the bouton and not the PN as a whole. The dense-core vesicles in the DCV-PNs (and DB-PNs) may exert a neuromodulatory effect on the processing of olfactory signals either within or between microglomeruli, but further consideration of this possibility must await identification of the vesicle contents. Neuropeptide signaling is functionally very diverse: a single neuropeptide may act as a circulating neurohormone, as a locally released neuromodulator or as a cotransmitter with classical fast-acting neurotransmitters (Nässel, 2009). Although at least 40 genes in the *Drosophila* genome encode neuropeptide precursors, very few neuropeptides have been mapped in any detail in the adult CNS, and further study will be required to identify the contents and role of these dense-core vesicles in the PNs. To date, there have been no peptides or amines identified in PNs of any insect species. Two of the DCV-PNs observed here had populations of dense-core vesicles that were more electron-dense and larger in diameter than the other boutons, indicating that the contents of PN dense-core vesicles may vary. Excluding one possibility at least, sNPF has been ruled out as a candidate (Johard et al., 2008).

4.2 KENYON CELLS: STRUCTURE AND FUNCTION

The reconstructions of claw-shaped KC dendrites that encircle individual PN boutons coincide well with reports from light microscopy (Lee et al., 1999; Leiss et al., 2009), but suffer in most cases in being incomplete. Significantly, two presynaptic sites were for the first time found in one of the few KCs that could be reconstructed for much of its extent within the series. The postsynaptic elements could not be conclusively identified at these sites, and they could include ENs, PNs, or other KCs. Whether the synaptic input provided by KCs is excitatory or inhibitory is not known, and attempts to identify a KC neurotransmitter have so far been unsuccessful in all insects. Dopamine, tyramine/octopamine, glutamate, acetylcholine and GABA have from various lines of evidence been excluded as possible candidates in *Drosophila* however (Yasuyama et al., 2002; Johard et al., 2008). The amino acids taurine and aspartate have been immunodetected in subpopulations of KCs in the fly (Strausfeld et al., 2003), the moth

(Sjöholm et al., 2006), and the cockroach (Sinakevitch et al., 2001) but evidence that taurine and aspartate act as neurotransmitters in insects is lacking. A small portion of Kenyon cells may contain glutamate, as shown by immunolabeling experiments in crickets, cockroaches, honeybees, and flies (Bicker et al., 1988; Schürmann et al., 2000; Sinakevitch et al., 2001; Strausfeld et al., 2003). The pattern of glutamate-immunoreactivity could not be replicated in *Drosophila* however, neither by immunocytochemical means nor by using genetic markers for vesicular glutamate transporter (vGluT), and so it remains unclear whether glutamate in KCs is vesicle bound and used as a neurotransmitter, or if it is present as a metabolic intermediate (Johard et al., 2008). Recently, sNPF has been localized to a large subset of KCs (Johard et al., 2008), and possibly corresponds to the dense-core vesicles observed here.

KC presynaptic sites could have important implications for the way olfactory information is transformed in the calyx, depending on the identity of the postsynaptic cells at these synapses and their receptor types. One possibility is that there could be synapses between KCs, and perhaps these engage in lateral inhibition, in a manner similar to that first reported in the visual system of the horseshoe crab *Limulus* (Hartline et al., 1956). For example, if one KC were to receive a stronger olfactory signal from a PN than a neighboring KC, it may inhibit that KC more strongly than the neighbour inhibits it, serving to increase the difference, or contrast in their response intensities. Interestingly, since there are different classes of KCs that project to different lobes, which appear to have unique roles in short- and long-term memory (Zars et al., 2000), it is possible that the KCs may, to some extent, regulate the strength of the signals reaching each of the olfactory lobes. One of the cells postsynaptic to the KC was tentatively identified as an EN. Since ENs are presynaptic to all three types of calycal neurons (PNs, KCs, and ENs), input from KCs could have significant implications for local processing of olfactory signals within the calyx. Finally, the KC could be presynaptic to PN axons or boutons. PNs provide most of the input to KCs, so that KC synapses back to PNs could serve to provide feedback to that PN input. It is also possible that KCs are presynaptic to any combination of these elements, like the ENs. Presynaptic KC neurites in the calyx, however, appear to be very infrequent and may not occur in all KCs. Presynaptic sites

were found in only a single KC, and have not been previously reported in any insect, although frequent synapses are found between KC fibres in the peduncle (Schürmann, 1987). Therefore, these KC presynaptic sites may play a highly selective role in the calyx, and might not even be present in all of the three classes of KCs.

4.3   FUNCTIONAL IMPLICATIONS OF MICROGLOMERULAR MICROCIRCUITS

Microglomeruli in several insect species have been investigated using single section EM, and in the best studied cases of the honeybee and the fruit fly all comprise an individual PN bouton surrounded by numerous tiny KC dendrite profiles as well as GABA-containing ENs (Ganeshina and Menzel, 2001; Yasuyama et al., 2002). Serial section EM observations made here provide important additions to our knowledge of microglomerular composition, in what is the most extensive report to date of the wiring of the calyx in any insect. PNs contact numerous KC dendrites at individual synapses and very rarely, an EN. In turn, ENs provide synaptic input to the PNs and the KCs, as previously reported (Yasuyama et al., 2002). The present study now reports the existence of extensive connections between the ENs which were not previously known. It is important to note that the organization of the adult mushroom body calyx differs from the simpler organization of the larval calyx (Masuda-Nakagawa et al., 2005; Ramaekers et al., 2005).

Widespread input to microglomeruli from ENs has been shown here and in previous EM studies (Ganeshina and Menzel, 2001; Yasuyama et al., 2002). Most ENs are GABA immunoreactive (Yasuyama et al., 2002), and some, if not all, of the ENs observed here are therefore probably also GABA-immunopositive. The connectivity map of the inputs and outputs derived for four EN neurites contacting a single PN bouton illustrates the complexity of connections existing within a single microglomerulus. If these ENs are presumed to be GABA-expressing, and therefore inhibitory in signal, then the transmission of olfactory signals involves a complex web of local inhibition and disinhibition. The EM series here reveals that some of this inhibition could be local, with PNs providing cholinergic and excitatory input to both KCs and ENs. The ENs could then provide inhibitory feedback to a PN, modifying the output of the PN both to itself

and to the postsynaptic KCs. ENs probably influence the response properties of individual KCs through direct and indirect contacts. For example, EN4 is presynaptic to a KC dendrite, but also to EN3, thus potentially relieving the inhibition on the KCs postsynaptic to EN3. Furthermore, by inhibiting the actions of EN3, its inhibition on EN1 could be relieved by disinhibition at two separate sites where EN3 is presynaptic to EN1. This would increase EN1 transmission to its postsynaptic partners, a KC and a PN. This arrangement would also permit a single KC to receive multiple inputs from three ENs, depending on their relative states of activation, since EN4, EN1, and EN3 are all presynaptic to the same KC. As a result, when EN4 is activated, this single KC would receive input from EN4 and EN1, and otherwise would receive input only from EN3. It is also possible that in addition to these already complex interactions within a microglomerulus, these circuits could also provide a means to disinhibit or inhibit other microglomeruli, because single GABA-positive ENs are thought to contribute to multiple microglomeruli (Yasuyama et al., 2002). Disinhibition could occur if an EN inhibited the action of another EN that in turn provided inhibitory input to another PN and population of KCs. Inhibition of neighboring microglomeruli could occur if an EN were postsynaptic at one PN bouton then presynaptic to a different PN bouton. Indeed, such an arrangement was observed in this series, as EN2 was both post and presynaptic to two separate PN boutons. Alternatively, these EN connections might facilitate a more global inhibitory network, as in the locust, in which lateral horn interneurons periodically inhibit KCs (Laurent, 2002; Perez-Orive et al., 2002), although there is no evidence so far that ENs play a similar role in the *Drosophila* calyx (Turner et al., 2008).

Complex as they are even to enumerate in words, these speculations require the confirmation of many important assumptions. Most obviously lacking are: clear substantiation that all synaptic contacts seen in EM are functional, even though model synapses with similar ribbon synapses, such as photoreceptor tetrads (Saint Marie and Carlson, 1982) and neuromuscular junctions (Atwood et al., 1993), obviously are; the additional possibilities for transmission offered by gap junctions between the elements of the microglomerulus, although there has been no analysis yet of gap junctions in the calyx; and evidence that the neurotransmitter phenotype can be correctly used to predict

the polarity of transmission (for which postsynaptic receptor expression studies are required). This issue will be considered next.

To further our understanding of the physiological function of GABA-positive ENs in the calyx it will be necessary to identify the type of GABA receptors on cells postsynaptic to GABA-positive ENs. In the insect central nervous system, GABA acts on ion channel receptors for fast, inhibitory transmission (Sattelle et al., 1991; Buckingham et al., 2005) and on G-protein-coupled receptors for a slow or modulatory action (GABA$_B$R; Mezler et al., 2001). Since ENs provide synaptic input to all calycal neurons, it is expected that there should be widespread distribution of at least one of these receptor types in the calyx. Indeed, both types of GABA receptors are widely expressed throughout the calyx (Enell et al., 2007). It will be interesting to determine if all cells postsynaptic to ENs exhibit a mixture of both receptor types or whether some are restricted to express just one. A hint may come from the finding that the mushroom body lobes and penduncle, which comprise all the KCs, are immunoreactive for an ionotropic receptor subunit, RDL (Resistant to Dieldrin), but not for subunits of GABA$_B$R, suggesting that KCs only experience fast, inhibitory input from GABAergic ENs (Enell et al., 2007). There is some evidence for this from electrophysiological recordings of cultured KCs (Su and O'Dowd, 2003). This does not exclude the possibility that KC dendrites in the calyx may still express GABA$_B$R alone or with ionotropic GABA receptors.

A more conclusive interpretation of the results also depends on further resolution of the origins and identities of ENs contributing to these circuits. Important questions include not only their neurotransmitter phenotype(s) but also the number of EN cells and their source(s) of activation. So far, the use of immunolabels and genetic reporters has identified candidate GABAergic cells as a large source of EN input to the calyx (Yasuyama et al., 2002; Enell et al., 2007; Liu and Davis, 2009). A greater or lesser part of this input almost surely originates from the anterior paired lateral (APL) neuron, a cell that densely innervates the whole mushroom body structure, including the calyx (Liu and Davis, 2009). Its cell body lies laterally to the calyx, near the lateral horn, and bifurcates into two branches, one entering through the calyx and the other at the waist of the vertical

lobes. Reduction of GABA synthesis in this cell enhances olfactory learning, suggesting that the APL neuron suppresses learning by releasing GABA. Similarly, there are GABA-positive feedback neurons in the honeybee that connect the lobes of the mushroom body to the calyx and that are suggested to be involved in olfactory memory formation (Grünewald, 1999). Whether the APL neuron is the *Drosophila* counterpart of these feedback neurons remains unclear, because in the bee these cells are considered postsynaptic in the lobes but the APL neuron shows markers for presynaptic specializations (Liu and Davis, 2009). Furthermore, GABA-positive terminals in the calyx are presynaptic in *Drosophila* (Yasuyama et al., 2002).

The inability to identify the cells of origin of EN terminals reconstructed in this study opens two significant possibilities. First, if the reconstructed EN terminals derive from different ENs, these could constitute the networks discussed above, through the serial synapses that connect EN profiles. One of the contributing cells is most likely the APL cell of Liu and Davis (2009), which from the density of its arborization should form at least some of the EN profiles. The numerical extent of that contribution is not known however and cannot readily be assessed from a published confocal image. Despite being dense and widespread in the calyx, EN terminals identified by EM in this study could outnumber those of the APL cell alone, a possibility that will require independent assessment, for example using the GAL4 line to drive HRP expression for EM evaluation. If an additional cell or cells were to contribute extensive EN terminals, these may also be GABA-positive, but need not be, but in any case have not been identified from existing GAL4 lines. The connections identified between reconstructed EN terminals indicates that there could be at least three independent EN terminals, if none was to synapse upon itself. Second, no less interesting, it may be that EN terminals do in fact synapse upon themselves to form so-called autapses (Ikeda and Bekkers, 2006). Not just an anatomical oddity, autapses have now been identified in a number of networks, for example between GABA networks of the neocortex (Tamás et al., 1997) where they have been proposed to improve spike-timing (Bacci and Huguenard, 2006). If the APL cell were to contribute all or most EN profiles in the calyx, it may play such a role in the mushroom body, too.

4.4 PROGRESS TOWARDS A CONNECTIVITY MODEL OF THE CALYX

There is growing interest in reconstructing and mapping entire regions of the insect brain, so that virtual neural networks can be built and a greater knowledge of how sensory information is processed and stored in the nervous system can be obtained. In addition, circuit diagrams of the brain are an essential, albeit insufficient means to understand behaviour, for which they are its neural substrate.

In the *Drosophila* calyx, KC responses to odours are highly selective and sparse, compared with the source of their inputs, the PNs from the antennal lobe (Tanaka et al., 2008). The sparseness of calycal responses has been observed from electrophysiological recordings in several species of insects, leading to the suggestion that KCs act as coincidence detectors, responding to coordinate input from PNs (Laurent, 2002; Perez-Orive et al., 2002; Turner et al., 2008). Several mechanisms appear to underlie this transformation of the olfactory signal in *Drosophila*: excitatory synaptic potentials from PNs decay rapidly, limiting temporal integration, KC firing thresholds are high, and PN convergence onto individual KCs is low (Turner et al., 2008; Leiss et al., 2009). These mechanisms ensure that individual KCs respond infrequently to any given odour, and require both spatial and temporal summation of coincident input from PN boutons in order to trigger an action potential. It is also possible that synaptic inhibition (from recurrent local interneurons of the lateral horn, as in the locust, Perez-Orive et al., 2002) and KC active conductances work together to make KCs coincidence detectors of PN input, by ensuring that KCs can summate PN input only briefly and periodically (Laurent, 2002), although electrophysiological recordings from *Drosophila* KCs provide no evidence so far for this suggestion (Turner et al, 2008). The study by Perez-Orive et al. (2002), which first raised the topic of coincidence detection by KCs was based on electrophysiological recordings in the locust, and appeared in parallel with the anatomical descriptions of Yasuyama et al. (2002) on *Drosophila*. The first report of EN input to the KC dendrites appeared in the latter account and provided anatomical evidence for convergence directly upon KC dendrites. The inputs for that convergence derive from both a PN bouton (excitatory) and ENs, some of which at least are GABA-positive and therefore likely inhibitory. Indeed, spontaneous excitatory and inhibitory synaptic

currents in cultured *Drosophila* KCs are respectively mediated by acetylcholine and GABA receptors (Su and O'Dowd, 2003). This study, however, has identified that postsynaptic KC profiles receive about 70 times the number of inputs from PNs compared with ENs, suggesting that unlike in the locust, convergence of excitatory PN input and inhibitory EN input may not have as large, or any, influence on coincidence detection (Perez-Orive et al., 2002). This conclusion rests on the assumption that the synaptic gain at all anatomical contacts is of similar size. Although it cannot be excluded that some KCs do not receive input from other, untraced ENs outside of the vicinity of the microglomerulus from which these counts were made, it seems clear that EN input to KCs is far outnumbered and therefore possibly outweighed by PN input. Identification of this extreme imbalance was only possible in the analysis here, because this was based on EM series, but not from the analysis of Yasuyama et al. (2002), a difference that illustrates the detection biases in synaptic maps reported from simple searches of single EM sections.

Turner et al. (2008) roughly estimated that there are about 13 PN active zones per KC, extrapolated from the number of synapses counted on a single section of a single PN bouton and the assumption that PN boutons are spherical. The results from the EM series here show that the number of synapses per section is variable and PNs are heterogeneous in shape, so that the previous estimates from Turner et al. (2008) must be very approximate. In spite of these limitations, Turner's estimate falls within the range of the one obtained here using total counts of synapses in nine boutons. Therefore, both the estimate of Turner et al. (2008) and the results of this study show that because each KC receives its synaptic inputs from five or so PN boutons (Leiss et al., 2009), each PN bouton might only contribute about three synapses to an individual KC (see section 3.4). If each of these boutons originate from different PNs, it is possible that the KCs are acting as coincidence detectors. Alternatively, if the boutons originate from the same PN or a set of functionally related PNs, the KCs improve the signal-to-noise ratio.

4.5   AGE-RELATED CHANGES IN THE CALYCAL MICROGLOMERULI

The developing mushroom body calyx of *Drosophila* has a simpler organization than that of the adult (Yasuyama et al., 2002; Masuda-Nakagawa et al., 2005; Ramaekers et al., 2005), and there is extensive remodeling of PN and KC neurites during the larval and pupal stages of development (Lee et al., 1999; Jefferis et al., 2002; Marin et al., 2005). There is some evidence that the number of KC axons continues to fluctuate during the adult life span (Technau, 1984; Heisenberg et al., 1995) but such changes have yet to be studied in the fly at the microglomerular level. In the honeybee, at least, it has been hypothesized that maturation of local synaptic circuits in the calyx occurs after adult emergence (Ganeshina et al., 2006). Here it is reported in *Drosophila* that by the first day of emergence, distinct microglomeruli are formed, although a few are ensheathed in glia, not seen in the adult fly (this study; Yasuyama et al., 2002; Leiss et al., 2009). Glomeruli of the antennal lobe are enwrapped by glial processes, as are cricket calycal microglomeruli (Schürmann, 1974). No DB-PNs were found, and these must thus develop sometime between one and five days of age. Interestingly, the DCV-PNs were larger than those of the 5-day old fly, consistent with the possibility that boutons become smaller with age and/or experience. In contrast, PN boutons enlarge with age in ants (Seid et al., 2005). Although all possible precautions were taken to section and photograph the calyces of the two flies in the same region, these differences may nevertheless have resulted from the selection of slightly different areas for reconstruction, because it is unlikely that the two regions would have corresponded completely. The absence of CCV_PN boutons in the 1-day but not 5-day old fly provides some suggestion that the reconstructed areas indeed differed between the two series, rather than that dense core vesicles disappeared from some boutons with age.

Ribbon and non-ribbon PN synapses are formed by the first day of emergence, as well as their corresponding postsynaptic partners. As in the adult calyx, the postsynaptic partners were most often putative KC dendrites, but bouton-bouton contacts were also found. PN boutons are cholinergic (Yasuyama et al., 2002) and thus these may provide excitatory input to one another in the 1-day old fly, although the functional implications of such a synaptic arrangement remains unclear. The overall density of synapses in the boutons did

not differ from the 5-day old fly. Ribbon synapses were larger and correspondingly had more postsynaptic partners than those of the 5-day old fly, and non-ribbon synapses also typically had more postsynaptic partners. These results collectively suggest that there is selective pruning of PN boutons following adult emergence; boutons become smaller, some synapses are lost to maintain the density of presynaptic sites, and the remaining synapses become smaller and accordingly reduce their number of postsynaptic partners. Some of these dissembled synapses should include bouton-bouton synapses. A larger sample of microglomeruli and flies will be needed to adjudicate these initial findings.

4.6 CHARACTERIZING THE PHENOTYPICALLY GABAERGIC NETWORK OF THE MUSHROOM BODY CALYX USING THE GAL4-UAS SYSTEM

GABA-positive cells densely innervate the calyx (Ganeshina and Menzel, 2001; Yasuyama et al., 2002; Liu and Davis, 2009) and these could have an important role in olfactory learning (Liu and Davis, 2009). GAL4 lines that drive expression in GABA-positive cells should identify the number and location of cells that contribute GABA-positive processes to the calyx. Unlike antibodies that only mark the component of the neuron containing the antigen (most often the cell body or the terminals), GAL4 lines can drive expression of membrane-bound or cytosolic GFP, thus providing uniform illumination of the entire neuron. Furthermore, GAL4 lines could be used at the EM level to selectively drive expression of HRP in GABA-positive cells for serial section EM and reconstructions. Two lines designed to promote expression of marker genes in GABA-positive neurons, GAD1-GAL4 (Featherstone et al., 2000) and vGAT-GAL4 (Simpson, unpublished) were investigated as potential candidates. There are various reasons why such indirect reporters may provide misleading evidence, of course, not least that they fail to identify the presence of the neurotransmitter itself, nor even the proteins that synthesize or pump the neurotransmitter, but rather they only reveal expression of the promoter for the gene that codes for such proteins; the promoter is not always specific to the gene of interest. A different problem is that even antibodies, which should reveal the presence of an amine or other molecule that can function as a neurotransmitter, do not reveal whether the molecule is in fact used in that role. For example, glutamate is a

common metabolic precursor, including for GABA, so that all cells including ones that are GABA-positive should contain glutamate.

As an example of how misleading reporter lines may be, both the vGAT-GAL4 and GAD1-GAL4 drivers revealed a similar pattern of GFP labeling in a large population of KCs, although KCs are not GABA-positive (Featherstone et al., 2000; Yasuyama et al., 2002; Johard et al., 2008). KC bodies, axons and dendrites were strongly labeled in both lines. The pattern of GFP expression was very similar to an immunolabel for aspartate (Strausfeld et al., 2003), showing the four fascicles composed of KCs. These arise from the posterior and emerge from under the calyx to extend into the pedunculus. With respect to the label obtained using the GAD1-GAL4 line, it is possible that KCs may use glutamate as a neurotransmitter, a precursor to GABA, and utilize GAD1 for a non-neurotransmitter function. For example, glutamatergic motor neurons require GAD1 for proper clustering of glutamate receptors on the postsynaptic muscle (Featherstone et al., 2000). Several lines of evidence do not support this hypothesis, however. Firstly, only a small subset of KCs contain glutamate (Strausfeld et al., 2003), and many KCs were labeled using GAD1-GAL4. Secondly, the pattern of GFP expression driven by GAD1-GAL4 did not correspond with a GAD1 immunolabel. Furthermore, since KCs are not GABA-positive (Yasuyama et al., 2002), they should not contain the vGAT even if for misleading reasons they may express GAD1. It therefore appears that both GAD1-GAL4 and vGAT-GAL4 drive ectopic expression of marker genes in KCs, the significance of which is not clear.

These results are not easily interpreted, but it seems most likely that the promoters used are not specific to vGAT and GAD1 and both require further dissection. Although the GAL4-UAS system is celebrated for its ability to drive expression of genes in a stage and tissue-specific manner, the pattern of expression is only as specific as that of the promoter sequence. It appears that in this case, some unknown portion of the promoter sequences may direct GFP expression in KCs. Such occurrences are not rare, but the limitations of GAL4 lines can be unknown or the lines are sometimes still used as a matter of convenience. For example, a well-established and often used line (GH146-

GAL4) considered to drive gene expression in PNs (e.g. Ng et al., 2002; Jefferis et al., 2007) was recently revealed also to drive expression in the GABA-expressing MB-APL neuron (Liu and Davis, 2009). Furthermore, the GAD1-GAL4 line has been used in different studies to drive expression in both GABA-containing cells (Enell et al., 2007; Leiss et al., 2009) and KCs (Johard et al., 2008). These results illustrate that GAL4 lines should always be used with care, and whenever possible the pattern of GFP expression validated with an antibody directed against the neurotransmitter itself. The GAD1-GAL4 and vGAT-GAL4 lines should not be used to drive expression in GABA-positive cells in the calyx, although they may still be useful for cells elsewhere in the nervous system (Ng et al., 2002). Alternatively, they can be used to visualize KCs and the entire mushroom body structure (this study; Johard et al., 2008).

Several GAL4 lines that drive gene expression in calycal ENs were identified in a large genetic screen (Tanaka et al., 2008). Given the widespread innervation of the calyx by GABA-containing cells (Yasuyama et al., 2002), it was hypothesized that at least one of these lines should drive expression in GABA-positive ENs. These lines permitted the visualization of the MB-C1 cell, MB-C2/C3 cells, and the MB-CP1 cell. None of these cells was GAD1-positive here. Interestingly, MB-C1 did not show the same coarse reticular pattern as originally identified (Tanaka et al., 2008). Instead, punctate and spherical structures were obvious. The same pattern was found using a marker for cytosolic GFP and membrane-bound GFP. These results indicate that several ENs arborize in the calyx that are not GABA-positive. It is possible that some of these cells may correspond to the uncharacterized cells observed in the EM series, the dense granule containing cell type and the cell with a cytoplasm filled with dense-core vesicles. It is also possible that some of these MB-cells correspond to the reconstructed ENs. Although these ENs were suspected to be GABA neurons, there was some evidence that they constituted a heterogeneous population, for example from differences in vesicle diameters and synaptic densities. Further characterization of these MB-cells will require double immuno-labels to determine if they are presynaptic in the calyx, and the nature of their neurotransmitter contents.

CHAPTER 5   CONCLUSION

The results of this study have revealed several new properties of the calyx:

1) The calyx contains three ultrastructurally distinct types of PN boutons that are heterogeneous in shape and exhibit subtle differences in synaptic densities.

2) All PN boutons form both ribbon and non-ribbon synapses, and from their smaller size and fewer postsynaptic partners, non-ribbon synapses may possibly become converted to ribbon synapses after activity; the olfactory signal may then be transmitted more strongly and efficiently at ribbon synapses.

3) PN boutons with an electron-dense cytoplasm have the most ribbon synapses per unit area of membrane as well as the highest ratio of ribbon to non-ribbon synapses, and thus may be more active and efficient than other boutons.

4) KC neurites are not exclusively postsynaptic in the calyx and can form occasional ribbon synapses, the functional interpretation of which awaits identification of their postsynaptic partners and vesicle contents, and clearly has important implications for olfactory information processing in the calyx.

5) PN boutons form an estimated 17-22 active zones per KC, and each KC probably receives synaptic inputs at it claws from about 5-7 PN boutons, so that each PN bouton may contribute input to a single dendritic KC claw at roughly only 3 presynaptic sites. For the postsynaptic side, there are about 11-13 KC claw-like branches per PN bouton, but each bouton contains approximately 40 presynaptic sites (30 with presynaptic ribbons, each having six postsynaptic partners, and 10 non-ribbon synapses, each with two to three postsynaptic partners), totaling about 200 postsynaptic elements. As a result, a single claw receives input from individual presynaptic sites that must be highly redundant.

6) There may be important processing of the olfactory signal by local circuits formed by ENs in the calyx; ENs form synaptic connections with PNs, KCs, and other ENs, and if presumed to be GABAergic, a single microglomerulus may incorporate a complex of inhibition and disinhibition.

7) Extensive serial synapses link EN terminals into a network, presumed to be GABAergic and inhibitory, that extends between microglomeruli and that may be autaptic.

8) The structure and synaptic connectivity of microglomeruli may undergo changes after adult emergence.

9) vGAT and GAD1-GAL4 lines drive ectopic expression of marker genes in KCs and are not reliable reporters of GABA-positive cells.

10) Previously identified calycal ENs (MB-C1, MB-C2/C3, MB-CP1) are not immunopositive for GAD1, a marker of GABA-containing cells, and thus contribute unidentified processes into the calyx.

11) A network of ENs consisting of neurons expressing a GABA phenotype differently innervates anatomically and functionally discrete areas of the honeybee calyx, although the density of innervation may change with alterations in age or experience (see Appendix).

REFERENCES

Abercrombie M (1946) Estimation of nuclear population from microtome sections. Anat Rec 94:239-247

Acebes A, Ferrús A (2001) Increasing the number of synapses modifies olfactory perception in *Drosophila*. J Neurosci 21:6264-6273

Aso Y, Grübel K, Busch S, Friedrich AB, Siwanowicz I, Tanimoto H (2009) The mushroom body of adult *Drosophila* characterized by GAL4 drivers. J Neurogenet 23:156-172

Atwood HL, Govind CK, Wu CF (1993) Differential ultrastructure of synaptic terminals on ventral longitudinal abdominal muscles in *Drosophila* larvae. J Neurobiol 24:1008-24

Bacci A, Huguenard JR (2006) Enhancement of spike-timing precision by autaptic transmission in neocortical inhibitory interneurons. Neuron 49:119-30

Benton R, Vannice KS, Gomez-Diaz C, Vosshall LB (2009) Variant ionotropic glutamate as chemosensory receptors in *Drosophila*. Cell 136:149-162

Bicker G, Schäfer S, Kingan TG (1985) Mushroom body feedback interneurones in the honeybee show GABA-like immunoreactivity. Brain Res 360:394-397

Bicker G, Schäfer S, Ottersen OP, Storm-Mathisen J (1988) Glutamate-like immunoreactivity in identified neuronal populations of insect nervous systems. J Neurosci 8:2108-2122

Brand AH, Perrimon N (1993) Targeted gene expression as a means of altering cell fates and generating dominant phenotypes. Development 118:401-415

Brändstatter J, Shaw SR, Meinertzhagen IA (1991) Terminal degeneration and synaptic disassembly following receptor photoablation in the retina of the fly's compound eye. J Neurosci 11:1930-1941

Buckingham S, Biggin P, Sattelle B, Brown L, Sattelle D (2005) Insect GABA receptors: Splicing, editing, and targeting by antiparasitics and insecticides. Mol Pharmacol 68:942

Bullock TH (1990) Goals of neuroethology. Bioscience 40:244-248

Bullock TH, Horridge GA (1965) Structure and function in the nervous system of invertebrates. San Francisco: W.H. Freeman and Co.

Busch S, Selcho M, Ito K, Tanimoto H (2009) A map of octopaminergic neurons in the *Drosophila* brain. J Comp Neurol 513:643-667

Butcher NJ (2008) The structural and physiological analyses of endocytotic organelles and proteins in the fruit fly *Drosophila melanogaster*. Honours thesis, Dalhousie University, Halifax, Canada

Chiang RG, Govind CK (1986) Reorganization of synaptic ultrastructure at facilitated lobster neuromuscular terminals. J Neurocytol 15:63-74

Crittenden J, Skoulakis E, Han K, Kalderon D, Davis RL (1998) Tripartite mushroom body architecture revealed by antigenic markers. Learn Memory 5:38-51

de Belle J, Heisenberg M (1994) Associative odor learning in *Drosophila* abolished by chemical ablation of mushroom bodies. Science 263:692-695

Dowling J, Boycott BB (1966) Organization of the primate retina: Electron microscopy. Proc R Soc Lond B Biol Sci 15:80-111

Dowling J (1987) The retina: An approachable part of the brain. Cambridge, MA: Belknap Press

Duffy JB (2002) GAL4 system in *Drosophila*: A fly geneticist's Swiss army knife. Genesis 34:1-15

Durst C, Eichmoller S, Menzel R (1994) Development and experience lead to increased volume of subcompartments of the honeybee mushroom body. Behav Neur Biol 62:259–263

Ehmer B, Gronenberg W (2002) Segregation of visual input to the mushroom bodies in the honeybee (*Apis mellifera*). J Comp Neurol 451:362–373

Enell LE, Hamasaka Y, Kolodziejczyk A, Nässel DR (2007) Ɣ-Aminobutyric acid (GABA) signaling components in *Drosophila*: Immunocytochemical localization of GABAB receptors in relation to the GABAA receptor subunit RDL and a vesicular GABA transporter. J Comp Neurol 505:18 -31

Fahrenbach WH (1985) Anatomical circuitry of lateral inhibition in the eye of the horseshoe crab, *Limulus polyphemus*. Proc R Soc Lond Ser B 225:219-249

Farris SM, Robinson GE, Fahrbach SE (2001) Experience- and age-related outgrowth of intrinsic neurons in the mushroom bodies of the adult worker honeybee. J Neurosci 21:6395-6404

Featherstone D, Rushton E, Hilderbrand-Chae M, Phillips A, Jackson F, Broadie K (2000) Presynaptic glutamic acid decarboxylase is required for induction of the postsynaptic receptor field at a glutamatergic synapse. Neuron 27:71–84

Feeney CJ, Karunanithi S, Pearce J, Govind CK, Atwood HL (1998) Motor nerve terminals on abdominal muscles in larval flesh flies, *Sarcophaga bullata*: Comparisons with *Drosophila*. J Comp Neurol 402:197-209

Fei H, Chow DM, Chen A, Romero-Calderón R, Ong WS, Ackerson LC, Maidment NT, Simpson JH, Frye MA, Krantz DE (2010) Mutation of the *Drosophila* vesicular GABA transporter disrupts visual figure detection. J Exp Biol 213:1717-1730

Fiala A, Spall T, Diegelmann S, Eisermann B, Sachse S, Devaud J, Buchner E, Galizia CG (2002) Genetically expressed cameleon in *Drosophila melanogaster* is used to visualize olfactory information in projection neurons. Curr Biol 12:1877-1884

Fiala JC (2005) Reconstruct: A free editor for serial section microscopy. J Microsc 218:52-61

Fishilevich E, Vosshall LB (2005) Genetic and functional subdivision of the *Drosophila* antennal lobe. Curr Biol 15:1548-1553

Ganeshina O, Menzel R (2001) GABA-immunoreactive neurons in the mushroom bodies of the honeybee: An electron microscopic study. J Comp Neurol 437:335-349

Ganeshina O, Vorobyev M, Menzel R (2006) Synaptogenesis in the mushroom body calyx during metamorphosis in the honeybee *Apis mellifera*: An electron microscopic study. J Comp Neurol 497:876-897

Gehring K (2008) Structural organization and plasticity of neurons in the mushroom bodies of the honeybee *Apis mellifera*. Doctoral dissertation, University of Würzburg, Würzburg, Germany

Gerschenfeld HM (1973) Chemical transmission in invertebrate central nervous systems and neuromuscular junctions. Physiol Rev 53:1-119

Govind CK, Chiang RG (1979) Correlation between presynaptic dense bodies and transmitter output at lobster neuromuscular terminals by serial section electron microscopy. Brain Res 161:377-388

Groh C, Tautz J, Rössler W (2004) Synaptic organization in the adult honey bee brain is influenced by brood-temperature control during pupal development. Proc Nat Acad Sci USA 101:4268-4273

Groh C (2009) Personal communication, University of Würzburg, Würzburg, Germany

Gronenberg W (2001) Subdivisions of hymenopteran mushroom body calyces by their afferent supply. J Comp Neurol 435:474–489

Grünewald B (1999) Morphology of feedback neurons in the mushroom body of the honeybee, *Apis mellifera.* J Comp Neurol 404:114-126

Hallem EA, Ho MG, Carlson JR (2004) The molecular basis of odor coding in the *Drosophila* antenna. Cell 117:965-979

Hartline HK, Wagner HG, Ratliff F (1956) Inhibition in the eye of *Limulus*. J Gen Physiol 39:651-673

Heisenberg M, Borst A, Wagner S, Byers D (1985) *Drosophila* mushroom body mutants are deficient in olfactory learning. J Neurogenet 2:1–30

Heisenberg M, Heusipp M, Wanke T (1995) Structural plasticity in the *Drosophila* brain. J Neurosci 15:1951-1960

Heisenberg M (2003) Mushroom body memoir: From maps to models. Nat Rev Neurosci 4:266-275

Helmstaedter M, Briggman KL, Denk W (2008) 3D structural imaging of the brain with photons and electrons. Curr Opin Neurobiol 18:633-641

Hofer S, Dircksen H, Tollbäck P, Homberg U (2005) Novel insect orcokinins: Characterization and neuronal distribution in the brains of selected dicondylian insects. J Comp Neurol 490:57-71

Ito K, Okada R, Tanaka NK, Awasaki T (2003) Cautionary observations on preparing and interpreting brain images using molecular biology-based staining techniques. Microsc Res Techniq 62:170-186

Ito K, Suzuki K, Estes P, Ramaswami M, Yamamoto D, Strausfeld NJ (1998) The organization of extrinsic neurons and their implications in the functional roles of the mushroom bodies in *Drosophila melanogaster* Meigen. Learn Memory 5:52-77

Jefferis GS, Marin EC, Watts R, Luo L (2002) Development of neuronal connectivity in *Drosophila* antennal lobes and mushroom bodies. Curr Opin Neurobiol 12:80-86

Jefferis GS, Potter C, Chan A, Marin E, Rohlfing T, Maurer C, Luo L (2007) Comprehensive maps of *Drosophila* higher olfactory centers: Spatially segregated fruit and pheromone representation. Cell 128:1187–1203

Johard H, Enell L, Gustafsson E, Trifilieff P, Veenstra J, Nässel DR (2008) Intrinsic neurons of *Drosophila* mushroom bodies express short neuropeptide F: Relations to extrinsic neurons expressing different neurotransmitters. J Comp Neurol 507:1479–1496

Kasuya J, Ishimoto H, Kitamoto T (2009) Neuronal mechanisms of learning and memory revealed by spatial and temporal suppression of neurotransmission using *shibire*[ts1], a temperature-sensitive dynamin mutant gene in *Drosophila melanogaster*. Front Mol Neurosci 2:1-6.

Keene AC, Waddell S (2007) *Drosophila* olfactory memory: Single genes to complex neural circuits. Nat Rev Neurosci 8:341-354

Kenyon F (1896) The brain of the bee. J Comp Neurol 6:133-210

Kim S, Atwood HL, Cooper RL (2000) Assessing accurate sizes of synaptic vesicles in nerve terminals. Brain Res 877:209-217

Laissue PP, Reiter C, Hiesinger PR, Halter S, Fischbach KF, Stocker RF (1999) Three-dimensional reconstruction of the antennal lobe in *Drosophila melanogaster*. J Comp Neurol 405:543-552

Laughlin SB, de Ruyter van Steveninck RR, Anderson JC (1998) The metabolic cost of neural information. Nat Neurosci 1:36-41

Laurent G (2002) Olfactory network dynamics and the coding of multidimensional signals. Nat Rev Neurosci 3:884-895

Lee T, Lee A, Luo L (1999) Development of the *Drosophila* mushroom bodies: Sequential generation of three distinct types of neurons from a neuroblast. Development 126:4065-4076

Leiss F, Groh C, Butcher NJ, Meinertzhagen IA, Tavosanis G (2009) Synaptic organization in the adult *Drosophila* mushroom body calyx. J Comp Neurol 517:808-824

Lichtman JW, Sanes JR (2009) Ome sweet ome: What can the genome tell us about the connectome? Mol Cell Biol 18:346-353

Liu X, Davis RL (2009) The GABAergic anterior paired lateral neuron suppresses and is suppressed by olfactory learning. Nat Neurosci 12:53-59

Luo L, Callaway E, Svoboda K (2008) Genetic dissection of neural circuits. Neuron 57:634-660

Macagno ER, Lopresti V, Levinthal C (1973) Structure and development of neuronal connections in isogenic organisms: Variations and similarities in the optic system of *Daphnia magna*. Proc Natl Acad Sci USA 70:57-61

Mao Z, Davis RL (2009) Eight different types of dopaminergic neurons innervate the *Drosophila* mushroom body neuropil: Anatomical and physiological heterogeneity. Front Neural Circuits 3:1-17

Marin EC, Watts RJ, Tanaka NK, Ito K, Luo L (2005) Developmentally programmed remodeling of the *Drosophila* olfactory circuit. Development 132:725-737

Masuda-Nakagawa L, Tanaka N, O'Kane C (2005) Stereotypic and random patterns of connectivity in the larval mushroom body calyx of *Drosophila*. Proc Natl Acad Sci USA 102:19027-19032

Meinertzhagen IA (1993) The synaptic populations of the fly's optic neuropil and their dynamic regulation: Parallels with the vertebrate retina. Prog Retin Res 12:13-39
Meinertzhagen IA (2010) The organisation of invertebrate brains: Cells, synapses and circuits. Acta Zoologica 91:64-71

Meinertzhagen IA, Govind CK, Stewart BA, Carter JM, Atwood HL (1998) Regulated spacing of synapses and presynaptic active zones at larval neuromuscular junctions in different genotypes of the flies *Drosophila* and *Sarcophaga*. J Comp Neurol 393:482-492

Meinertzhagen IA, Hu X (1996) Evidence for site selection during synaptogenesis: The surface distribution of synaptic sites in photoreceptor terminals of the flies *Musca* and *Drosophila*. Cell Mol Neurobiol 16:677-698

Meinertzhagen IA, O'Neil S (1991) Synaptic organization of columnar elements in the lamina in the wild type in *Drosophila melanogaster*. J Comp Neurol 305:232-263

Meinertzhagen IA, Sorra KE (2001) Synaptic organization in the fly's optic lamina: Few cells, many synapses and divergent microcircuits. Prog Brain Res 131:53-69

Mezler M, Müller T, Raming K (2001) Cloning and functional expression of GABA(B) receptors from *Drosophila*. Eur J Neurosci 13:477-86

Midorikawa M, Tsukamoto Y, Berglund K, Ishii M, Tachibana M (2007) Different roles of ribbon-associated and ribbon-free active zones in retinal bipolar cells. Nat Neurosci 10:1268-1276

Mobbs PG (1982) The brain of the honeybee *Apis mellifera*. Proc R Soc Lond Ser B 298:309-354

Msghina M, Govind CK, Atwood HL (1998) Synaptic structure and transmitter release in crustacean phasic and tonic motor neurons. J Neurosci 18:1374-1382

Muenz T, Oberwallner B, Gehring K, Rössler W (2008) Plasticity of synaptic complexes in the mushroom bodies of the honeybee brain depends on age, experience and season. FENS Abstr 4:143

Namiki S, Haupt SS, Kazawa T, Takashima A, Ikeno H, Kanzaki R (2009) Reconstruction of virtual neural circuits in an insect brain. Front Neurosci 3:206-213

Nässel DR (1993) Neuropeptides in the insect brain: A review. Cell Tissue Res 273:1-29

Nässel DR (2009) Neuropeptide signaling near and far: How localized and timed is the action of neuropeptides in brain circuits? Invert Neurosci 9:57-75

Nässel DR, Elekes K (1992) Aminergic neurons in the brain of blowflies and *Drosophila*: Dopamine- and tyrosine hydroxylase-immunoreactive neurons and their relationship with putative histaminergic neurons. Cell Tissue Res 267:147-167

Nässel DR, Enell LE, Santos JG, Wegener C, Jefferis GS (2008) A large population of diverse neurons in the *Drosophila* central nervous system expresses short neuropeptide F, suggesting multiple distributed peptide functions. BMC Neurosci 9:90-125

Ng M, Roorda R, Lima S, Zemelman B, Morcillo P, Miesenböck G (2002) Transmission of olfactory information between three populations of neurons in the antennal lobe of the fly. Neuron 36:463–474

Nicol D, Meinertzhagen IA (1982) An analysis of the number and composition of the synaptic populations formed by photoreceptors of the fly. J Comp Neurol 207:29-44

Nishino H, Mizunami M (1998) Giant input neurons of the mushroom body: Intracellular recording and staining in the cockroach. Neurosci Lett 246:57-60

Otsuna H, Ito K (2006) Systematic analysis of the visual projection neurons of *Drosophila melanogaster*. I. Lobula-specific pathways. J Comp Neurol 497:928–958

Ott SR, Rogers SM (2010) Gregarious desert locusts have substantially larger brains with altered proportions compared with the solitarious phase. Proc R Soc B *In Press*

Parsons T, Sterling P (2003) Synaptic ribbon. Conveyor belt or safety belt? Neuron 37:379-382

Perez-Orive J, Mazor O, Turner GC, Cassenaer S, Wilson RI, Laurent G (2002) Oscillations and sparsening of odor representations in the mushroom body. Science 297:359-365

Phelps CB, Brand AH (1998) Ectopic gene expression in *Drosophila* using the GAL4 system. Methods 14:367-379

Ramaekers A, Magnenat E, Marin EC, Gendre N, Jefferis GS, Luo L, Stocker RF (2005) Glomerular maps without cellular redundancy at successive levels of the *Drosophila* larval olfactory circuit. Curr Biol 15:982-992

Robinson GE (1992) Regulation of division of labor in insect societies. Annu Rev Entomol 37:637-665

Rybak J, Meinertzhagen IA (1997) The effects of light reversals on photoreceptor synaptogenesis in the fly *Musca domestica*. Eur J Neurosci 9:319-33

Saint Marie RL, Carlson SD (1982) Synaptic vesicle activity in stimulated and unstimulated photoreceptor axons in the housefly. A freeze-fracture study. J Neurocytol 11:747-61

Sanes JR, Zipursky SL (2010) Design principles of insect and vertebrate visual systems. Neuron 66:15-36

Sattelle DB, Lummis SC, Wong JF, Rauh JJ (1991) Pharmacology of insect GABA receptors. Neurochem Res 16:363-374

Schäfer S, Bicker G (1986) Distribution of GABA-like immunoreactivity in the brain of the honeybee. J Comp Neurol 246:287-300

Schmitz F (2009) The making of synaptic ribbons: How they are built and what they do. The Neuroscientist 15:611-624

Schürmann FW (1974) Bemerkungen zur funktion der Corpora Pedunculata im Gehirn der insekten aus morphologischer sicht. Exp Brain Res 19:406-432

Schürmann FW (1987) Arthropod brains: Evolution, development, structure, and function. A Gupta. New York: John Wiley & Sons

Schürmann FW, Ottersen OP, Honegger HW (2000) Glutamate-like immunoreactivity marks compartments of the mushroom bodies in the brain of the cricket. J Comp Neurol 418:227-239

Seid MA, Harris KM, Traniello JF (2005) Age-related changes in the number and structure of synapses in the lip region of the mushroom bodies in the ant *Pheidole dentata*. J Comp Neurol 488:269-277

Seid MA, Wehner R (2008) Ultrastructure and synaptic differences of the boutons of the projection neurons between the lip and collar regions of the mushroom bodies in the ant, *Cataglyphis albicans*. J Comp Neurol 507:1102–1108

Shanbhag S, Müller B, Steinbrecht R (1999) Atlas of olfactory organs of *Drosophila melanogaster* 1. Types, external organization, innervation and distribution of olfactory sensilla. Int J Insect Morphol Embryol 28:377-397

Sinakevitch I, Farris SM, Strausfeld NJ (2001) Taurine-, aspartate- and glutamate-like immunoreactivity identifies chemically distinct subdivisions of Kenyon cells in the cockroach mushroom body. J Comp Neurol 367:352-367

Sitaraman D, Zars M, Laferriere H, Chen Y, Sable-Smith A, Kitamoto T, Rottinghaus GE, Zars T (2008) Serotonin is necessary for place memory in *Drosophila*. Proc Natl Acad Sci USA 105:5579-5584

Sjöholm M, Sinakevitch I, Strausfeld NJ, Ignell R, Hansson BS (2006) Functional division of intrinsic neurons in the mushroom bodies of male *Spodoptera littoralis* revealed by antibodies against aspartate, taurine, FMRF-amide, Mas-allatotropin and DC0. Arthropod Struct Dev 35:153-68

Steiger U (1967) Über den Feinbau des Neuropils im Corpus pedunculatus der Waldameise. Z Zellforsch 81:511-536

Stieb SM, Muenz TS, Wehner R, Rössler W (2010) Visual experience and age affect synaptic organization in the mushroom bodies of the desert ant *Cataglyphis fortis*. Dev Neurobiol 70:408-423

Stocker RF (1994) The organization of the chemosensory system in *Drosophila melanogaster*: A review. Cell Tissue Res 275:3-26

Stocker RF, Lienhard M, Borst A, Fischbach K (1990) Neuronal architecture of the antennal lobe in *Drosophila melanogaster*. Cell Tissue Res 262:9–34

Strausfeld NJ, Sinakevitch I, Vilinsky I (2003) The mushroom bodies of *Drosophila melanogaster*: An immunocytological and Golgi study of Kenyon cell organization in the calyces and lobes. Microsc Res Techniq 62:151-169

Stuart AE, Borycz J, Meinertzhagen IA (2007) The dynamics of signaling at the histaminergic photoreceptor synapse of arthropods. Prog Neurobiol 82:202-27

Su H, O'Dowd DS (2003) Fast synaptic currents in *Drosophila* mushroom body Kenyon cells are mediated by α-bungarotoxin-sensitive nicotinic acetylcholine receptors and picrotoxin-sensitive GABA receptors. J Neurosci 23:9246-9253

Tamás G, Buhl EH, Somogyi P (1997) Massive autaptic self-innervation of GABAergic neurons in cat visual cortex. J Neurosci 17:6352-64

Tanaka J, Matsuzaki M, Tarusawa E, Momiyama A, Molnar E, Kasai H, Shigemoto R (2005) Number and density of AMPA receptors in single synapses in immature cerebellum. J Neurosci 25:799-807

Tanaka NK, Awasaki T, Shimada T, Ito K (2004) Integration of chemosensory pathways in the *Drosophila* second-order olfactory centers. Curr Biol 14:449-457

Tanaka NK, Tanimoto H, Ito K (2008) Neuronal assemblies of the *Drosophila* mushroom body. J Comp Neurol 508:711-755

Technau GM (1984) Fiber number in the mushroom bodies of adult *Drosophila melanogaster* depends on age, sex and experience. J Neurogenet 1:113-126

Tolbert L, Hildebrand JG (1981) Organization and synaptic ultrastructure of glomeruli in the antennal lobes of the moth *Manduca sexta*: A study using thin sections and freeze-fracture. Proc R Soc Lond Ser B 213:279-301

Turner GC, Bazhenov M, Laurent G (2008) Olfactory representations by *Drosophila* mushroom body neurons. J Neurophysiol 99:734-746

Vallés A, White K (1988) Serotonin-containing neurons in *Drosophila melanogaster*: Development and distribution. J Comp Neurol 268:414-428

Vosshall LB, Wong A, Axel R (2000) An olfactory sensory map in the fly brain. Cell 102:147–159

Vosshall LB, Stocker RF (2007) Molecular architecture of smell and taste in *Drosophila*. Annu Rev Neurosci 30:505-533

Ware RW, Lopresti V (1975) Three-dimensional reconstruction from serial sections. Int Rev Cytol 40: 325-440

Wegener S (2007) Maturation-dependent synaptic plasticity of GABAergic neurons in the mushroom body calyx of the honeybee brain. MSc thesis, University of Würzburg, Würzburg, Germany

White J, Southgate E, Thomson J, Brenner S (1986) The structure of the nervous system of the nematode *C. elegans*. Proc R Soc Lond Ser B 314:1-340

Williams RW, Rakic P (1988) Three-dimensional counting: An accurate and direct method to estimate numbers of cells in sectioned material. J Comp Neurol 278:344-352

Wilson EO (1976) Behavioral discretization and the number of castes in an ant species. Behav Ecol Sociobiol 1:141-154

Winston M (1987) The biology of the honey bee. Cambridge, MA: Harvard University Press

Winther AM, Siviter RJ, Isaac RE, Predel R, Nässel DR (2003) Neuronal expression of tachykinin-related peptides and gene transcript during postembryonic development of *Drosophila*. J Comp Neurol 464:180-196

Wojtowicz J, Marin L, Atwood H (1994) Activity-induced changes in synaptic release sites at the crayfish neuromuscular junction. J Neurosci 14:3688-3703

WormAtlas, Altun ZF, Herndon LA, Crocker C, Lints R, Hall DH (eds) (2002-2010) http://www.wormatlas.org

Yang C, Zhang J, Yazulla S (2003) Differential synaptic organization of GABAergic bipolar cells and non-GABAergic (glutamatergic) bipolar cells in the tiger salamander retina. J Comp Neurol 455:187-197

Yasuyama K, Meinertzhagen IA, Schürmann FW (2002) Synaptic organization of the mushroom body calyx in *Drosophila melanogaster*. J Comp Neurol 445:211–226

Zars T (2000) Behavioral functions of the insect mushroom bodies. Curr Opin Neurobiol 10:790-795

Zars T, Fischer M, Schulz R, Heisenberg M (2000) Localization of a short-term memory in *Drosophila*. Science 288:672-675

Zhai R, Bellen H (2004) The architecture of the active zone in the presynaptic nerve terminal. Physiology 19:262-270

Zhu S, Chiang A, Lee T (2003) Development of the *Drosophila* mushroom bodies: Elaboration, remodeling and spatial organization of dendrites in the calyx. Development 130:2603-2610

APPENDIX A   Plasticity in the Mushroom Body Calyx of the European Honeybee, *Apis mellifera*

A.1   INTRODUCTION

The mushroom bodies are large and pronounced structures of the honeybee brain. Each hemisphere features a pair of cup-shaped calyces composed of anatomically and functionally distinct regions, the lip, collar, and basal ring (Mobbs, 1982; Gronenberg, 2001). The lip receives olfactory input from the antennal lobes and the collar receives visual input from the medulla and the lobula (Gronenberg, 2001; Ehmer and Gronenberg, 2002). The basal ring receives both olfactory and visual inputs. As in *Drosophila*, described in this study as well as others (Yasuyama et al., 2002; Leiss et al., 2009), the honeybee calyces are composed of microglomeruli, repeating spherical structures with a projection neuron (PN) bouton at the centre, surrounded by tiny Kenyon cell (KC) dendrites (Ganeshina and Menzel, 2001; Groh et al., 2004). GABA-immunoreactive extrinsic neurons (ENs) also make important contributions to microglomeruli (Ganeshina and Menzel, 2001). These ENs are considered inhibitory feedback neurons, providing a putative flow of information from the mushroom body lobes back to the calyx (Bicker et al., 1985; Schäfer and Bicker, 1986). For example, GABA-positive EN terminals are presynaptic to KCs in the calyx (Ganeshina and Menzel, 2001), and KCs carry sensory information to the mushroom body lobes, where they could contact postsynaptic specializations of the GABA-positive ENs, which could then act as feedback neurons to the calyx.

Honeybee division of labour is characterized by temporal polyethism. Young worker bees attend to tasks within the dark hive, like comb cleaning and brood care. At about three weeks of age, they switch to foraging outside the hive (Winston, 1987; Robinson, 1992). Behavioural maturation appears to coincide with structural changes of the mushroom bodies, including the calyx. During this time, the volume of the calyx increases and the microglomerular density (number of microglomeruli per unit area of the calyx) decreases (Durst et al., 1994; Muenz et al., 2008). These changes are the probable

outcome of growth by KC dendritic branches with increasing age and experience (Farris et al., 2001; Gehring, 2008). There is also some evidence that innervation of the calyx by GABA-positive cells, presumably the feedback neurons, becomes less dense with maturation, as shown from the percentage of the calyx covered by GABA-immunoreactive profiles (Wegener, 2007). However, these results must be interpreted with caution, because the number of bees analyzed in the study was small (as few as three), and microscope parameters were not held constant during image acquisition. Furthermore, glutaraldehyde fixation was necessary, resulting in poor penetration of the GABA antibody beyond the initial 3μm of the tissue and difficulty in co-labeling with other reagents.

In this study, protocols were developed for two markers of GABA-immunoreactive neurons, vGAT (*Drosophila* vesicular GABA transporter; Enell et al., 2007) and GAD1 (*Drosophila* glutamic acid decarboxylase, Featherstone et al., 2000), selected because they provide a bright immunolabel of neurites in the formaldehyde-fixed *Drosophila* calyx (Enell et al., 2007). GAD1 provided the superior immunolabel of the two, and was thus used to investigate if innervation by neurites expressing a GABA phenotype differs between the lip and the collar, and if innervation of these areas changes with age. Phalloidin, an F-actin probe, was used to visualize the mushroom bodies and individual microglomeruli, as previously reported (Groh et al., 2004).

A.2 MATERIALS AND METHODS

A.2.1 Bees

Both 1-day old and foraging worker honeybees (*Apis mellifera carnica*) from the same queen were collected for GAD1 analysis. To obtain 1-day old bees, a frame containing pupae was removed from a colony (departmental bee station, University of Würzburg) and incubated at 33°C until emergence. Approximately 350 bees that emerged from the frame were marked on the back of the thorax and introduced back into the colony. The marked bees were then collected from the colony after 1 day. Foraging honeybees were collected at the entrance of the hive and identified by the presence of pollen loads on their hind legs (Winston, 1987). The vGAT antibody was tested on bees from a separate

marked cohort from the same queen and colony as those used for GAD1 analysis, at ages of 1-day, 7-days, 9-days and 15-days.

A.2.2 Immunocytochemistry

Worker bees were decapitated and heads embedded in wax or pinned for brain dissection in Ringer's solution. The brains were fixed in 4% formaldehyde in phosphate buffered saline (PBS) overnight at 4°C, then washed three times for 10 minutes each in PBS. The brains were embedded in 5% agarose and sectioned at a thickness of 100µm on a Vibratome (Leica). The sections were washed twice for 10 minutes in 0.2% Triton-X 100 in PBS before incubating for at least one hour at 23°C in 10% normal goat serum (NGS) and 0.2% Triton-X 100 in PBS. The sections were then incubated in mouse anti-synapsin (SYNORF 1, 1:10), Alexa Fluor Phalloidin (0.2 units), and rabbit anti-vGAT for four days at 4°C (1:250, 1:500, 1:1000, 1:2000, 1:4000), or rabbit anti-GAD1 (1:1000) with 5% NGS in PBS. Anti-synapsin was kindly provided by Dr. E. Buchner, anti-vGAT from Dr. D. Nässel, and anti-GAD1 from Dr. F. R. Jackson. The tissues were then washed five times in PBS for 10 minutes each and incubated in Alexa 568 goat anti-rabbit (1:250, MoBiTec) and Alexa 405 goat anti-mouse (1:250, MoBiTec) with 2% NGS in PBS for two hours at room temperature. Sections were then transferred to 60% glycerol in PBS for 30 minutes at 23°C or overnight at 4°C, and mounted in 80% glycerol in PBS on slides beneath a 00 coverslip sealed with nail polish.

A.2.3 Confocal Microscopy, Image Processing and Data Analysis

Specimens were examined with a Leica TCS SP confocal microscope (Wetzlar, Germany) using an immersion objective, 63x/1.4 Plan Apochromat, and a 1.75X digital zoom. Series of optical sections were obtained in the section plane containing the ellipsoid body of each bee, in the two most medial lips and collars, for a total z-depth of 20µm captured in 0.8µm intervals. All stacks used for statistical analyses were collected using the same detection parameters (e.g. gain), which were chosen from an initial assessment of a few randomly selected, well-labeled sections. Image processing was performed with Image J and Adobe Photoshop.

Quantification of the innervation density of GAD1-positive cells, defined as the percentage of the selected area covered by GAD1-positive profiles (Wegener, 2007), in 1-day old (n=9) and forager bees (n=9), was performed using Image J. Density measurements were made for the entire lip and collar (Figures A1-A,B; A2-A,B), as well as for smaller areas containing only microglomeruli (Figures A1-C,D; A2-C,D) in the first 3μm of the tissue, to provide a comparison with the values obtained by Wegener (2007), and the first 20μm, the observed depth of GAD1 antibody penetration. First, the collected image stacks were collapsed into single z-projection images containing the maximum point of intensity for each optical section in the phalloidin channel, to permit the visualization of individual microglomeruli and the borders of the calyx. The region of interest (collar or lip) was then outlined in its entirety (Figures A1-A; A2-A) or in small areas containing only microglomeruli. These small areas were two circles in the lip, each with a total area of 400μm^2 (Figure A1-C) and the dense region of the collar (Figure A2-C). The corresponding z-projection of the GAD1 channel was then converted to a binary image (Figures A1-B,D; A2-D,B). It was ensured that all well-labeled profiles visible in the GAD1 z-projection were accurately represented in the binary image (Figures A1, A2). To test for differences of the phenotypically GABAergic innervation density of the calyx between ages (1-day old and forager) and region (lip and calyx), data were evaluated using a 2X2 ANOVA (p<0.05 for significance).

A.3 RESULTS AND DISCUSSION

The vGAT antibody yielded non-specific labeling of the entire brain, regardless of the age of the bees, dissection method or antibody dilution examined (not shown). Surprisingly, the synapsin label was completely abolished in the presence of vGAT, possibly because synapsin and vGAT both localize to synaptic vesicles. The vGAT signal did not improve in the absence of synapsin or phalloidin, however, and thus the vGAT antibody was not used in the remainder of this study. The GAD1 antibody showed a very similar pattern of immunolabeling to direct GABA antibodies (Figure A3-A-C; e.g. Bicker et al., 1985; Schäfer and Bicker, 1986; Wegener, 2007). Phalloidin but not synapsin yielded a strong signal in conjunction with GAD1. A GABA-positive tract previously described by Schäfer and Bicker (1986), which extends from near the antennal

lobes to run alongside the medial antennocerebral tract, was found to terminate in the lower division of the central complex (Figure A3-D-F). GAD1-immunoreactive (GAD1-ir) fibres branch between the medial and lateral calyx, before running along the inner periphery of the calyx and invading the basal ring, the collar, and the lip (Figure A3-G-I; Figure A4). The lip was densely innervated by GAD1-positive fibres, as was a small region of the basal ring that anatomically corresponds to an area exclusively receiving input from the medulla (Figure A4; Ehmer and Gronenberg, 2002). The GAD1-ir profiles were located between microglomeruli and followed a beads-on-a-string motif (Figure A5). Microglomeruli appeared to have a more regular structure and were easier to identify individually than in the fly (compare with Figure 13). Often there was one GAD1-positive profile per microglomerulus, but occasionally there were two. More rarely, a single GAD1-ir profile was co-localized with two microglomeruli. These results correspond well to those previously obtained using direct GABA antibodies at both the light (Wegener, 2007) and the electron (Ganeshina and Menzel, 2001) microscope level.

Analyses of the innervation density of the first 20μm of the tissue revealed that the lip was more densely innervated than the collar, but the innervation of each region at both ages was very similar (Table A1). Accordingly, both the entire calyx and the microglomeruli-only containing areas showed an effect of region (respectively, $F_{(1,32)}=190.0$, $p<0.001$; $F_{(1,32)}=207.6$, $p<0.001$) but no effect of age ($F_{(1, 32)}=0.230$, $p=0.635$; $F_{(1, 32)}=0.001$, $p=0.977$). There was no interaction between age and region ($F_{(1,32)}=0.236$, $p=0.630$; $F_{(1,32)}=0.070$, $p=0.793$). For the tissue depth of 3μm, again there were negligible differences between the innervation densities of the entire structure and the area containing only microglomeruli. The following statistical values thus refer only to the microglomeruli-only areas: an effect of age ($F_{(1,32)}=5.78$, $p= 0.022$), region ($F_{(1,32)}=90.783$, $p<0.001$), and an interaction between age and region ($F_{(1,32)}=6.217$, $p=0.018$) was observed. Given the presence of an interaction, pairwise comparisons of the means were then calculated (1-way ANOVA followed by Scheffe's test). The pairwise comparisons indicated that the lip becomes increasingly innervated with age ($p=0.003$) but the innervation of the collar remains constant ($p=1.0$). Furthermore, the

innervation of the lip was greater than that of the collar in both 1-day old (p<0.001) and foraging bees (p<0.001).

These results collectively show that the lip is more densely innervated by neurites immunoreactive to GAD1 at any age than the collar, as previously indicated by Wegener (2007). It appears, however, that the density of innervation in the lip and collar remains constant as the bees age and transform from in-hive to outside-hive tasks, although increased innervation of the lip was found when the analysis was restricted to the first 3µm of the tissue. These results may be more accurate than those obtained from analyzing the first 20µm of tissue. Analyzing a short depth of the tissue from its surface provides the advantage of more uniform antibody penetration; antibodies are unlikely to penetrate the tissue of individual bees identically, and this is compounded as the depth of the tissue increases. Regardless, these findings stand in contrast to the previous study by Wegener (2007), who showed that the innervation of the calyx by GABA-positive cells decreases with age. The difference in findings cannot be easily explained, but could be due to the previously mentioned limitations of the original study. Alternatively, the amount of GAD1 in the calyx might not strongly correlate with the level of GABA, and thus it is possible that there could simultaneously be a decrease in the amount of GABA in the calyx, and no change or an increase in the amount of GAD1. Counts of microglomeruli are needed to assess more accurately whether the results here have functional implications for an individual microglomerulus. For example, if innervation by GAD1-positive profiles remains the same over the lifespan, there could still be a net increase of innervation per microglomerulus if the microglomulus density decreases with age (Muenz et al., 2008).

A.4 TABLES AND FIGURES

Table A1 Innervation densities of GAD1-immunoreactive fibres in the lip and the collar of the calyx (mean±standard deviation), as measured by the percentage of GAD1-positive profiles covering the area of interest in a selected depth of tissue.

		20µm		3µm	
Area of interest	Region of calyx	1 day old	Forager	1 day old	Forager
Entire calyx	Lip	21.6±1.9	21.6±3.9	5.9±1.1	8.4 ±2.2
	Collar	10.5±1.6	9.7±1.9	2.4±1.3	2.4±1.0
Microglomeruli-only	Lip	24.4±2.6	24.7±5.3	6.3±1.0	8.9±2.1
	Collar	9.4±1.5	9.2±1.9	2.0±1.0	2.0±0.8
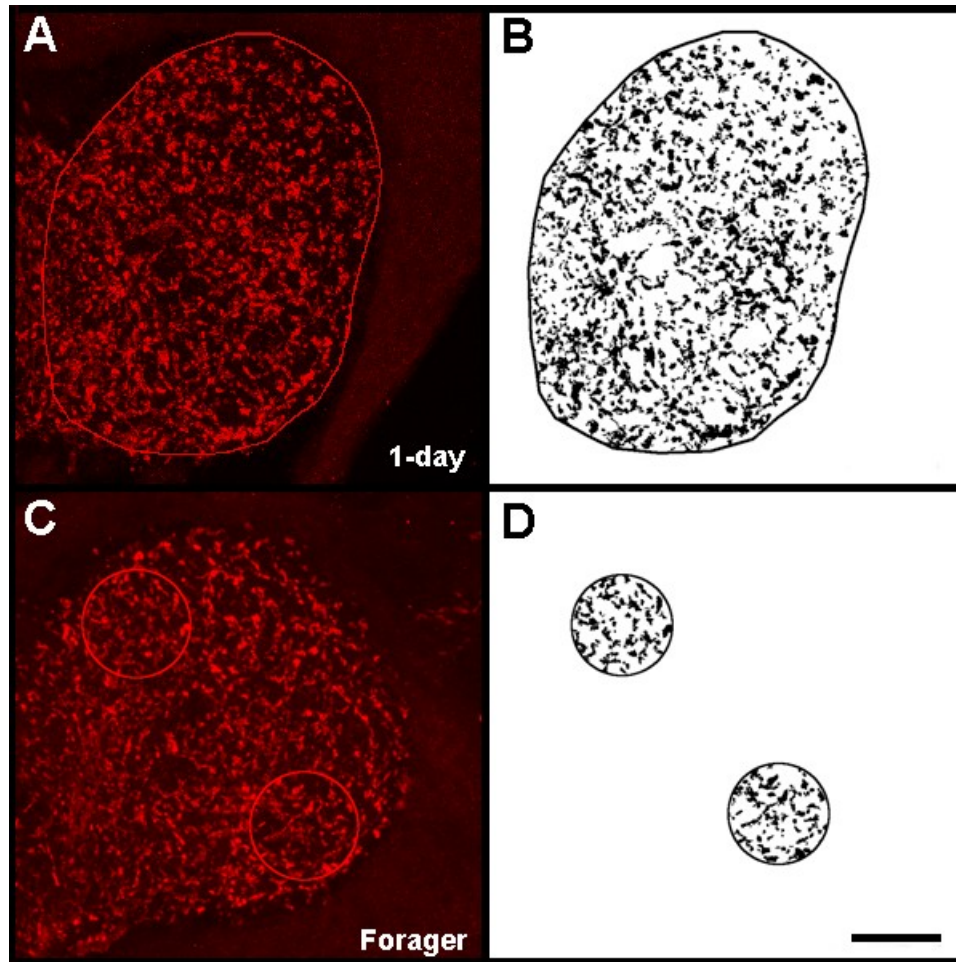
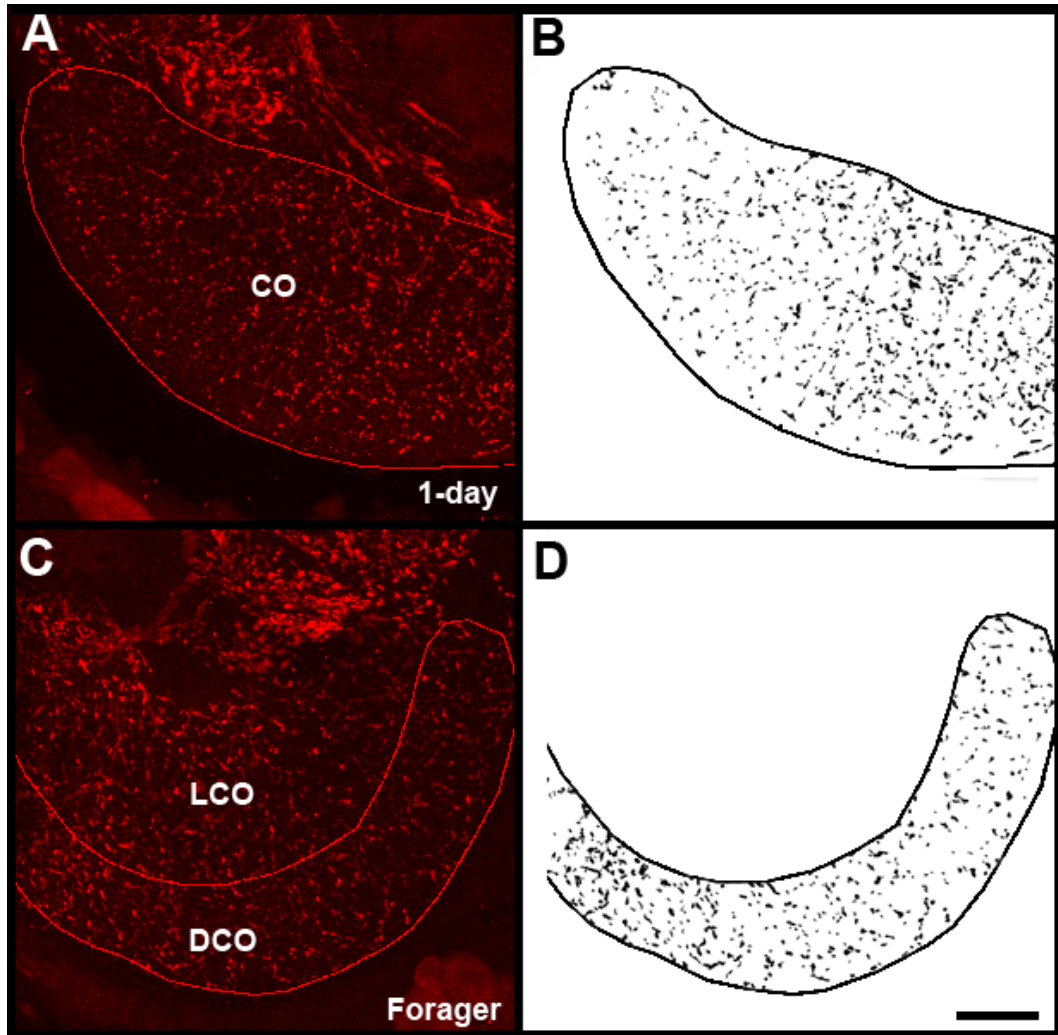Figure A1 Immunofluorescence labeling of GAD1 innervation in the lip of a 1-day old
bee and a forager bee. A) The entire lip region and (C) two circular areas
(400µm^2 each) were converted to binary images (B,D, respectively) to
calculate GAD1-ir innervation for the entire lip region as well as an area
solely containing microglomeruli. Scale bar, 20µm; 20µm stack of 25
sections.

Figure A2 Immunofluorescence labeling of GAD1 innervation in the collar of a 1-day old bee and a forager bee. A) The entire collar (CO) region and (C) the dense region of the collar (DCO) were converted to binary images (B,D, respectively) to calculate GAD1-ir innervation for the entire collar region as well as an area solely containing microglomeruli. Scale bar, 20µm; 20µm stack of 25 sections; LCO, loose collar region).
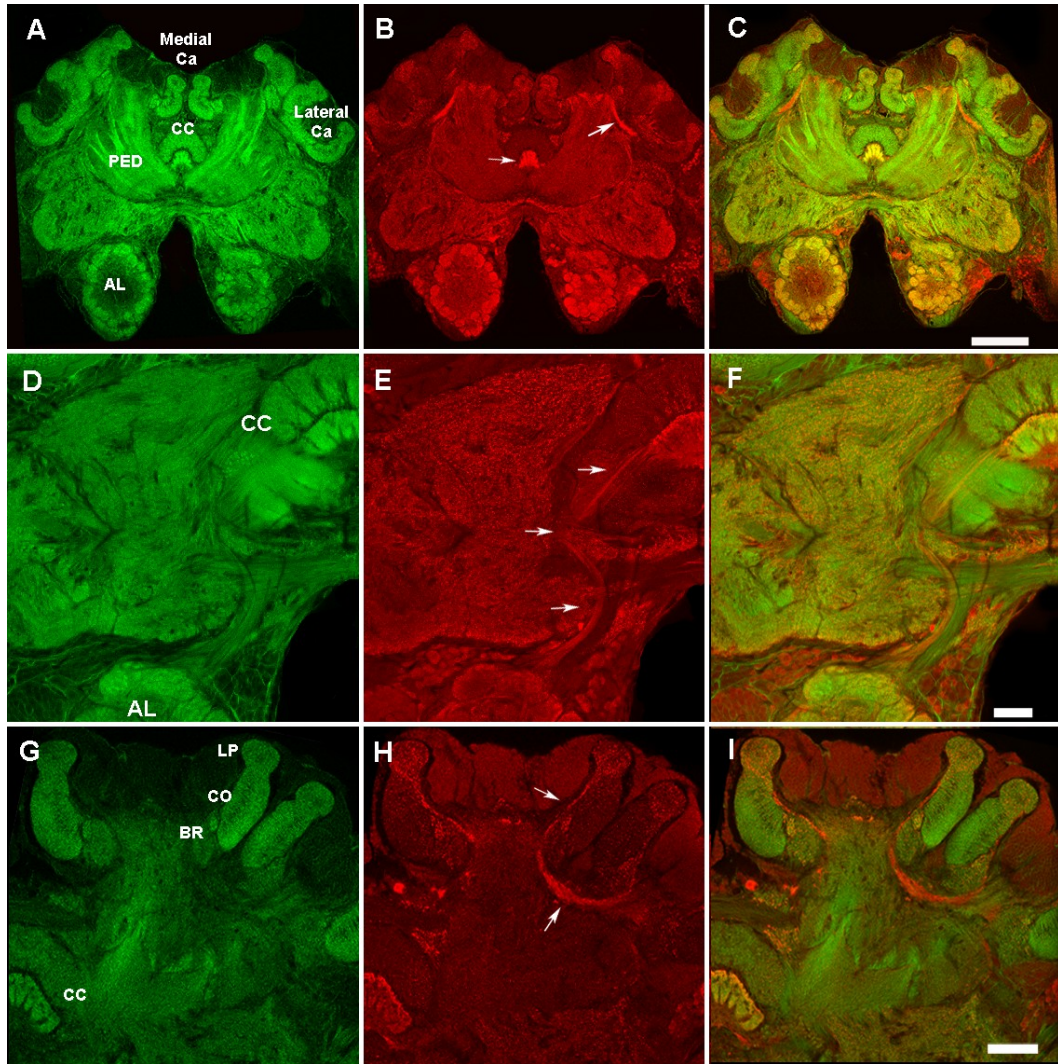
Figure A3 Immunofluorescence labeling of GAD1-ir (red) tracts of the honeybee brain. Brain structure is labeled with phalloidin (green) to show actin enrichment. A-C) The antennal lobes (AL), the lower division of the central complex (CC, arrow), the mushroom body calyces (Ca), and the tracts that innervate calyces (arrow), show high immunoreactivity to GAD1. D-F) A GAD1-ir tract (arrows) extends from near the antennal lobes to the lower division of the CC, running in part along the median antennoglomerular tract (13.0µm stack of 16 sections). G-H) GAD1-ir fibres (arrows) branch between the medial and lateral calyx, before running along the inner periphery of the calyx and invading the basal ring (BR), the collar (CO), and the lip (LP). Scale bar for A-C, 250µm; D-I, 100µm.
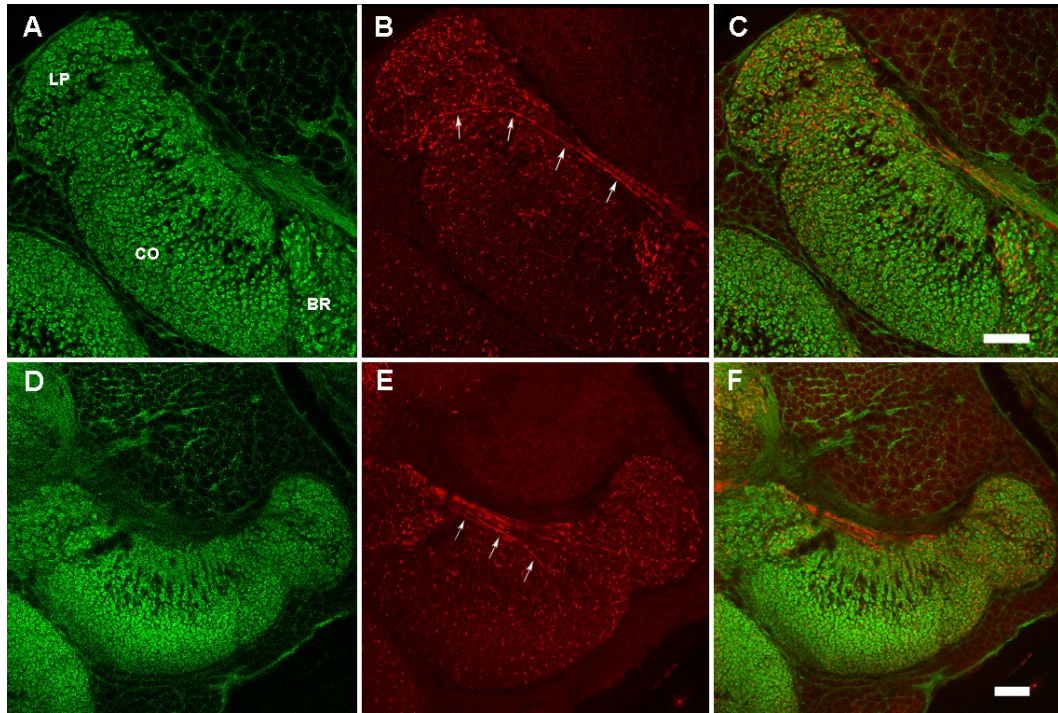
Figure A4 GAD1-ir (red) fibres invade all components of the mushroom body calyx. Microglomeruli are labeled with phalloidin (green). A-C) GAD1-ir fibres (arrows) branch extensively and densely innervate the microglomeruli of the lip (LP) of the calyx. D-F) GAD1-ir fibres also innervate the collar (CO). C,F) A small portion of the basal ring shows high immunoreactivity to GAD1. All scale bars, 25µm.
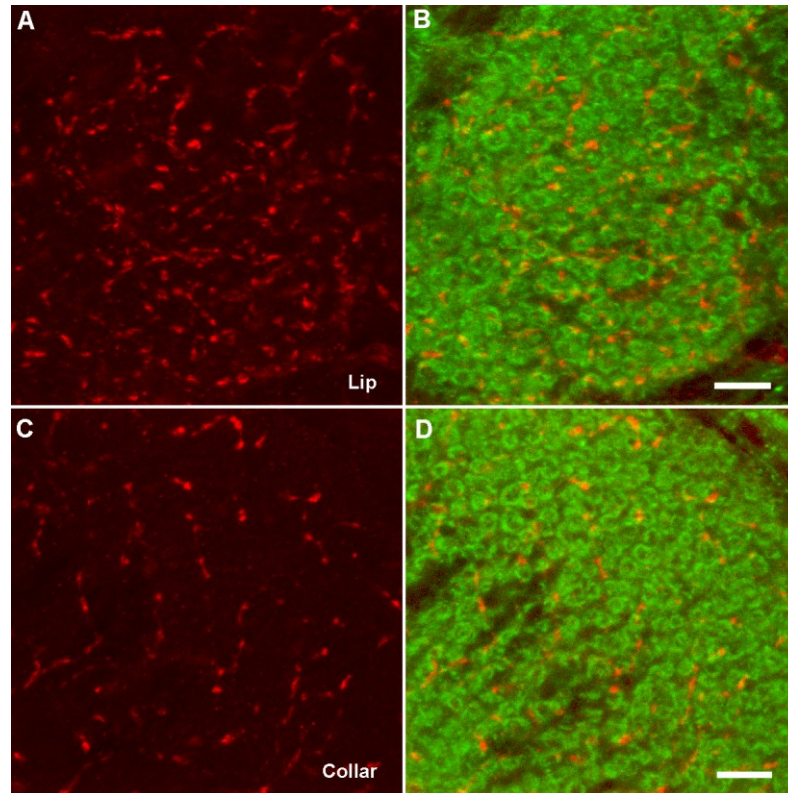
Figure A5 GAD1-ir (red) neurons form contacts with microglomeruli in the lip and collar
of the calyx. Microglomeruli are labeled with phalloidin (green), which
detects a halo of actin enrichment encircling each microglomerulus. A,B) The
lip is densely innervated with GAD1-ir profiles, often taking a large,
encircling trajectory, while the collar (C,D) is sparsely innervated by long,
branching GAD1-ir neurons showing small, spherical swellings. All scale
bars, 5µm; 3.59µm stack of 7 sections; forager bees.